Implementation of Anatomical Navigators for Real Time Motion Correction in Diffusion Tensor Imaging

Alkathafi A. Alhamud

Department of Human Biology

University of Cape Town

Thesis presented for the degree of

Doctor of Philosophy

February 2012

Abstract

Thesis: **Implementation of Anatomical Navigators for Real Time Motion Correction in Diffusion Tensor Imaging**

Author's Name: Alkathafi A. Alhamud Date: 10-02-2012

Diffusion Tensor Imaging (DTI) is used to detect microstructural changes in the human brain. Although echo planar imaging (EPI) has been implemented in diffusion pulse sequences to minimize the effect of subject motion, motion artifacts may reappear in the diffusion volume images when scanning the brain repeatedly with different diffusion directions and strengths. Both retrospective and prospective motion correction approaches have been implemented in DTI to correct for misalignments in diffusion volume images. Most of these methods rely on the contrast differences between the diffusion weighted images and a target image, which renders the registration for motion correction inaccurate, especially in acquisitions with high diffusion weightings. In order to develop a motion correction method that is independent of the diffusion contrast, a separate motion tracking technique has been introduced using a volumetric 3D-EPI navigator. This technique performs prospective motion correction in diffusion weighted images without having to reacquire volumes during which motion occurred, unless motion exceeded some pre-set thresholds. The additional scan time for the navigator and feedback is only 526 ms per diffusion volume, which takes 9500 ms to acquire.

The navigated diffusion sequence (vNav) was validated using a water phantom, and *in vivo* in sixteen children (aged 5-6 years) and 6 adults. A multiecho MPRAGE sequence was also acquired in paediatric and adult subjects. FreeSurfer was used to automatically extract volumes of interest (VOI's). The mean and the histogram-derived measurements of the FA and MD for the whole brain (WBH) and for different VOI's were analysed. Our results show that adding the navigator does not alter the DTI data. In the paediatric and adult scans acquired using the standard diffusion sequence, subject head motion caused significant changes in all the DTI measures, except FA of the whole brain white matter in children. Retrospective motion correction did not recover diffusion measures but instead resulted in decreased FA and generated spurious fiber tracts in the corpus callosum. The DTI measures are recovered substantially in the prospective motion corrected data acquired using the navigated sequence.

Contents

List of Figures

List of Tables

Preface

This thesis presents and evaluates the performance of a novel method to improve the efficacy of *in vivo* DTI studies at the Cape Universities Brain Imaging Centre (CUBIC), South Africa. This work originated due to the limitations of methods that are currently available for motion correction in DTI. The main objective was to implement a technique that would be independent of diffusion weighting, easy to apply, and affordable, specifically for use in paediatric scans.

This thesis includes three independent articles. These articles are to be found in chapters two, three and four. Each chapter documents and evaluates various aspects of the methodology, research, and findings. A comprehensive introduction provides the necessary background and context to the work. This style facilitates direct access and concise evaluation of the different methodologies and follows the logical progression of the work. However, as a complete document, it contains necessary repetition due to the fact that each core chapter is being presented as an independent article. For the purpose of thesis examination the contributions from co-authors are given below.

Chapter one provides the background and rationale for the current study, as well as basic MRI physics, diffusion MRI, and an overview of current methods for motion correction in MRI. It also provides the background theory and principles of the pulse sequences being used in the remainder of the thesis.

Chapter two is an article that, at the time of writing, is in press in *Magnetic Resonance in Medicine*. The chapter presents the implementation of a novel echo planar imaging volumetric navigator in DTI to correct motion and reacquire uncorrected corrupted diffusion volumes during which excessive motion occurred. This chapter also demonstrates the effect of motion and retrospective motion correction on the DTI-derived metrics (MD and FA maps) for the whole brain of adult subjects.

André van der Kouwe and Ernesta Meintjes (supervisor) supervised and directed the work. Dylan Tisdall and Aaron Hess together developed the initial proof of concept for an EPI-based motion correction navigator. Khader M. Hasan provided assistance in analysing the DTI data. The novel idea of how to extend and implement the EPI navigator to perform motion correction in real time in DTI was that of the candidate, Alkathafi A. Alhamud. The EPI-based navigator

for motion correction for the scanner at CUBIC, its implementation in the DTI sequence, algorithm development, the methods, data acquisition, validation, and processing were performed by Alkathafi A. Alhamud. The article was drafted by Alkathafi A. Alhamud and handed over to the co-authors for editorial and scientific commentary.

Chapter three is a manuscript that, at the time of writing, is under review by NeuroImage. The chapter demonstrates the potential misinterpretation of FA and MD values that may occur as a result of subject head motion. The analyses presented in this chapter uses automatic tissue segmentation by FreeSurfer to explore changes in regional FA and MD measures in gray and white matter, and compares the performance of retrospective motion correction to prospective motion correction on these measures.

André van der Kouwe and Ernesta Meintjes (supervisor) supervised and directed the work. Khader M. Hasan provided assistance in processing of the DTI data. The idea to investigate the impact of motion on interpretation of abnormal DTI measures was that of Alkathafi A. Alhamud. The candidate acquired and analysed all the data. The article was drafted by Alkathafi A. Alhamud and handed over to the co-authors for editorial and scientific commentary.

Chapter four is also a prepared manuscript that will be submitted for publication. It demonstrates the use of the navigated diffusion pulse sequence in young children (aged 5-6 years). The chapter compares the performance of the standard diffusion sequence to the navigated diffusion sequence. The differences in the whole brain histograms (WBHs) of the FA between paediatric and adult subjects are characterized. Automatic tissue segmentation with FreeSurfer was used in this chapter to explore changes in regional FA and MD measures in children in gray and white matter resulting from subject head motion.

André van der Kouwe and Ernesta Meintjes (supervisor) supervised and directed the work. Barbara Laughton recruited the children, scheduled and arranged the paediatric scans. The idea to investigate the impact of motion on DTI measures in young children was that of Alkathafi A. Alhamud. The candidate analysed all the data. The article was drafted by Alkathafi A. Alhamud and handed over to the co-authors for editorial and scientific commentary.

Chapter five is a comprehensive discussion that summarises the findings of the previous chapters, highlights limitations, and suggests possible improvements to the current implementation of the navigator. Chapter six presents the conclusions of the current study. It summarizes all the salient points that have been detected throughout this study.

Acknowledgments

Ernesta Meintjies supervised the work and André van der Kouwe has been a supportive advisor through out my work. They provided the context, expert ideas, advice, support, and numerous resources required for the implementation of this work. I would like to thank them for their significant contributions, as without them this would not have been possible. Khadar M. Hasan offered several ideas and important points in the analysis of the DTI data. M. Dylan Tisdall and Aaron A. Hess provided advices on the EPI navigator.

I would like to present my sincere gratitude to my family in specific my wife who supported me during my PhD studies, to my mother and my deceased father.

The following organisations have provided the resources used in this work: The University of Cape Town, Cape Universities Brain Imaging Centre (CUBIC), and the Athinoula A. Martinos Center for Biomedical Imaging.

Funding was provided by the South African Research Chairs Initiative of the Department of Science and Technology and National Research Foundation of South Africa, Medical Research Council of South Africa, NIH grants R21AA017410, R21EB008547, R21MH096559, R01HD071664, R01NS05574, P41RR014075, the Ellison Medical Foundation, and the University of Cape Town.

Chapter 1

Introduction

This thesis presents a novel method to correct, in real time, errors and artifacts caused by subject head motion in Diffusion Tensor Imaging (DTI) using an EPI volumetric anatomical navigator. In this chapter, MR physics, the basic principles of diffusion imaging, diffusion pulse sequences, effects of motion in DTI, and current mechanisms for addressing these are presented. Chapter 2 describes the implementation and the validation of an EPI volumetric navigator (vNav) to correct these errors, in real time, in DTI. Since prospective motion correction occurs at the onset of each diffusion acquisition, volumes during which significant motion occur may be corrupted. The mechanism for the reacquisition of these corrupted diffusion volumes is also described. Chapter 3 explores the effects of subject head motion on regional DTI measures, in particular fractional anisotropy (FA) and mean diffusivity (MD), in gray and white matter using automatic tissue segmentation with FreeSurfer. We explore the extent to which either retrospective motion correction or the prospectively motion corrected diffusion sequence, both without and with reacquisition of corrupted diffusion volumes, can recover the DTI measures in the presence of motion. Chapter 4 presents differences due to motion in the DTI measures of different brain regions in young (5-6 years) children, information regarding how much children in this age range tend to move, and the success with which the prospectively motion corrected DTI sequence can recover the DTI measures. Children were scanned using both the basic DTI sequence and the prospectively motion corrected sequence with reacquisition. Chapter 5 is a comprehensive discussion, summarising the main findings of the previous chapters and their implications for DTI. The final chapter presents the conclusions.

1.1 Background and Motivation

Histological examination of the human brain reveals that it is comprised of more than 100 billion neurons that communicate with each other via axons for the formation of complex neural networks. The structural mapping of such networks during healthy and diseased states is important for understanding brain function. Previously, imaging of the white matter was, for the most part, undertaken during post-mortem studies. The development of diffusion tensor imaging (DTI) was a major breakthrough for studies of brain tissue connectivity (Basser et al., 1994). DTI is a non-invasive technique that can measure white matter organization in vivo.

DTI is based on measuring differences in water diffusion in different directions in different brain tissue. It requires scanning the brain repeatedly (i.e. multiple volumes of the brain where each volume can consist of 72 slices with 2mm thickness) with different magnetic field gradients applied in different directions. DTI, when compared to conventional MRI imaging techniques, is characterized firstly by the application of very strong magnetic field gradients and secondly by a lengthy scan time. This drawn out acquisition time renders DTI acquisition susceptible to subject head motion especially in paediatric and non-cooperative subjects. Some of the factors that determine the accuracy of the DTI measures are the quality of individual DTI volumes, the alignment of the individual DTI volumes, and the accuracy of the diffusion weighting. Subject motion can result in significant misalignment between diffusion gradient directions (scanner coordinate system) and subject anatomy (subject coordinate system), resulting in artifacts and errors in diffusion measures.

Several techniques have been proposed for motion correction in DTI, but all the existing methods are fraught with limitations and drawbacks such as, for example, a substantial lengthening of scan time (Kober et al., 2011). Some prospective methods require cameras and markers (Aksoy et al., 2011), while others are limited by low signal to noise ratio at high diffusion weightings (Benner et al., 2010). Retrospective motion correction is also widely used (Rohde et al., 2004; Helton et al., 2006; Qiu et al.,2008; Leemans and Jones 2009; Rosas et al., 2010).

The aim of this study was to develop a method for prospective motion correction in DTI that overcomes many of the limitations of previous methods. To this end, we implemented a novel three-dimensional echo planar imaging (3D-EPI) navigator into the DTI sequence. The current

method is not influenced by the strong magnetic field gradients used to acquire DTI data, as the navigator images are acquired prior to application of the diffusion gradients. Furthermore, the navigator only causes a minimal increase in scan time compared to other methods (Kober et al., 2011). The navigator was developed on a Siemens 3 T Allegra (Erlangen, Germany) scanner at Cape Universities Brain Imaging Centre (CUBIC) in South Africa, with prototype development performed on a Siemens 3 T Tim Trio scanner located at the Athinoula Martinos Center for Biomedical Imaging (Boston, MA, USA).

1.2 Theory

1.2.1 MRI Physics

The basic principle underlying magnetic resonance imaging (MRI) is the use of natural magnetic properties; the spin phenomenon of the water proton (i.e. hydrogen nucleus), and its interaction with the magnetic field. Any proton that is subjected to a magnetic field starts to precess around the axis of that magnetic field at a frequency (ω_0) given by the Larmor equation

$$\omega_0=\gamma B_0 \tag{1.1}$$

where γ is the gyromagnetic ratio of the nucleus being imaged (typically hydrogen) and B_0 is the strength of the static main magnetic field. The precession of millions of magnetic dipole moments gives rise to a net magnetization vector, M, initially parallel to B_0, where B_0 also defines the Z axis. To generate a signal, a transverse magnetic field ($\boldsymbol{B}1$) needs to be applied perpendicular to the main magnetic field $\boldsymbol{B}0$. This transverse magnetic field is generated by applying a radiofrequency (RF) pulse to a coil. If the RF pulse is applied at the Larmor precession frequency, which is termed the resonance condition, it causes the net magnetization $\boldsymbol{M}$ to precess around the direction of the transverse magnetization at frequency $\omega_1 = \gamma B_1$, while simultaneously precessing around $\boldsymbol{B}0$ at the Larmor precession frequency. The net effect of these combined motions is to flip the magnetization from the longitudinal (Z) direction into the transverse (XY) plane with a spiralling type motion. The magnetization will continue precessing around B1 for as long as the RF pulse is applied. The flip angle α is a function of the time *t* that the RF pulse is applied and is given by equation (1.2).

$$\alpha = 2\pi\gamma B_1 t. \tag{1.2}$$

If the ***M*** is flipped completely into the transverse plane, it is called a 90 degree flip angle, while a 180 degree flip angle will invert the magnetization. When the RF pulse is turned off the magnetization will revert to precessing only around ***B***0 at the Larmor precession frequency. This precessing ***M*** causes a change in flux in a receiving coil, which induces a current in the coil according to Faraday's law. This current is the MRI signal.

The ***M*** does not continue to precess forever, but relaxes back to its equilibrium position parallel to ***B***0. Since it is only the transverse component of the magnetization that induces current in the receiving coil, the MRI signal decreases over time. The signal is typically a decaying exponential and is termed the free-induction decay (FID), since it is measured in the absence (ie. 'free') of an RF pulse. The equation of motion of the magnetization ***M*** is given by the Bloch equation (1.3).

$$\frac{dM}{dt} = M \times \gamma B - \frac{M_x i + M_y j}{T_2} - \frac{(M_z - M_0)k}{T_1} \tag{1.3}$$

The three terms in the Bloch equation describe (1) precession of the magnetization around ***B***, (2) decay of the transverse magnetization with time constant T2, and (3) re-growth of the longitudinal magnetization with time constant T1.

The decay of the transverse component of the magnetization Mxy is termed T2 relaxation, or spin-spin dephasing. T2 relaxation is a consequence of the fact that the individual hydrogen nuclei that comprise the net magnetization are all located in distinct chemical environments with different neighbouring atoms. Each individual hydrogen nucleus will therefore experience a slightly different local magnetic field, causing the precessional frequencies to vary. This variation will cause the individual hydrogen nuclei to become progressively more out of phase, and result in a decreasing Mxy. T2 contrast can be manipulated in the MR image by changing the time to echo (TE), which defines how long after the RF pulse the signal will be acquired.

The re-growth of the longitudinal magnetization is termed T1 or spin-lattice relaxation. During this process the nuclei will transfer the energy absorbed during excitation back to the lattice. The efficiency of this process depends on how well the precession frequency of the magnetization matches the frequency of motion of spins in the lattice. T1 contrast may be manipulated in the

images by varying the repetition time (TR), which defines the time between successive RF pulses.

Spatial localisation or encoding is achieved in MRI by applying three mutually orthogonal field gradients at different times during the imaging sequence. Arbitrary orientations of the linear gradients can be achieved through the simultaneous application of fixed-orientation gradients in three axes, X, Y, and Z. The basis of spatial localisation is the fact that the nuclear precession frequency is directly proportional to the magnetic field (eq. 1.1). The gradients induce linearly varying magnetic fields, resulting in spatially encoded precessional frequencies. For example, by applying the gradient during excitation, only spins that match the resonance condition will be excited. In this way an imaging slice is selected. Similarly, by applying the gradient during readout, the location from which signal with a specific frequency originated can be determined, yielding a 'profile' image. In order to produce a topographic image, it is necessary to acquire multiple profile images, so that signal excitation needs to be repeated many times with allowances for relaxation time between excitation. The program that controls the timings and order of the different components of the imaging sequence is termed a pulse sequence.

1.2.2 Pulse Sequences

An MR pulse sequence diagram is a simple way of showing how the RF and gradients are applied during an acquisition. The vertical axis represents amplitude and the horizontal axis is time. Enormous numbers of pulse sequences have been developed, each with its own application. Some of the most widely used sequences for diffusion imaging are described briefly below (McRobbie et al., 2007).

Gradient Echo (GE)

The gradient echo (GE) sequence is the most basic MRI sequence. It comprises a series of excitation pulses that are each separated by a repetition time TR. Data is acquired at a specific time after the application of the excitation pulse and this is defined as the echo time TE. TE is defined as the time between the mid-point of the excitation pulse and the mid-point of the data acquisition window. The contrast in the image will vary with changes to both TR and TE. GE is suitable for fast imaging due to the low flip angles that can be used, facilitating ultra-short TR's.

The disadvantages of this sequence are difficulty to generate good T_2 contrast, sensitivity to B_0 inhomogeneities and sensitivity to changes in susceptibility. Figure 1.1 shows the basic elements of the standard gradient echo sequence.

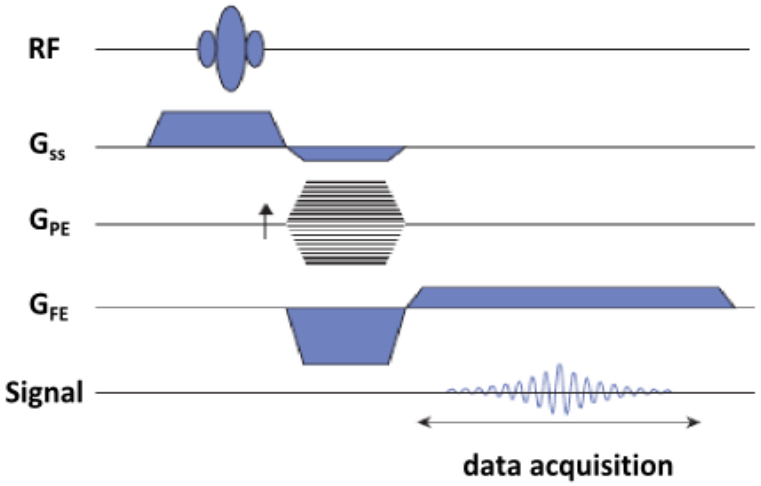

Figure 1.1: The basic elements of the gradient echo MR imaging sequence. Amplitude is shown vertically, time horizontally. RF is the excitation pulse, G_{ss} is the slice selective gradient, G_{PE} is the phase encoding gradient, G_{FE} is the frequency encoding gradient. The sequence is repeated for many different values of G_{PE}.

Spin Echo (SE)

The SE sequence is similar to the GE sequence with the exception that there is an additional 180^o refocusing pulse present. The additional 180^o pulse is placed exactly halfway between the excitation pulse and the echo (Fig. 1.2). The 180^o pulse is usually applied in conjunction with a slice selective gradient in the Z direction. The advantages of this sequence are high signal-to-noise ratio (SNR), true T2 weighting, and relative insensitivity to the effects of B0 inhomogeneity. The major disadvantage is longer scan time.

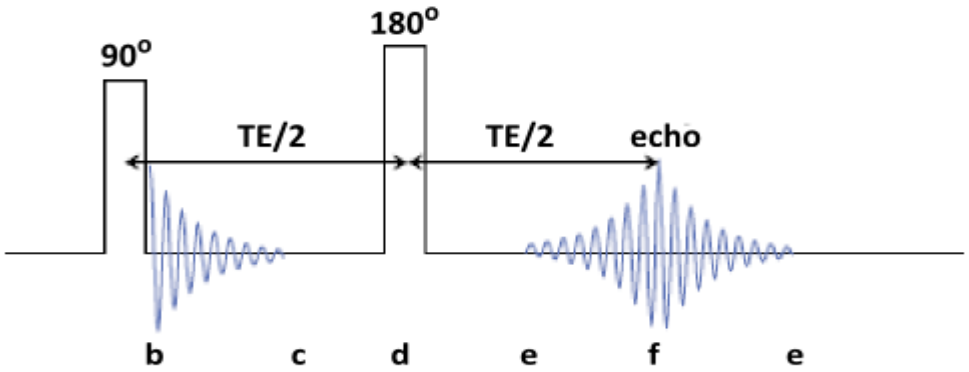

Figure 1.2: Spin-echo sequence with the 180° refocused RF pulse. Following the RF pulse, the spins are initially in phase (b) but dephase during the period labeled (c). At time (d), a 180° pulse is applied. During period (e) the spins recover their phase. The signal is maximal at (f) whereafter the spins again dephase.

Crusher Gradients

When a shaped RF pulse is applied together with a field gradient (Fig 1.1) it is called a selective RF pulse. Selective slices are not uniform in the selection direction, but have a variation in flip angle perpendicular to the image plane. As a result there will generally be signal from regions with unwanted magnetization included in the FID signal.

For the 180° refocusing pulse a pair of 'crusher' gradients can be used to eliminate any unwanted magnetization. These two gradients are equal in size and they are placed on either side of the refocusing pulse. The refocused magnetization that generates the echo will experience both gradients, and because of refocusing, will remain unaffected. By contrast, the unwanted magnetization produced by an imperfect refocusing pulse will be dephased by the single crusher gradient lobe that it experiences. The possibility of crushers on the readout (X) and phase encoding (Y) directions also exists. Figure 1.3 shows the spin echo sequence with the crusher gradients placed on both sides of the 180° RF pulse (i.e. in the Z-direction only).

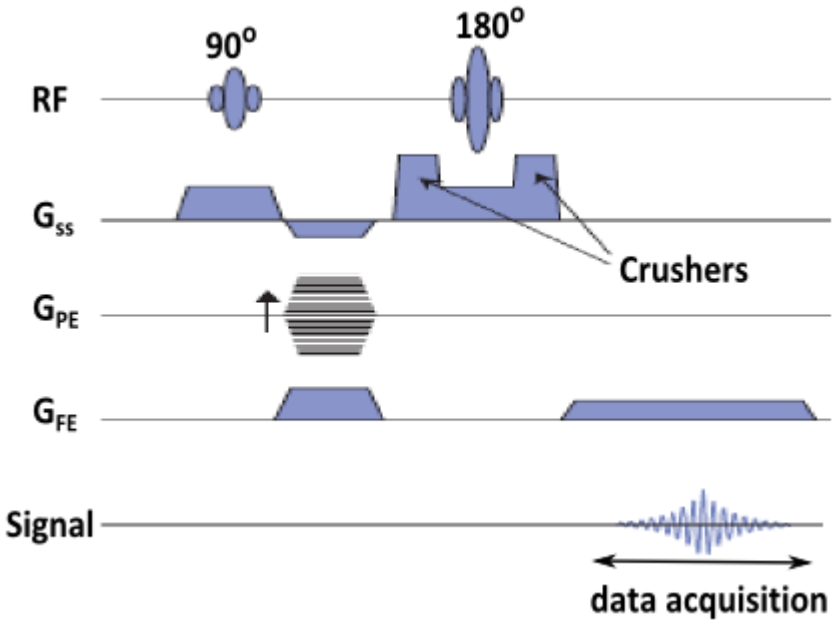

Figure 1.3: The spin-echo pulse sequence with the crusher gradients on both sides of the 180° refocusing RF pulse. The crusher gradients are used to dephase the unwanted magnetization (FID signal) created by the refocusing pulse.

Echo Planar Imaging (EPI)

For both the GE and SE sequences, the entire sequence needs to be repeated for a series of phase encoding steps in order to generate the whole image. This increases the scan time and also renders the data subject to motion artifacts. Echo planar imaging (EPI) is one of the fastest acquisitions in MRI. Single-shot EPI fills the entire k-space matrix in a zig-zag fashion after a single excitation. Each image can be acquired in less than 100 ms, albeit with low spatial resolution. Since a slice is imaged in a single shot, motion is effectively frozen during the acquisition. EPI is now the gold standard for clinical diffusion MRI (Le Bihan et al., 2006). Depending on how the phase-encoding gradient is applied, the EPI can be either blipped or unblipped. In blipped EPI, which is used in the current DTI sequence, a small phase-encoding gradient 'blip' is placed at each readout gradient reversal. This blip is of constant size and adds further phase encoding to the previous blip making the acquisition easier and quicker. While in the unblipped EPI, a constant phase-encode gradient is continuously used during the oscillating read out gradient (Fig. 4b).

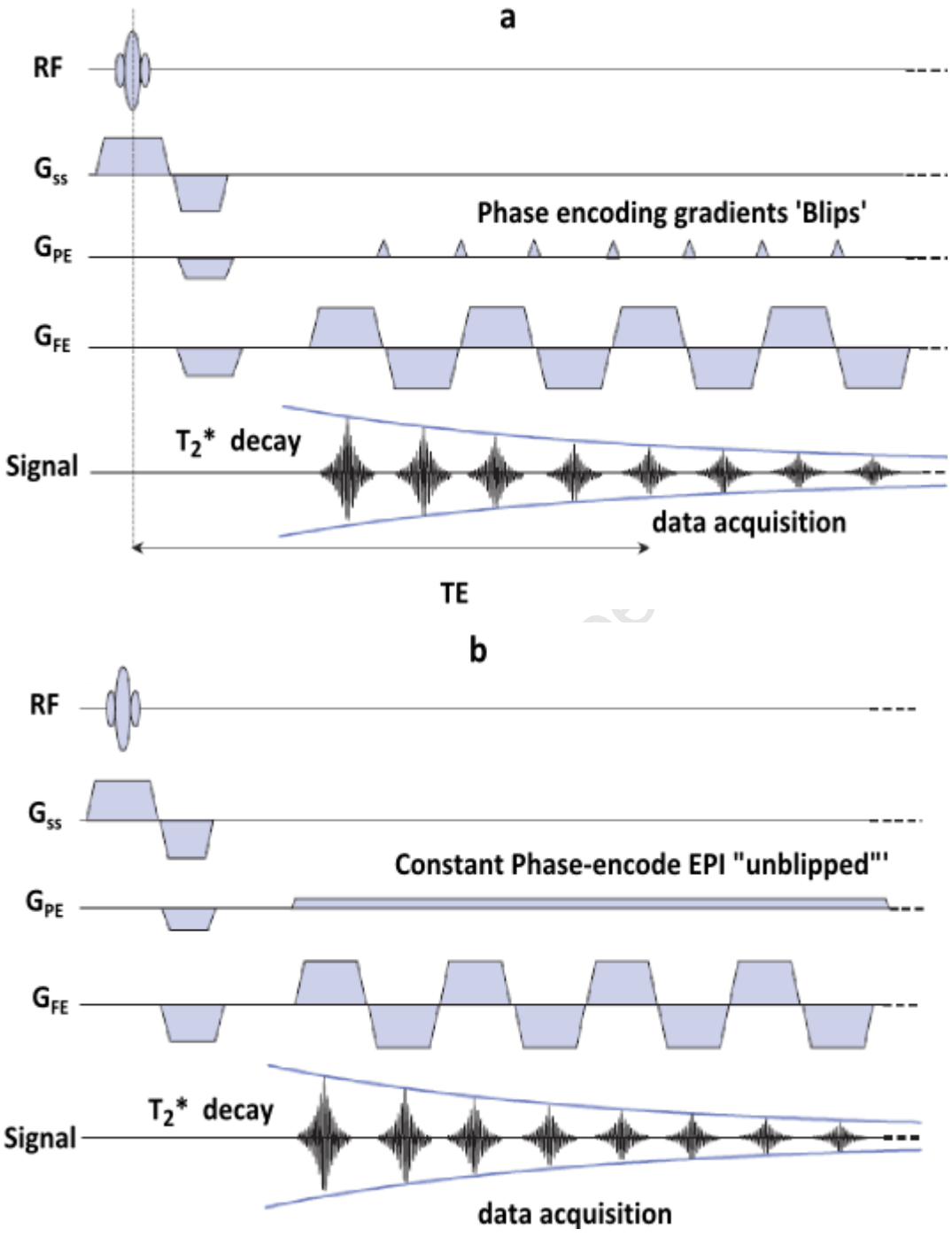

Figure 1.4: (a) In a 'Blipped' single-shot GE-EPI sequence a small phase-encoding gradient 'blip' is placed at each readout gradient reversal; (b) In a 'Unblipped' single-shot GE-EPI a constant phase-encode is applied continuously along the readout gradient reversal. In both modalities the whole image is acquired following a single excitation.

There are several drawbacks to EPI acquisition; among these are the N/2 ghost and the high sensitivity to chemical shift artifacts; i.e. fat-shift, in the phase-encoding direction, due to the comparatively low bandwidth in that orientation (Nagy and Weiskopf, 2008). For these reasons, effective fat suppression and phase correction are important factors in EPI.

Fat Suppression

Hydrogen in fat has a lower Larmor frequency than hydrogen in water and this difference is called the chemical shift. It is approximately 3.5 ppm. In order to improve fat/water soft-tissue contrast it is often useful to 'null' or suppress the signal from the fat.

Several methods have been developed to achieve fat suppression. Most of these rely on either relaxation time differences between water and fat or differences in the resonant frequencies of fat and water (chemical shift). The latter was used in the current DTI pulse sequence. This method exploits the chemical shift between fat and water to initially excite only the fat protons. A narrow range of RF frequencies centred on the Larmor frequency of fat is used to flip the hydrogen nuclei in fat through 90^{o}, leaving the water protons unexcited. This is known as the CHEmical Shift Selective (CHESS) pulse sequence. Crusher gradients are applied immediately after the CHESS pulse to dephase the transverse fat magnetization (Fig. 1.5). Since there is no remaining net magnetization from fat, fat will not contribute to the signal generated by the subsequent imaging sequence.

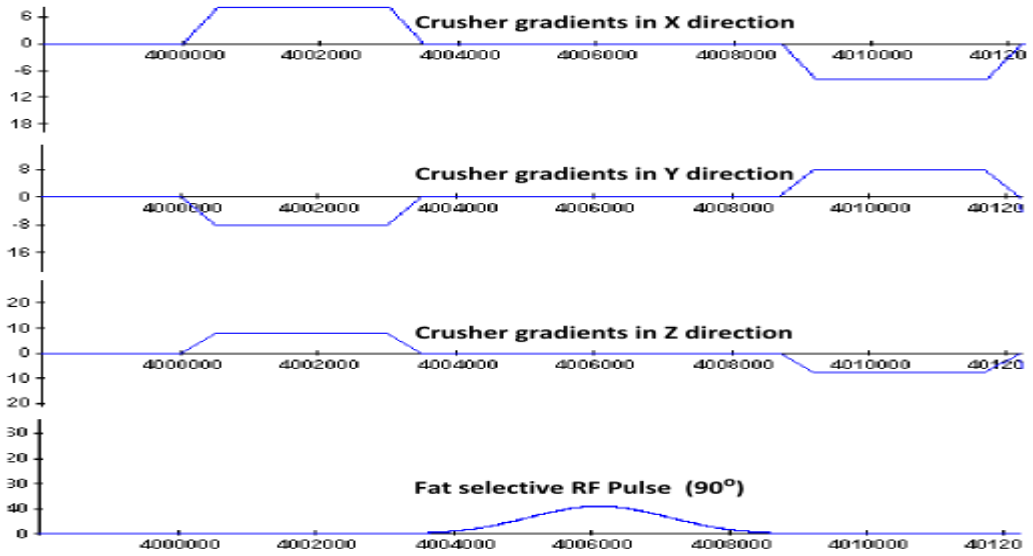

Figure 1.5: CHESS (CHEmical Shift Selective) sequence diagram. The x axis is the time in μs, the y axis is the magnitude. From top to bottom, the crusher gradients are applied in all three directions, X,Y and Z, respectively. The bottom trace illustrates the timing of the fat selective (CHESS) RF pulse. The crushers are used to destroy the phase coherence of transverse fat magnetization. This diagram was generated by the Sequence Development Environment Software (IDEA) provided by Siemens by simulating the DTI pulse sequence.

Phase Correction

Another serious artifact that is associated with EPI is the N/2 ghost. This ghost occurs because of cumulative phase differences between odd and even echoes over the echo train caused by eddy currents from the rapidly switching readout gradients. Phase correction can be achieved from a reference scan that is identical to a full scan but without the phase encoding gradient.

1.2.3 Diffusion

Diffusion is defined as the random movement of gas or liquid molecules through thermal agitation as a function of temperature above 0 Kelvin. In pure water, collisions between molecules cause random movement without any preferred direction, this is known as Brownian motion (Brown R., 1828). Over time, this random "walk" process produces net displacement. These displacements are randomly distributed when considering large molecular populations (Le Bihan et al., 1991). The probability that a molecule travels a distance *r* during a time interval *t* can be estimated. When the molecules move equally and freely in all directions, the diffusion is referred to as having a Gaussian distribution with zero mean, because the probability of

movement in one direction is the same as movement in any other direction. The variance of the distance travelled in all three dimensions is proportional to the time interval *t*, according to the so-called Einstein equation (equation 1.4).

$$\left\langle r^2 \right\rangle = 6Dt \tag{1.4}$$

D is known as the diffusion coefficient and characterizes the mobility of molecules within, and relative to, the diffusion medium which is expressed in $mm^2\ s^{-1}$. Fick's law demonstrates that diffusion also occurs from a region of higher concentration to a region of lower concentration. In biological tissue, there is a high probability that water molecules interact with structures such as cell membranes and macromolecules that reduce or impede their motion. Water exchange between intercellular and extracellular compartments, as well as the shape of extracellular space and tissue cellularity, affects diffusion. The term apparent diffusion coefficient (ADC) represents the measured diffusion constants in tissues and is commonly reported in units of $cm^2\ s^{-1}$ or $mm^2\ s^{-1}$. In the human brain, random translational diffusion of water molecules can be either isotropic or anisotropic. Isotropic diffusion occurs when there is no preferred direction for molecular motion such as in CSF and gray matter. In this case, the measured apparent diffusivity is largely independent of the orientation of the tissue at the voxel length scale and it is usually sufficient to describe the diffusion characteristics with a single (scalar) apparent diffusion coefficient (*ADC*). Anisotropic diffusion occurs when water molecules diffuse more along certain directions in comparison to others. In brain white matter fibers the presence of cellular membranes and the surrounding myelin sheaths hinder the motion of water molecules perpendicular to the fibers. In this case, the measured apparent axial diffusivity (parallel to tracts) is higher than radial diffusivity (perpendicular to tracts).

1.2.4 Diffusion Weighted Imaging (DWI) Pulse Sequence

All MRI pulse sequences are, to some extent, sensitive to diffusion, but it is not possible to produce a measurable signal attenuation that reflects the diffusion directly. To make MRI pulse sequences sensitive to the diffusion of water molecules, additional gradient pulses are introduced. A significant improvement in diffusion measurements was observed when a single spin echo sequence incorporating very large but short diffusion gradients (hundreds of gauss per centimetre during a few milliseconds) was introduced by Stejskal and Tanner (1965). The gradient pulses are placed on each side of the 180^o spin echo refocusing pulse (Fig 1.6) and are

balanced for "static" spins. Signal attenuation due to residual ***B***0 field inhomogeneities become negligible in comparison with the signal loss that occurs in moving molecules as a result of dephasing due to the large diffusion gradients This allows accurate measurements of very small diffusion coefficients (Le Bihan et al., 1991).

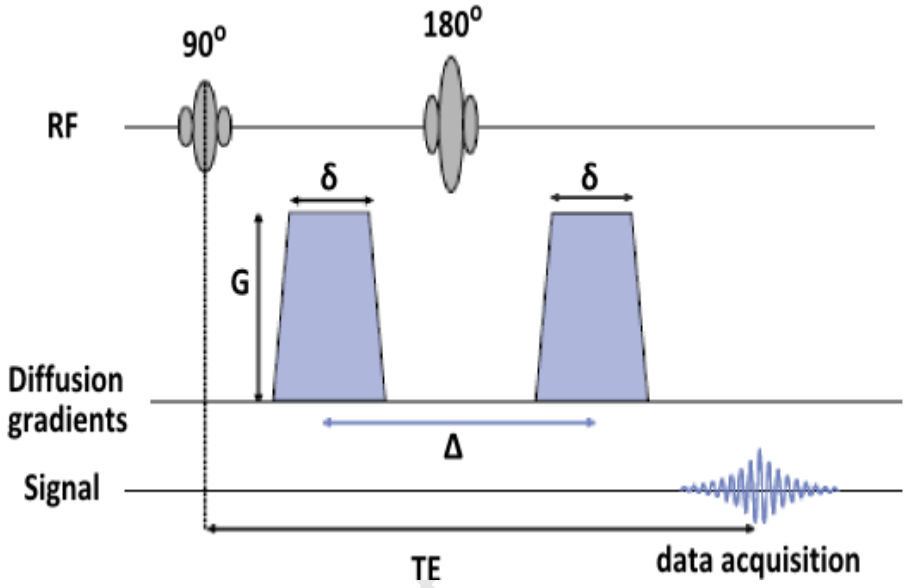

Figure 1.6: Illustration of the main components of the Stejskal and Tanner spin echo diffusion sequence that is designed to measure the diffusion coefficient along the direction of the diffusion gradient. δ is the duration of the diffusion gradient, Δ is the center-to-center spacing, and G is the magnitude of the diffusion gradient in mT/m. Other sequence elements were omitted for clarity.

The effect of the diffusion gradient pulses is to induce a spatially-dependent phase shift in each excited nucleus. The phase shift is proportional to the magnetic field. As such, for stationary spins, the second gradient lobe will rephase the spins that were dephased by the first gradient lobe. For spins that have moved between the application of the two gradient lobes, there will be a net phase shift proportional to the distance travelled. This phase shift results in signal attenuation and is given by equation (1.5).

$$S = S_0 \exp(-b.ADC) \qquad (1.5)$$

where S_0 is the signal intensity without diffusion weighting (termed the b_0 image), S is the attenuated signal, b is a measure of the diffusion weighting (DW), and ADC is the apparent

diffusion coefficient. The factor *b* depends on the strength, duration, and interval between the diffusion gradients and is given by equation (1.6).

$$b = \gamma^2 * G^2 * \delta^2 (\Delta - \delta / 3) \quad (1.6)$$

In equation (1.6), γ is the gyromagnetic ratio for hydrogen, *G* is the strength of the diffusion gradient pulse in mT/m, δ is the duration of the pulse, and Δ is the center-to-center spacing. (Δ-δ/3) is known as the diffusion time *t* and is related to molecular motion through the Einstein equation (1.4). To extract information about the diffusion properties of a particular voxel, the diffusion coefficient (ADC) is calculated by rearranging equation (1.5). To obtain an image of ADC values at least two acquisitions are necessary. Since diffusion is directional, three orthogonal measurements are often performed and the images averaged to produce an image with isotropic diffusion weighting (Wong et al., 1995; Mori and Zijl, 1995; Jones et al., 1999).

Due to the long diffusion encoding period, diffusion imaging is highly sensitive to motion artefacts. Since diffusion MRI aims to calculate the diffusion of water over distances on the order of tens of micron, any bulk motion (such as subject motion) or even involuntary physiological motion (such as cardiac pulsation) can significantly degrade the image quality. If diffusion weighted imaging (DWI) data is obtained using traditional multi-shot image acquisition strategies such as GE or SE sequences, each acquisition (TR) will have a unique phase shift due to motion between diffusion gradient lobes. This introduces a significant ghost in the reconstructed image along the phase encoding direction (Fig. 1.7). For this reason, it becomes necessary to use single-shot acquisition echo planar imaging (EPI) or navigator phase correction for in vivo DW-MRI.

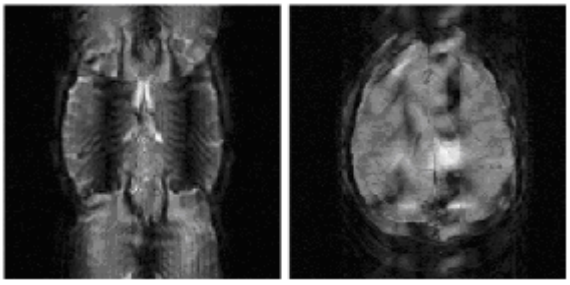

Figure 1.7: Typical motion artefact: ghost and signal variation across diffusion images (Le Bihan et al., 2006).

The diffusion gradient pulse is relatively strong causing a sizeable eddy current to be generated in the diffusion gradient coils. This eddy current produces a geometric distortion in the diffusion

images (Fig. 1.8). Several diffusion-weighting preparations have been proposed in the past that aim to reduce the effective eddy currents during data acquisition by incorporating additional gradient lobes, often in combination with extra RF pulses. These additional gradient lobes cause their own eddy currents, but their polarities and durations are adjusted to reduce the cumulative eddy current effect of all gradient pulses involved. The twice-refocused spin echo (TRSE) pulse sequence (Reese et al., 2003) successfully reduces the cumulative eddy current effect by adjusting the timings of the gradient lobes (Fig. 1.9), at the expense of increased echo time, and hence somewhat decreased SNR.

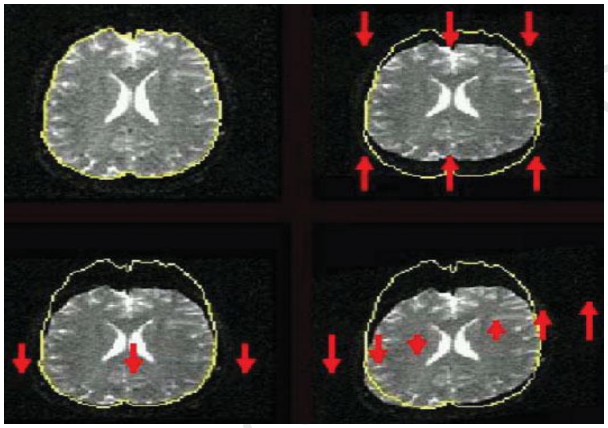

Figure 1.8: Images showing geometrical distortions resulting from eddy currents that are associated with the use of strong diffusion gradients: contraction (top right), shift (bottom left), and shear in the bottom right (Le Bihan et al., 2006).

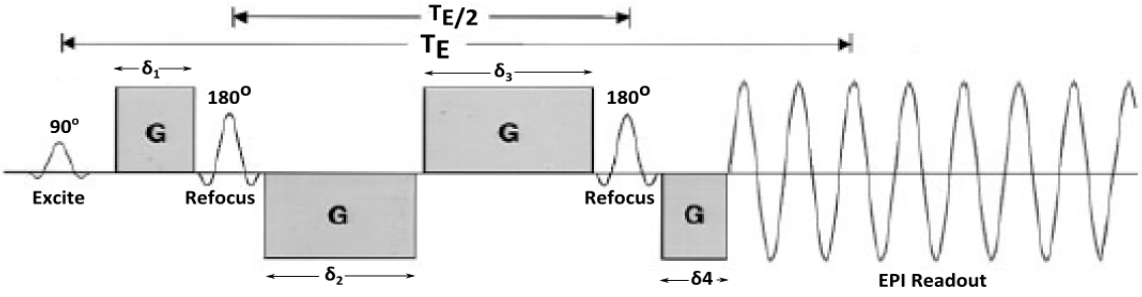

Figure 1.9: Diagram of the standard twice-refocused spin echo (TRSE) sequence that successfully reduces the effect of eddy currents (Reese et al., 2003). Shown are the 90° RF pulse for excitation and the two 180° refocusing RF pulses. G is the strength of the diffusion gradients. The duration of the diffusion gradients are δ_1, δ_2, δ_3, and δ_4, respectively, and the data is acquired using an EPI readout. Other sequence elements were omitted for clarity.

1.2.5 Elements of a DWI sequence

In diffusion imaging many of the sequence elements that were discussed in preceding sections are used in combination to overcome different obstacles that are associated either with the diffusion gradients or with EPI. Figure 1.10 illustrates how these different elements are used in a DWI sequence. The DWI sequence employs a CHESS pulse to perform fat suppression (a in Fig. 1.10), an extra readout to correct for phase differences between even and odd echo's in the EPI readout (b in Fig. 1.10), crusher gradients that are placed on both sides of the two 180^{o} refocusing RF pulses to destroy unwanted magnetization that arises from the refocusing pulses (c in Fig. 1.10), two 180^{o} RF refocusing pulses to overcome ***B***0 inhomogeneity (d in Fig. 1.10), and diffusion gradients implemented using the twice-refocused technique to overcome eddy current effects (e in Fig. 1.10). The EPI readout with blipped phase encoding is indicated by f in figure 1.10.

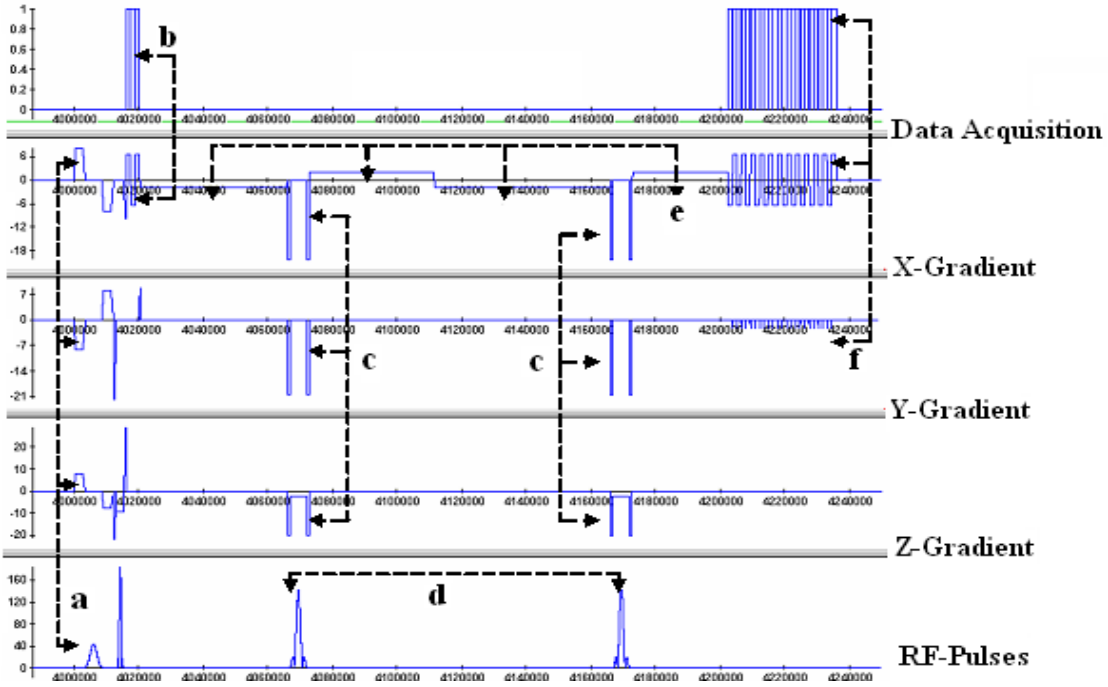

Figure 1.10: Illustration of the sequence elements of the single-shot DTI pulse sequence used in the current study. The elements are (a) the CHESS pulse, (b) additional readout for phase correction, (c) the crusher gradients, (d) two 180^{o} refocusing pulses, (e) diffusion gradients implemented using the twice-refocused pulse technique. The elements of the blipped EPI readout are indicated by f. The x axis represents the time and the y axis represents the magnitude of the different components. This diagram was generated by the Sequence Development Environment Software (IDEA) provided by Siemens by simulating the DTI pulse sequence.

1.3 Diffusion Tensor Imaging (DTI)

1.3.1 From DWI to DTI

As already mentioned, diffusion in the brain white matter is not the same along every direction due to the presence of natural barriers. In white matter the principal barrier to diffusion is the myelin sheaths of axons. Bundles of axons, known as fiber tracts, run in parallel creating an environment in which water diffuses more along the length of the nerve fibers than in directions perpendicular to them. Diffusion Tensor Imaging 'DTI' (Basser et al., 1994), which is an extension of diffusion MRI, exploits the anisotropic properties of diffusion in white matter to map the white matter tracts in the brain. A *single apparent diffusion coefficient* can no longer be used to characterize the anisotropic diffusion. The diffusion coefficient D or ADC is now represented by a *second rank tensor* $\underline{D}$ (1.7) defined by

$$\underline{D} = \begin{pmatrix} D_{xx} & D_{xy} & D_{xz} \\ D_{yx} & D_{yy} & D_{yz} \\ D_{zx} & D_{zy} & D_{zz} \end{pmatrix} \qquad 1.7$$

Since the tensor is symmetric (i.e. $D_{yx}=D_{xy}$, $D_{zx}=D_{xz}$, and $D_{zy}=D_{yz}$), the diffusion tensor can be calculated from a minimum of 6 diffusion-weighted volume images each with diffusion weighting applied along a different direction.

In each voxel of the image it is important to determine the principal directions of diffusion, called eigenvectors, and the diffusion values, called eigenvalues. When the diffusion tensor $\underline{D}$ is fully diagonalized and the covariance between displacements in orthogonal directions is zero, the diagonal elements of the tensor are equal to the eigenvalues λ_1, λ_2, and λ_3. Many parameters can be derived from the eigenvalues, in particular fractional anisotropy (FA) and mean diffusivity (MD). FA is one of the most widely used parameters derived from DTI acquisitions (Pierpaoli and Basser, 1996) and provides information about the microstructural integrity of highly oriented microstructures. FA is defined in equation (1.8) and MD in equation (1.9).

$$FA = \frac{\sqrt{(\lambda_1 - \lambda_2)^2 + (\lambda_1 - \lambda_3)^2 + (\lambda_2 - \lambda_3)^2}}{\sqrt{2(\lambda_1^2 + \lambda_2^2 + \lambda_3^2)}} \quad \text{, and} \tag{1.8}$$

$$MD = \frac{(\lambda_1 + \lambda_2 + \lambda_3)}{3} \tag{1.9}$$

Diffusion is considered isotropic if the three eigenvalues are equal, and anisotropic, if the eigenvalues are different in magnitude. The FA values range from one (absolutely directed diffusion) to zero (completely isotropic diffusion). MD is a measure of average molecular motion independent of any tissue directionality.

The main directions of the diffusivities are exploited in Tractography (Basser et al., 2000) to reconstruct the trajectory of white matter pathways and to derive connectivity among different parts of the brain. There are several software resources that are freely available on the internet for fiber tracking as well as to generate all the diffusion maps, such as Diffusion Toolkit and Trackvis (http://trackvis.org/). Trackvis, which was used in the current work, is based on deterministic tractography. Deterministic tractography relies on the hypothesis that the main eigenvector that corresponds to the highest eigenvalue is parallel to the underlying dominant fiber orientation in each voxel. Based on this assumption, a single pathway along the direction of maximum water diffusivity is propagated.

1.3.2 Effects of Subject Head Motion in DTI

Although echo planar imaging (EPI) has been implemented in the diffusion pulse sequence mainly to minimize the effect of subject motion by acquiring the whole image within a single shot, motion artifacts may reappear in the diffusion volume images when scanning the brain repeatedly with different gradient directions for calculating the diffusion tensor.

Head motion causes misalignment of the diffusion volume images and furthermore, individual voxels are exposed to a slightly different diffusion encoding direction/gradient than the desired one (Aksoy et al., 2008). Motion during diffusion sensitization gradients also causes signal dropouts in the images (Fig. 1.11). Both uncorrected diffusion volumes and errors in diffusion encoding can cause serious artifacts in DTI, which can result in erroneous estimations of the diffusion tensor information such as FA and MD.

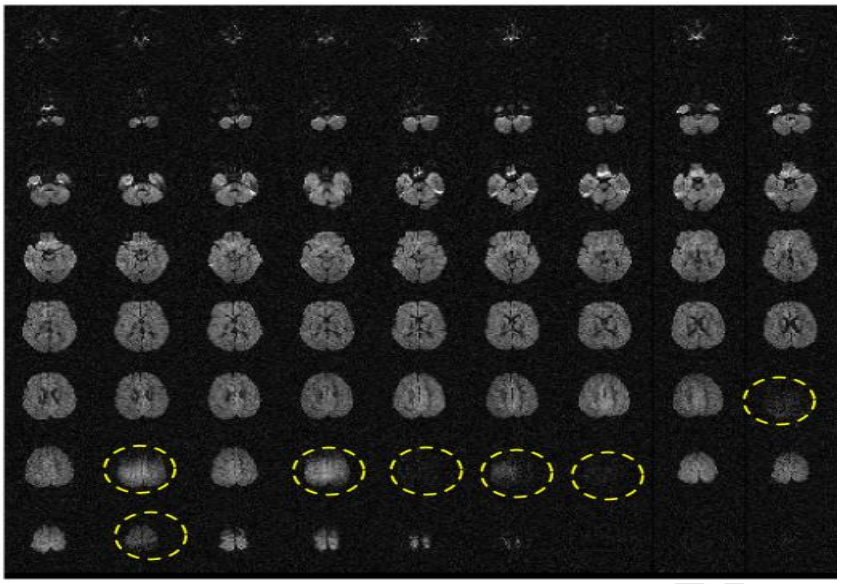

Figure 1.11: Data affected by signal dropouts are indicated by circles. Information for these slices is typically lost, leading to reduced SNR or biased results. The DTI acquisition for this example consisted of 34 measurements or diffusion volumes, each with 72 slices, with a maximum b value of 1000 sec mm^{-2}. The current volume was # 7.

1.3.3 Motion Correction in conventional MRI

Subject movement during MR examination renders MR data inaccurate. Consequently, a range of techniques have been developed to correct human movement that occurs both voluntarily (such as subject head motion) and involuntarily (such as cardiac pulsation). These techniques are able to measure and correct the subject specific frame of reference to varying degrees during a scan. A variety of tools or methods are available to accomplish this. One set of methods requires modifying the pulse sequence to include a navigator. A second method utilizes information inherent in the MRI images themselves, while a third method requires additional hardware and software such as external optical tracking devices and microcoils. We present below a review of these three different approaches to motion correction in MRI.

Navigator Techniques in MRI

Ehman and Felmlee (1989) first suggested that a navigator could be used with interleaved excitation to produce a one dimensional (1D) projection of a plane. The 1D displacement along the readout direction could then be determined by using an image space cross-correlation or k-

space phase roll. 1D navigators are widely used in cardiac MRI to track the motion of the right hemi-diaphragm or the heart directly in order to correct for respiratory motion.

Subsequently, orbital navigators were developed by Fu et al. (1995). Their aim was to sample a circle of k-space at a prescribed radius and plane. Since a rotation is equivalent in k-space and image space, a rotation around the prescribed axis can be measured using cross-correlation of two acquisitions. Out of plane rotation that may occur, however, invalidates the procedures and thereby greatly reduces the efficiency of this method. By combining these two principles, van der Kouwe et al. (2006) developed the clover navigator with 3D k-space traversal, measuring three orthogonal arcs and three orthogonal lines through the centre of k-space. By co-registering the clover navigator to a reference map, one can solve the six degrees of freedom in a rigid body transformation completely. Welch et al. (2002) proposed a different method that measures all six degrees of freedom by fully sampling a sphere of k-space. Rotations are estimated from sphere to sphere co-registration and translations from the linear phase roll between each navigator acquisition.

Although the previous navigators were very fast, imaging navigators with small flip angles have been proposed for situations where there is a long preparation time before the start of the next RF excitation pulse. Interference with the magnetization relaxation process is avoided by using a very small flip angle of the order of 2 to 8 degrees. Spectroscopy and Magnetization Prepared Rapid Gradient Echo (MPRAGE) sequences (Mugler and Brookeman, 1990) have been modified in this way to generate a complete image or set of images during the magnetization recovery/preparation time. Two previously reported imaging navigators include PROspective MOtion (PROMO) and a 3D EPI volumetric navigator (vNav). PROMO proposed by White et al. (2010) uses spiral imaging for the acquisition of three orthogonal images that are then co-registered to a map of such spiral images. In order to achieve sufficient accuracy and stability PROMO acquires a set of five navigators every 100 ms in imaging applications or five every 300 ms in Single Voxel Spectroscopy (SVS). The 3D EPI imaging navigator has been implemented to correct for motion in SVS by Hess et al. (2011) and in a multiecho MPRAGE sequence by Tisdall et al. (2011). This method acquires a complete three dimensional low-resolution EPI navigator within each TR.

Methods that use Information Inherent in the Images

Motion correction can also be achieved using information inherent in the MRI acquisition itself. One such method termed Periodically Rotated Overlapping ParallEL Lines with Enhanced Reconstruction (PROPELLER) (Pipe, 1999) acquires data in k-space in strips of parallel lines, where the lines acquired are the lowest phase-encoded lines in any Cartesian-based collection scheme. These strips are acquired for many different directions so that the centre of k-space is oversampled, yielding a propeller-like sampling pattern. The strips acquired in the centre portion of k-space for each of the acquisitions are used to construct low-resolution images that can be used to correct in-plane translation and phase errors. PROPELLER requires increased scan time and provides limited information at the corners of k-space.

Thesen et al. (2000) developed a Prospective Acquisition CorrEction (PACE) technique for functional MRI (fMRI). In fMRI multiple complete image volumes are acquired in rapid succession, approximately every 1 s to 3 s. Each successive measurement can be registered to the first volume using image volume based registration (Friston et al., 1995).

Additional Hardware for Motion correction

While most of the previous techniques require adding a 'navigator' acquisition to the pulse sequence or a specific strategy for data collection and acquisition, an alternative approach is to use optical tracking devices. This can be achieved using equipment ancillary and external to the MRI scanner namely, such as stereo cameras (Qin et al., 2009; Zaitsev et al., 2006), retrograde reflectors with a single camera (Zaitsev et al., 2010a), or laser positioning of retro reflectors (Eviatar et al., 1999). Cameras or lasers need to be firmly fixed inside the MR area onto the head coil (Qin et al., 2009) or outside the scanner bore (Eviatar et al., 1999; Zaitsev et al., 2010a; Zaitsev et al., 2006) and must be in line of sight of a specific marker or set of markers that are affixed to the head of the subject. These systems are costly and awkward to set up due to the presence of additional hardware and the adjuncts to the subject's head. Moreover the practicality of these systems is hindered by the head coil which affects the field view available, as well as the actual space limitations of an MR environment.

Microcoils or locator coils (Derbyshire et al., 1998; Ooi et al., 2009) are active markers that determine the position and orientation of the head by affixing three microcoils to the

subject's head. These microcoils are tuned to receive the MR signal from a water-filled bead within the coil.

1.3.4 Navigator Techniques in Diffusion MRI

The navigator echo technique was implemented in diffusion imaging by Ordidge et al. (1994) to correct for subject motion even before the invention of fast imaging. They inserted a one-dimensional navigator in the readout direction in a conventional 2DFT pulsed gradient spin-echo (PGSE) sequence. The variations of the navigator echo phase from one view to another were used to correct phase errors induced by translational motion in 2DFT. An improvement to the 'navigator echo' technique, which allowed correction not only for translation but also for rotation of the measured object, was implemented by Anderson and Gore (1994) and De Crespingy et al. (1995).

In these early navigator methods the 'navigator echo' was implemented in only one dimension (e.g. in readout direction), which caused a lack of rotational motion correction in other dimensions. This can be overcome by acquiring a second navigator echo in the phase-encoding direction. A 2D spiral navigator was proposed by Butts et al. (1997) in an interleaved echo-planar imaging (IEPI) sequence. The information from the navigator, which consisted of the constant and linear phase shifts across the head in both the x and y directions, was used to regrid the image data in k-space. A 2D Cartesian navigator echo was used in DW-IEPI (Atkinson et al., 2000) to correct for offsets of the diffusion images in k-space. In this technique, the scan was repeated four times to avoid violation of the Nyquist condition.

To overcome the many obstacles relating to post-acquisition correction, the first online motion correction in DWI was proposed by Norris et al., (2001). They used two orthogonal in-plane navigator echoes, one in the readout and the second in the phase encoding direction. These navigators were inserted before the readout gradients, meaning that they were affected by the diffusion contrast. Following the acquisition of the navigator echoes, the zeroth and first-order phase corrections were applied in less than 8 ms using the B(0) coil for the zeroth phase error and the appropriate magnetic field gradient pulses for the first order error.

Another approach to motion correction was to use information inherent in the MRI acquisition to calculate motion correction parameters. The 2D Periodically Rotated Overlapping ParallEL Lines with Enhanced Reconstruction (PROPELLER) method has also been

implemented in diffusion imaging (Pipe et al., 2002). In this method the centre portion of k-space, which is acquired on each strip, is used to remove some of the in-plane motion and reject some artifacts from through-plane motion. As with the previous navigators, motion correction with PROPELLER is affected by the diffusion weightings and is also limited to specific types of image acquisition.

1.3.5 Motion Correction in DTI

Retrospective motion correction has been the standard approach to correct for misalignment of diffusion volume images in DTI. Retrospective motion correction basically tries to align each diffusion volume to a target volume image, which is usually the first volume with no diffusion sensitization (the b0 volume image) since it has less distortion and higher SNR compared to the DW images. Following retrospective correction, each voxel is assumed to correspond to the same anatomical location in all diffusion volumes. The goodness of the match or alignment between the images is based on a cost function that is maximized or minimized using some optimization algorithm. Cost functions that are commonly used in image registration in MRI include cross-correlation, mutual information, and mean-squared difference. Mutual information (MI), which is a measure of statistical dependency between two data sets, is particularly suited to registration of images from different modalities and not just a single image type (Maes et al., 1997; Studholme et al., 1997). Several tools are available freely online to perform retrospective motion correction of diffusion volume images, such as FLIRT in FSL (FMRIB Software Library; http://www.fmrib.ox.ac.uk/fsl) and statistical parametric mapping (SPM).

Subject head motion does not only cause misalignment of diffusion volume images but the imaged subject will also be exposed to a different diffusion encoding gradient during motion. The correction of the b matrix is carried out by reorienting the b matrix to the correct diffusion encoding gradient either retrospectively (Rohde et al. 2004; Leemans and Jones, 2009) or prospectively (Benner et al., 2010; Kober et al., 2011; Alhamud et al., 2012)

Retrospective techniques have many limitations in the co-registration of conventional MR images, including blurring artifacts (Tong and Cox, 1999) and the influence of through-plane motion on the local history of magnetization (Muresan et al., 2005). Retrospective techniques face even greater difficulties in diffusion weighted imaging (DWI), particularly with high b-

value diffusion weighting. A robust retrospective method has been implemented by Rohde et al. (2004), in which mutual information is used to correct for the misalignment in the diffusion volume images as well as to reorient for each b matrix. The authors stated that: "This method may not be able to correctly register diffusion volumes acquired with diffusion weightings greater than 1100 s mm-2 due to the fact that most of the tissue/air boundaries, which are some of the main features that guide the image registration process, are nearly eliminated at high b-values".

Prospective motion correction has been proposed to address the problems associated with retrospective motion correction in DTI. Three studies have reported real-time motion correction in DTI. The optical system reported by Aksoy et al. (2011) uses a camera and markers. The requirement for specialized hardware and software that are not standard components of the scanner, is limiting. The second method or diffusion-weighted prospective acquisition correction (DW-PACE) was implemented by Benner et al. (2010) to correct misalignment in diffusion data. DW-PACE is based on registering the diffusion volumes in real time to the first reference volume that has the same diffusion weighting using the prospective acquisition correction (PACE) algorithm for estimating motion parameters (Thesen et al., 2000). DW-PACE requires sufficient signal-to-noise ratio (SNR) in the diffusion images for accurate image co-registration, which limits the application to low diffusion weightings, thus precluding applications such as q-space imaging (Assaf and Cohen, 1999), Q-ball imaging (Tuch et al., 2003), and diffusion spectrum imaging (Wedeen et al., 2005). The third method proposed by Kober et al. (2011) detects motion by performing a volume-wise comparison of the signal measured using a free induction decay (FID) navigator that is inserted after the slice rewinder gradient. While the authors report high sensitivity and specificity in detecting motion, the major disadvantage of this method is that the navigator contains no anatomical information, so that an extra b0 acquisition, two to allow time for feedback in the case of prospective motion correction, needs to be acquired each time motion is detected in order to compute the motion parameters, after which the diffusion volume is re-acquired in the updated gradient coordinate system. As such, two (in the case of retrospective correction) to three (for prospective correction) extra TR's are added to the sequence each time motion is detected, which could result in impractical long scan times in young uncooperative subjects that move often. The authors also note increased noise of the FID

navigator using this method at higher b-values, which they attribute to eddy current history effects, and difficulties detecting slow movements.

To address some of the limitations related to retrospective and prospective motion correction methods in DTI and also in order to develop a method that is independent of the diffusion contrast, a separate motion tracking technique has been introduced in this work using a volumetric 3D-EPI navigator (vNav). This work involved modifying the standard twice-refocused spin echo diffusion pulse sequence to acquire an anatomical or imaging navigator following the acquisition of each diffusion volume. The standard diffusion sequence was further modified to include an optional function included in the diffusion protocol for reacquisition of uncorrected diffusion volumes. Figure 1.12 shows an example of the sequence timing diagram for the standard diffusion sequence without the navigators (Fig. 1.12a) and the diffusion sequence with the imaging navigators (8 in this example) inserted between the diffusion volumes (Fig. 1.12b). The navigator adds very little scan time to each measurement (TR_{nav} = 526 ms) relative to the duration of the diffusion volume measurement (TR = 9500 ms).

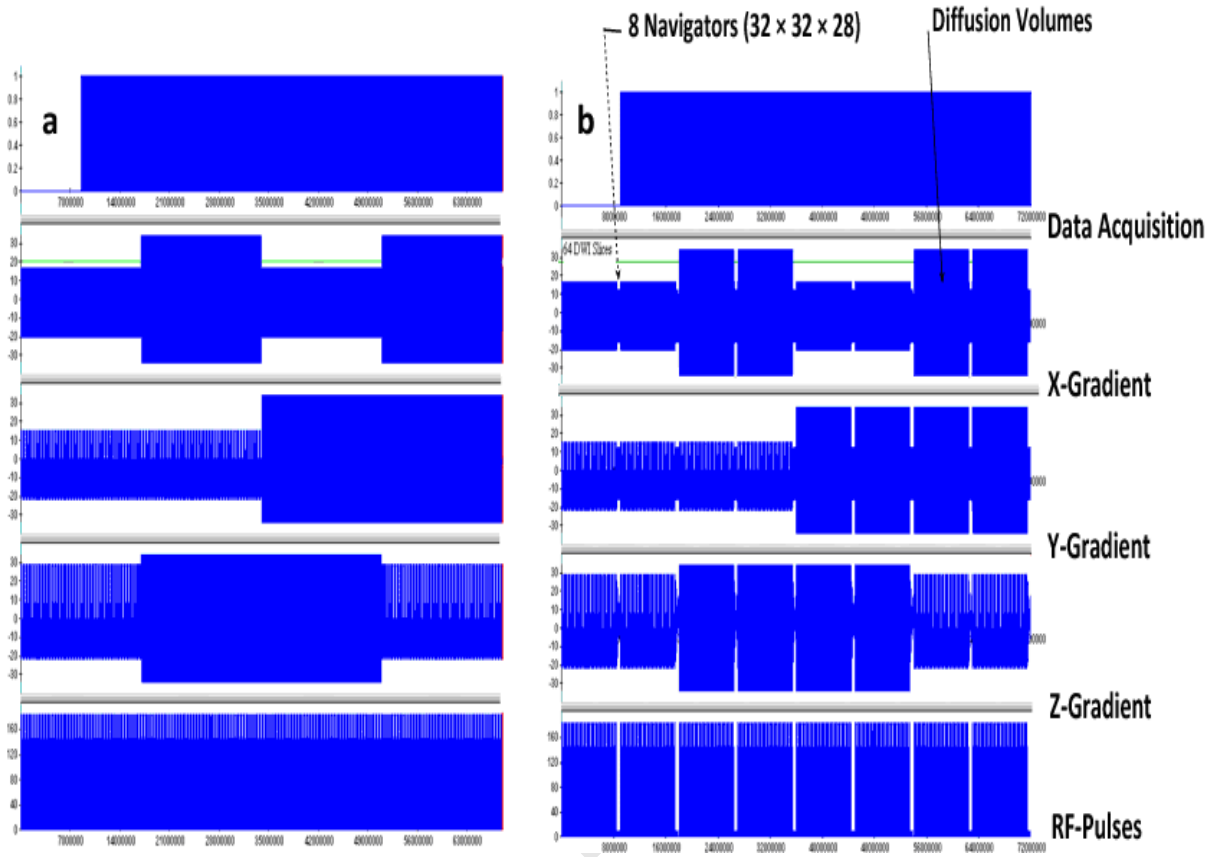

Figure 1.12: Comparison of the sequence timing diagram of the standard diffusion sequence without navigators (a) and the diffusion sequence with navigators inserted between the diffusion volumes (b). The diffusion protocol for this example was: 64 slices for each volume, one dummy scan, 7 diffusion volumes, one b0 volume image, 6 diffusion gradient directions with b value 1000 sec mm^{-2}. The scan time with the standard sequence was ~ 68 sec and with the navigated sequence was ~ 72 sec. The navigator acquisition matrix was 32 × 32 × 28 and the acquisition time for each navigator was 406 ms. The x axis represents the time and the y axis represents the magnitude of the sequence elements. This diagram was generated using the Sequence Development Environment Software (IDEA) provided by Siemens by simulating the DTI pulse sequence. During the timing diagram of the sequence several gradients and RF pulses are applied; excitation and refocusing RF pulses, gradients are applied in different directions X,Y and Z directions, ADC for data acquisition.

Chapter 2

Volumetric Navigators for Real Time Motion Correction in Diffusion Tensor Imaging[a]

A. Alhamud[1], M. Dylan Tisdall[2,3], Aaron T. Hess[1], Khader M. Hasan[4], Ernesta M. Meintjes[1] and André J.W. van der Kouwe[2,3]

[1]MRC/UCT Medical Imaging Research Unit, Department of Human Biology, University of Cape Town, South Africa

[2]Athinoula A. Martinos Center for Biomedical Imaging, MGH, Charlestown, MA, USA

[3]Department of Radiology, Harvard Medical School, Brookline, MA, USA

[4]University of Texas Health Science Center at Houston, TX, USA

[a]Published in Magnetic Resonance In Medicine and reproduced with permission from John Wiley & Sons.

Abstract

Prospective motion correction methods using an optical system, diffusion-weighted prospective acquisition correction, or a free induction decay navigator have recently been applied to correct for motion in diffusion tensor imaging. These methods have some limitations and drawbacks. This article describes a novel technique using a three-dimensional-echo planar imaging navigator, of which the contrast is independent of the *b*-value, to perform prospective motion correction in diffusion weighted images, without having to reacquire volumes during which motion occurred, unless motion exceeded some preset thresholds. Water phantom and human brain data were acquired using the standard and navigated diffusion sequences, and the mean and whole brain histogram of the fractional anisotropy and mean diffusivity were analyzed. Our results show that adding the navigator does not influence the diffusion sequence. With head motion, the whole brain histogram-fractional anisotropy shows a shift toward lower anisotropy with a significant decrease in both the mean fractional anisotropy and the fractional anisotropy histogram peak location ($P < 0.01$), whereas the whole brain histogram-mean diffusivity shows a shift toward higher diffusivity with a significant increase in the mean diffusivity ($P < 0.01$), even after retrospective motion correction. These changes in the mean and the shape of the histograms are recovered substantially in the prospective motion corrected data acquired using the navigated sequence.

2.1 Introduction

Diffusion Tensor Imaging (DTI) provides information that has been widely used in mapping the architecture of the central nervous system (Basser and Pierpaoli, 1996), in studying development and aging (Hasan et al., 2009a; Snook et al., 2005), and in detecting diverse pathological conditions of the human brain due to its ability to identify microstructural abnormalities (Chung et al., 2008). DTI data differ from other imaging modalities in that each voxel contains not only a single value, but a 3×3 positive definite matrix also known as a diffusion tensor (Basser et al.,1994). The diffusion tensor is calculated by scanning a volume of the brain repeatedly: one scan without diffusion sensitization, and the others with diffusion sensitization in non-collinear directions. Head motion causes misalignment of the diffusion volumes and furthermore, individual voxels are exposed to a slightly different diffusion encoding direction/gradient than the desired one (Aksoy et al., 2008). Motion during diffusion

sensitization gradients also causes signal dropouts in the images. Both uncorrected diffusion volumes and errors in diffusion encoding can cause serious artifacts in DTI, which can result in erroneous estimations of the diffusion tensor information. Generally, retrospective motion correction is used to correct for both the misalignment in the diffusion volumes as well as the b matrices. Retrospective techniques have many limitations in the co-registration of conventional MR images, including blurring artifacts (Tong and Cox, 1999) and the influence of through-plane motion on the local history of magnetization (Muresan et al., 2005). Retrospective techniques face greater difficulties with diffusion weighted imaging (DWI), especially diffusion weighting with high b-values. A robust retrospective method has been implemented by Rohde et al. (2004), in which mutual information is used to register the diffusion volumes and correct the b matrix. This method may not be able to correctly register diffusion volumes acquired with diffusion weightings greater than 1100 s mm^{-2} due to the fact that most of the tissue/air boundaries, which are some of the main features that guide the image registration process, are nearly eliminated at high b-values.

To avoid the limitations associated with retrospective motion correction, prospective motion correction in DTI has recently been proposed. Three studies have previously reported real-time motion correction in DTI. The optical system reported by Aksoy et al. (2011) uses a camera and markers. The requirement for specialized hardware and software, which are not standard components of the scanner, is limiting. The second method or diffusion-weighted prospective acquisition correction (DW-PACE) was implemented by Benner et al. (2010) to correct misalignment in diffusion data. DW-PACE is based on registering the diffusion volumes in real time to the first reference volume that has the same diffusion weighting using the prospective acquisition correction (PACE) algorithm for estimating the motion parameters (Thesen et al., 2000). DW-PACE requires sufficient signal-to-noise ratio (SNR) in the diffusion images for accurate image co-registration, which limits the application of DW-PACE to low diffusion weightings, thus precluding applications such as q-space imaging (Assaf and Cohen, 1999), Q-ball imaging (Tuch et al., 2003), and diffusion spectrum imaging (Wedeen et al., 2005). The third method proposed by Kober and colleagues (2011) detects motion by performing a volume-wise comparison of the signal measured using a free induction decay (FID) navigator that is inserted after the slice rewinder gradient. While the authors report high sensitivity and specificity in detecting motion, the major disadvantage of this method is that the navigator

contains no anatomical information, so that an extra b0 acquisition, two to allow time for feedback in the case of prospective motion correction, needs to be acquired each time motion is detected in order to compute the motion parameters, after which the diffusion volume is re-acquired in the updated gradient coordinate system. As such, two (retrospective correction) to three (prospective correction) extra TR's are added to the sequence each time motion is detected, which could result in impractical long scan times in young uncooperative subjects that move often. The authors also note increased noise using this method at higher b-values, which they attribute to eddy current history effects, and difficulties detecting slow movements.

Since most of the current self-navigating methods for motion correction in DTI rely on image contrast, the correction for the misalignment of the diffusion volumes is rendered inaccurate by the changes in the diffusion weighting, especially at high b-values. Navigator-based motion tracking methods typically take advantage of the k-space properties of rigid body transforms to subsample k-space in a time efficient manner. These include orbital (Fu et al., 1995; Ward et al., 2000), spherical (Welch et al., 2002) and cloverleaf (van der Kouwe et al., 2006) navigators. Despite these methods being very fast, imaging navigators, such as PROMO (White et al., 2010) and the echo planar imaging (EPI) volumetric navigator (Hess et al., 2011), are well suited to methods with long repetition times and have been implemented in spectroscopy. To date, imaging navigators have not been applied to DTI.

The current paper presents the first prospective motion correction technique in DTI that (1) uses a volumetric navigator that contains 3D anatomical information for direct computation of motion parameters, and (2) for which the accuracy of co-registration and motion estimates are not affected by the diffusion gradients even at high b-values. Using this method, prospective motion correction is performed without requiring reacquisition of volumes during which motion occurred. The additional scan time for the navigator and feedback is only 526 ms per TR (TR = 9500 ms). If selected in the protocol, reacquisition of volumes will only occur for large motions that exceed some pre-set threshold. In such cases, reacquisition of the motion-corrupted volume is performed in a single TR, thus minimising the extra scan time required. Also, the number of reacquisitions allowed is set at the start of the scan, thus limiting the increase in scan time.

2.2 Materials and Methods

2.2.1 Preparation of the 3D-EPI Navigator Sequence

The navigator is a three-dimensional multishot echo planar imaging (EPI) sequence element, in which a single complete slice of *k*-space is collected with a Cartesian sampling scheme after each excitation. The full navigator consists of a stack of *k*-space slices collected across multiple excitations. The navigator is implemented with a very small flip angle of 2° to minimize the impact of signal saturation on the diffusion sequence. The off-resonance distortions and T_2 blurring effect are relatively insignificant due to the use of a multishot technique, high bandwidth in readout direction 3906 Hz/px, a very short echo spacing time of 310 μs, and a very short TR of 14 ms per shot. The acquisition matrix size is 32 × 32 × 28 (8 mm isotropic) to achieve both a very short scan time and good estimation of motion. The field-of-view (FOV) in all three directions was selected to cover the subject's head. The navigator protocol is prepared and run on the scanner before starting the diffusion sequence. The aim of this process is to check and store the navigator protocol for future use in the modified diffusion sequence. Running the scan triggers the image reconstruction to store the navigator protocol and can be used to confirm that the brain is properly located in the navigator. This preliminary scan takes less than a second to run and once the protocol is saved does not need to be rerun unless the protocol changes.

2.2.2 Diffusion Pulse Sequence with 3D-EPI Navigator

A twice-refocused 2D diffusion pulse sequence (Reese et al., 2003) has been modified to acquire a 3D-EPI navigator following the acquisition of each diffusion volume. The navigator protocol, prepared in a preceding setup scan, is separate from the diffusion protocol. The diffusion sequence is enabled to read two separate protocols at the same time; one for the standard diffusion sequence and the other for the navigator. In order for the diffusion volumes to be spatially aligned in real time, each navigator volume, that follows the diffusion volume, has to be reconstructed and the transformation to a reference volume computed. The first navigator volume is chosen as the reference volume.

Both ICE (image calculation environment) and PACE (prospective acquisition correction) are Siemens software running on the scanner. Navigator image reconstruction and estimation of motion are performed in real time in ICE. PACE (Thesen et al., 2000), which uses

a least squares cost function for image alignment, is used to calculate the motion parameters for each navigator volume and provides the 6 parameter motion estimate. The navigator preparation process described in the previous step ensures that the navigator FOV covers the subject's entire head, which is necessary for accurate estimation of motion by PACE. When subject motion in any direction is greater than ±20 mm translation or ±8 degrees rotation, PACE terminates completely because it is likely that the subject will have moved outside the image volume resulting in inaccurate motion estimates. When the motion exceeds these limits, the navigated diffusion sequence continues to run as a standard sequence without prospective motion correction. The navigator volumes will, however, still be acquired and stored.

Insertion of the navigator increases the repetition time (TR) of the diffusion sequence by the total scan time of the navigator TR_{vNav}. An additional waiting period for feedback from ICE, $T_{feedback}$, is added to the modified TR to enable the sequence, in real time, to receive feedback and to update the slice positions and gradient coordinate system according to the new motion parameters in the TR immediately following the navigator. This feedback period is determined experimentally and depends on diffusion and motion calculations in ICE. Figure 2.1 summarizes the implementation of prospective motion correction in the volumetric navigated diffusion sequence.

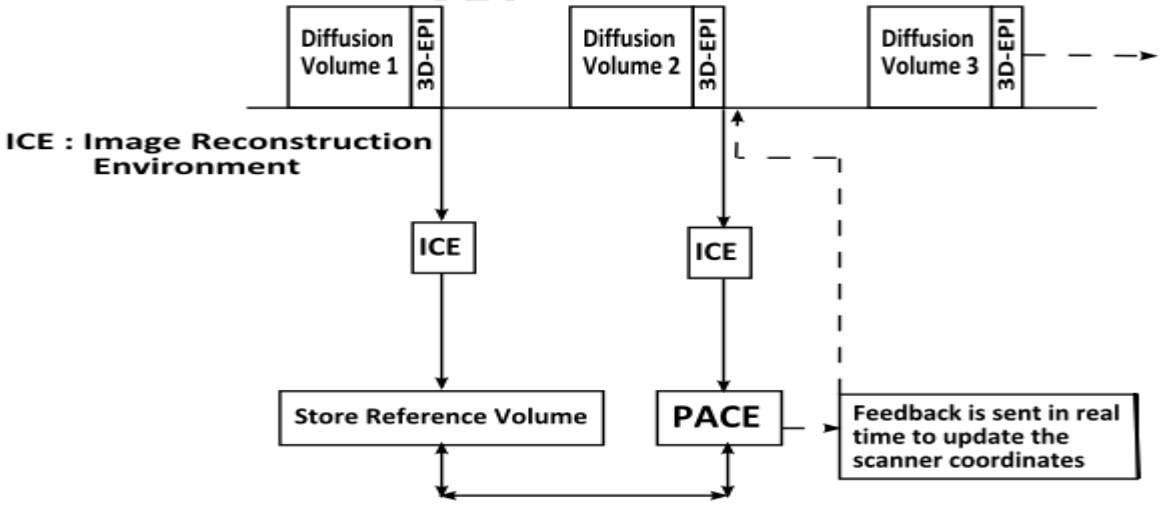

Figure 2.1: Flowchart of the modified diffusion pulse sequence with interleaved 3D-EPI navigator. Data is transferred to ICE, registration is performed by PACE, and the position and gradient system is updated before acquisition of the next diffusion volume.

2.2.3 Reacquisition

A limitation of prospective motion correction techniques, in general, is undetected motion. When ICE sends the motion parameters to the diffusion sequence, the sequence updates the slice orientation of the next diffusion volume, but the previously acquired volume is not corrected for motion that may have occurred during its acquisition. This uncorrected motion can cause an error in the estimation of the diffusion tensor if the motion is large and leads to high pixel misregistration between diffusion weighted volumes. Furthermore, motion during the diffusion sensitization gradients may cause signal dropout in the corresponding images. For this reason, the diffusion pulse sequence was further modified to reacquire volumes during which the motion exceeded some pre-defined threshold. The diffusion protocol was modified to include this feature, which may be selected on the user interface and will prompt the user to specify the number of reacquisitions to be performed (N_{reacq}). In ICE the image reconstruction pipeline was modified to include a new function that compares the PACE motion parameters to certain thresholds. If the motion parameters exceed these thresholds, ICE sends a signal, in addition to the motion parameters, to the sequence to update the gradient system and reacquire this volume. The volume is reacquired in the next TR. The thresholds set in ICE are translation in any direction $\geq$ 2.5 mm or rotation in any direction $\geq$ 1 degree. These thresholds were defined according to the amount of motion that was found to typically lead to volumes with slices of low signal. Every time the sequence reacquires a volume the scan time increases by another TR. All the additional times that are added to the original diffusion scan time are given by Equation (2.1).

$$T_t = (TR_{basic} + TR_{vNav} + T_{feedback}) * (N_{reacq} + N_{diff\_directions} + N_{prep}) \quad (2.1)$$

where T_t is the total scan time of the whole sequence, TR_{basic} is the repetition time of the standard diffusion sequence (9500 ms in the current protocol), TR_{vNav} is the total scan time of the navigator (406 ms in the current protocol), $T_{feedback}$ is the waiting period for the feedback (120 ms in the current protocol), N_{reacq} is the number of reacquisitions that were specified in the diffusion protocol (5 in the current protocol), $N_{diff\_directions}$ is the total number of diffusion directions plus the low b value acquisitions (34 in the current protocol), and N_{prep} is the number of preparation or dummy scans (1 in the current protocol).

The number of reacquisitions N_{reacq} might change from one protocol to another depending on how much extra time can be tolerated in the total diffusion acquisition time. Specifying the number of reacquisitions at the start of the scan ensures that scans do not become impractically long in cases where subjects frequently move a lot. Should there be no (or too few) occurrences of motion during the scan that trigger a reacquisition, the acquisition of the last diffusion volume will be repeated for each nonacquired reacquisition in order to keep the scan time correct. ICE is enabled to display the diffusion images for each TR. In the case where reacquisition has been enabled, ICE will generate both the uncorrected volume and the reacquired one, so that it is possible to study the effects of the modified sequence without or with reacquisition.

2.2.4 Feedback and Combination of Motion Parameters

The gradient pulses are programmed in the logical coordinate system defined by three directions: phase encoding, readout encoding and slice select encoding. The gradients in the logical coordinate system are transformed into the physical coordinate system using a rotation matrix which depends on the slice orientation. When the motion parameters are received from ICE in real time, the sequence updates the position and orientation of the next navigator and applies the updated navigator transformation matrix to adjust the position and the orientation for each diffusion slice. The gradients for both the navigator and the diffusion are adjusted to the new orientation by multiplying the gradients in the current logical coordinate system by the new rotation matrix.

2.2.5 Experimental Protocol

All scans were performed on a Siemens Allegra 3 T (Siemens Healthcare, Erlangen, Germany) scanner at the Cape Universities Brain Imaging Centre. The navigator parameters were the same for all scans. The acquisition parameters for the navigator were: TR = 14 ms, TE = 6.6 ms, voxel size = 8 x 8 x 8 mm^3, acquisition matrix size = 32 x 32 x 28, FOV 256 x 256 x 224 mm^3, the bandwidth in the readout direction = 3906 Hz/px, flip angle = 2 degrees, and total scan time = 406 ms.

The acquisition parameters for the diffusion sequence were: TR = 9500 ms without the navigator (basic sequence), TR = 10026 ms with the navigator (vNav sequence), TE = 86 ms, 72 slices, matrix size = 112 x 112, single channel birdcage head coil, slice thickness = 2 mm, 30

non-collinear diffusion gradient directions, b-values 0 and 1000 s mm^{-2}, and four low b-value scans. The waiting period for feedback (including all navigator-related computations in the sequence and in ICE) is 120 ms for each repetition time. For *in vivo* scans, reacquisition was enabled with five reacquisitions.

In order to ensure that insertion of the navigator in the diffusion sequence does not corrupt the diffusion data, we first performed DTI acquisitions of a stationary water phantom:

1) W_basic: water phantom stationary scans acquired using the basic diffusion sequence, repeated three times (W_basic1, W_basic2 and and W_basic3), and

2) W_vNav: scans of a stationary water phantom using the navigated (vNav) diffusion sequence with prospective motion correction, repeated three times (W_vNav1, W_vNav2, and W_vNav3).

Six healthy male subjects (24 to 30 years) were scanned. All subjects provided informed written consent prior to scanning according to protocols that had been approved by the Faculty of Health Sciences Human Research Ethics Committee of the University of Cape Town, South Africa. The experimental protocol comprised 4 different DTI acquisitions:

1) NoMo_basic: an at rest (no motion - NoMo) scan acquired with the basic (standard) diffusion sequence,

2) NoMo_vNav_NoCo: an at rest scan (NoMo) acquired using the navigated (vNav) diffusion sequence but without prospective motion correction enabled (no correction - NoCo),

3) Mo_basic: a scan with motion (Mo) acquired using the basic diffusion sequence , and

4) Mo_vNav_all: a scan with motion (Mo) acquired using the navigated (vNav) diffusion sequence with motion tracking and motion correction applied, and reacquisition enabled. The Mo_vNav_all data were analysed both without reacquisition (Mo_vNav_noReAq) and with reacquisition (Mo_vNav_ReAq) applied.

Two additional DTI acquisitions were performed for two subjects:

5) Mo_vNav_NoCo: a scan with motion (Mo) acquired with the navigated (vNav) sequence but with no prospective motion correction applied (NoCo). Using this scan, motion parameters could be logged for an acquisition without prospective motion correction, allowing us to compare the navigator motion estimates by PACE with motion estimates determined using retrospective motion correction techniques (Mo_vNav_NoCo_retro), and

6) NoMo_vNav_Co: an at rest scan (NoMo) acquired using the navigated (vNav) diffusion sequence with prospective correction (Co) applied.

During the 'at rest' (NoMo) scans, the subjects were asked to lie as still as possible. Since subjects were not anaesthetized, unexpected motion could occur. For the scans with motion, the subjects were instructed to change their head position upon verbal instruction. Five to six instructions (roughly one every 40 s) were given during the scan. The subjects were asked to repeat the same movements for each of the scans acquired with motion. The total scan time without the navigator is 5 minutes and 33 seconds, with the navigator it is 5 minutes and 50 seconds, and with five reacquisitions it is 6 minutes and 40 seconds.

2.2.6 Diffusion Data Processing

Diffusion volumes were processed after conversion from DICOM format to NifTi using Freesurfer tools (Athinoula A. Martinos Center for Biomedical Imaging; http://surfer.nmr.mgh.harvard.edu/). The diffusion data of the six subjects were quantified using Diffusion Toolkit (http://trackvis.org/) (including TrackVis), which generates all the diffusion maps and the track bundles from the NifTi data. From the whole track bundles, the histograms of the DTI-derived indices (MD and FA maps) were computed. In the current studies the whole track bundles of the whole brain were selected. TrackVis then measured the mean FA and the mean MD for each track in the bundle. Each track therefore represents a single data point; the data points were binned to create the histogram. The FA and the MD histograms were transferred to Matlab to calculate the histogram-derived measurements (peak location, skewness and

kurtosis). Each histogram contains 50 bins, for each of which the values were normalized by the total number of tracks that is estimated by TrackVis. The mean FA, the mean MD and the histogram-derived measurements were compared for the different acquisitions for the six subjects using a paired t-test implemented in Matlab. P-values less than 0.01 were considered statistically significant. The diffusion maps of the water phantom were processed in a similar way to the *in vivo* data also using Diffusion ToolKit, but the histogram parameters for the water phantom were calculated from the MD map, and normalized by the total number of pixels. Retrospective motion correction of the diffusion DICOM volumes was performed only for scans with motion that were acquired using the basic diffusion sequence (Mo_basic) and for the Mo_vNav_NoCo scan acquired using the navigated sequence without prospective motion correction. Two different registration methods were used to align all the diffusion volumes to the b0 volume, after which the corrected volumes were processed to extract all the diffusion maps in the same way as described above. The two methods include (1) the use of the linear image registration tool (FLIRT) in FSL (FMRIB Software Library; http://www.fmrib.ox.ac.uk/fsl) with a least squares cost function and 6 degrees of freedom, (2) statistical parametric mapping (SPM5 - http://www.fil.ion.ucl.ac.uk/spm/). We also investigated for three subjects whether eliminating motion corrupted volumes that have a low signal due to the motion improves retrospective motion correction.

2.3 Results

2.3.1 The Influence of the Navigator on the Diffusion Sequence

Water Phantom

Figure 2.2 shows the MD map of a single slice of the first baseline scan (W_basic1) of the water phantom, and the difference between the MD map of this slice for this acquisition and the same slice for each of the other acquisitions. The MD maps of all slices were averaged for the three basic scans and for the three prospectively corrected navigated scans. Shown in Figure 2.3 are the histograms of the averaged MD maps over the whole volume of the phantom for the two different sequences (W_basic and W_vNav). These figures demonstrate that the insertion of the navigator in the diffusion sequence does not corrupt the diffusion data of the water phantom

and that there were no potential or residual errors from PACE, which would have introduced diffusion errors.

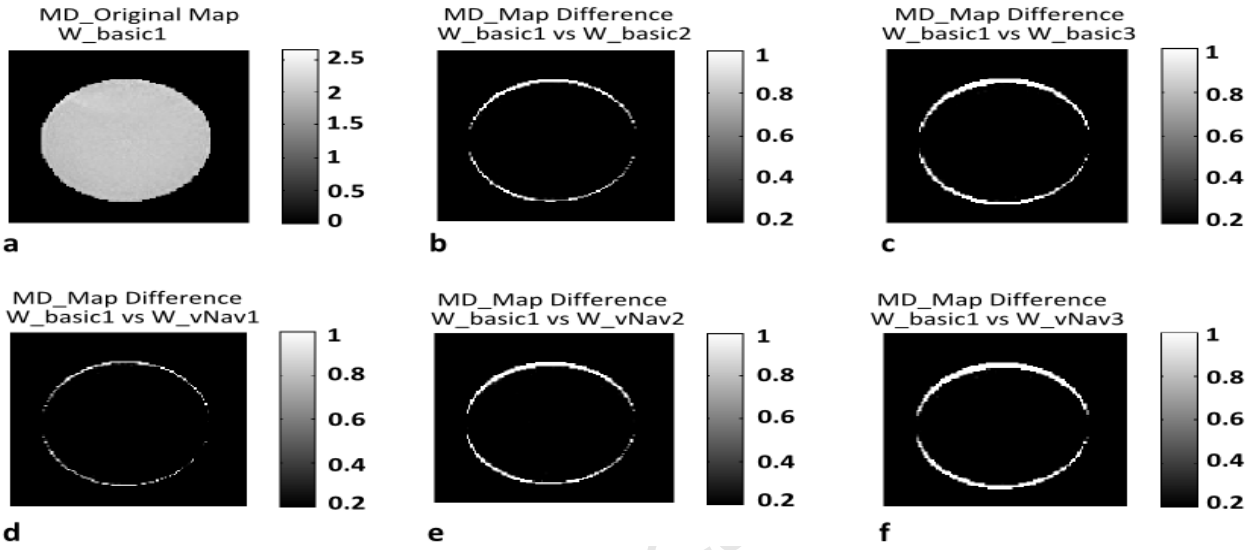

Figure 2.2: (a) The MD map for slice 38 of a stationary water phantom scanned using the basic diffusion sequence, and the difference between the MD map of this slice and the MD map of the same slice for scan (b) W_basic2, (c) W_basic3, (d) W_vNav1, (e) W_vNav2, and (f) W_vNav3, where W denotes water phantom scans, basic denotes scans acquired using the basic diffusion sequence, and vNav denotes scans acquired using the navigated prospective motion corrected diffusion sequence. All color bars have units 10^{-3} mm^2 s^{-1}.

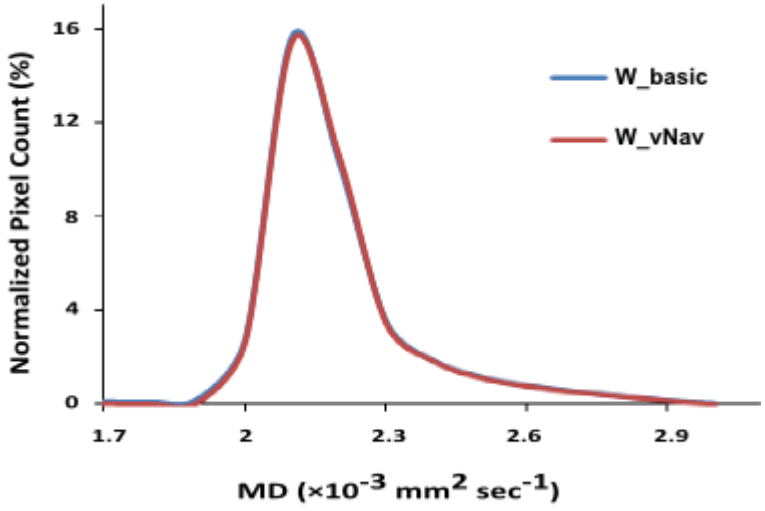

Figure 2.3: Histograms of the averaged MD for the three scans over the whole volume of the water phantom for the navigated prospective motion corrected diffusion sequence (vNav) and the basic diffusion sequence (basic).

In Vivo Data

Figure 2.4 shows for two subjects (2 and 5) that there is no difference due to insertion of the navigator in the whole brain histograms (WBHs) of FA for the at rest (NoMo) scans acquired with the basic diffusion sequence and with the navigated sequence without prospective motion correction (vNav_NoCo). The bottom row (Figure 2.4 c,d) shows the motion parameters that were estimated in ICE by PACE during the NoMo_vNav_NoCo scans. These data show that even when a subject has been asked to lie as still as possible, there may still be some small residual motion. For these small motions, motion in the 30 ms between diffusion encoding gradient lobes were, however, likely to be very small and well below the limits that have been found to cause low signal and dropout slices.

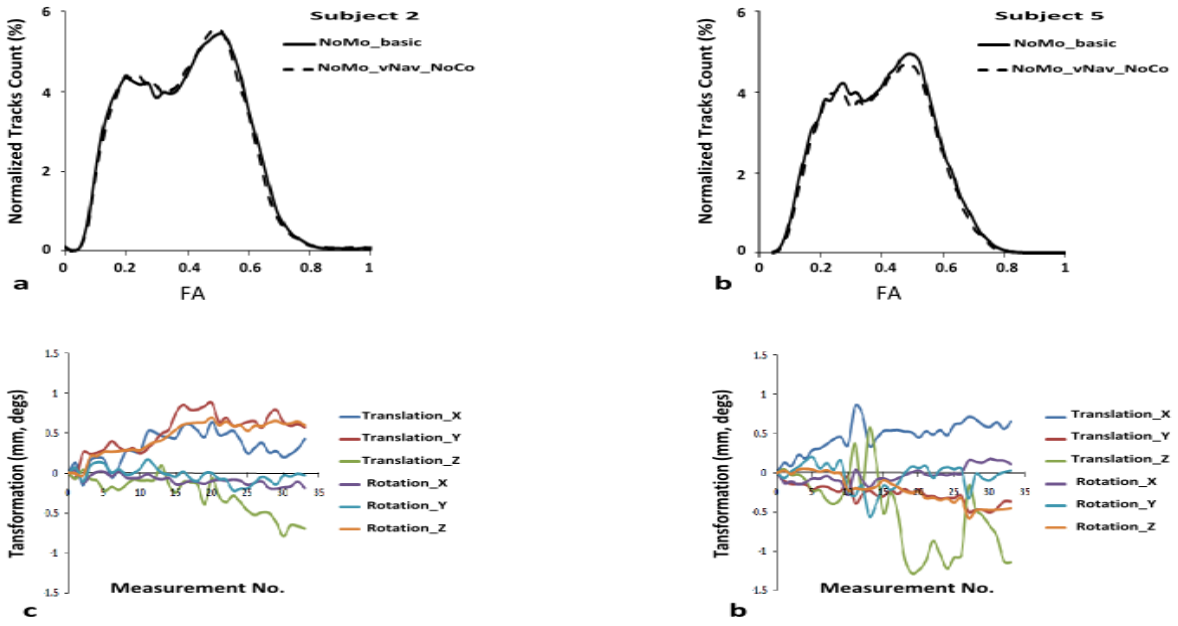

Figure 2.4: Normalized whole brain histograms (WBHs) of FA for two subjects (2 and 5) for the at rest (NoMo) scans acquired with the basic diffusion sequence and with the navigated sequence without prospective motion correction (vNav_NoCo). The plots in the bottom row are the corresponding motion parameters that were estimated in ICE by PACE during the NoMo_vNav_NoCo scans.

2.3.2 Subject Motion, Motion Correction and Reacquisition

In order to confirm that we are comparing diffusion data acquired under similar conditions of motion, we compare in figure 2.5 the motion parameter estimates for the first

subject generated by PACE and retrospective motion correction. Figures 2.5a and 2.5d show the motion parameters that were estimated in ICE by PACE for the Mo_vNav_NoCo and Mo_vNav_all scans, respectively. Figures 2.5b and 2.5e show the retrospective motion estimates for the navigated sequence without prospective motion correction (Mo_vNav_NoCo) using SPM and FLIRT, respectively, and same for the basic sequence in figures 2.5c and 2.5f. In figure 2.5d, since reacquisition was enabled, the number of measurements was 39, compared to 34 in all the other acquisitions.

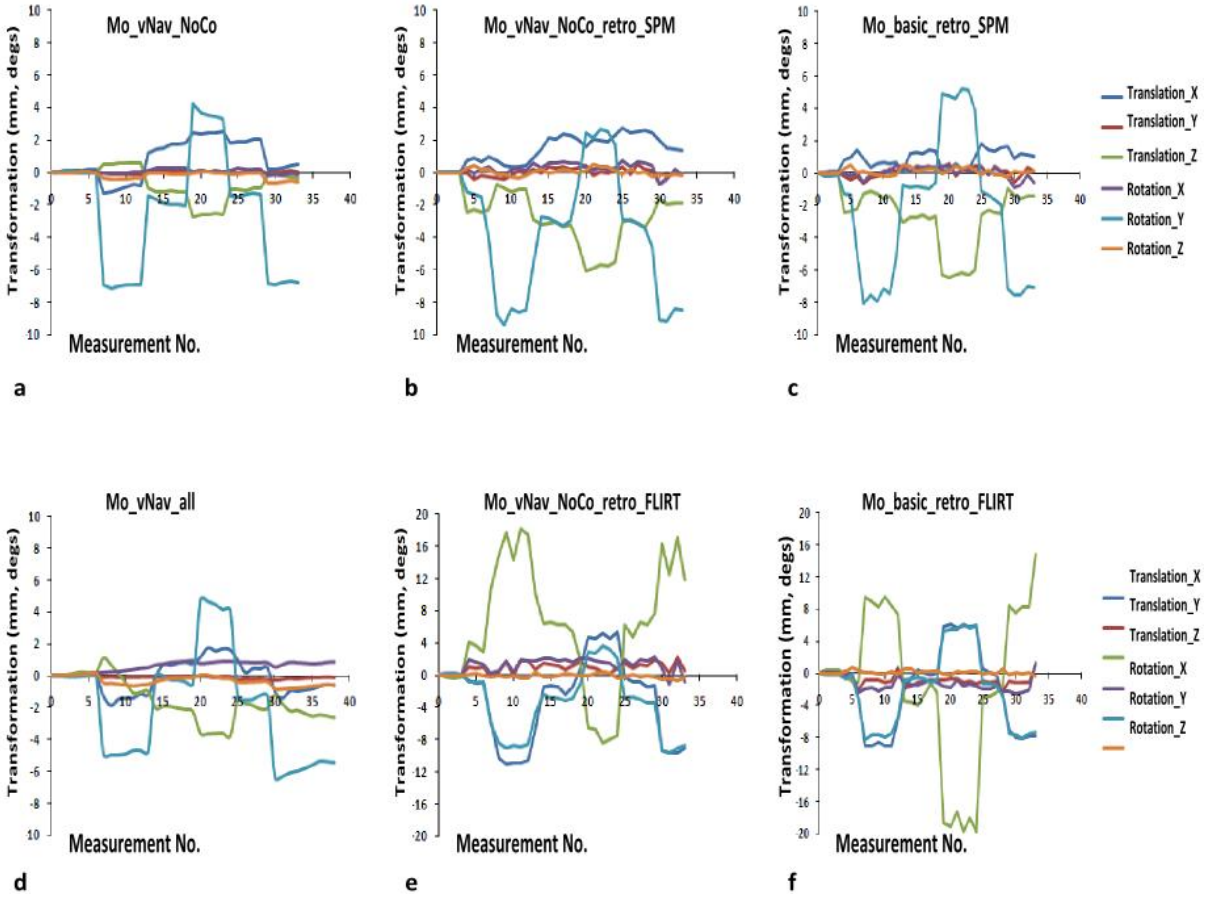

Figure 2.5: Comparison of motion parameter estimates generated by PACE and retrospective (retro) motion correction for the first subject. a and d show the motion parameters that were estimated in ICE by PACE for the Mo_vNav_NoCo and Mo_vNav_all scans, respectively. b and e show the retrospective motion estimates for the Mo_vNav_NoCo scan using SPM and FLIRT, respectively, and same for the basic diffusion sequence in c and f. Mo denotes a scan with motion, vNav the navigated diffusion sequence, NoCo without prospective motion correction, and all a scan with prospective motion correction and reacquisition enabled. Subjects moved upon verbal instruction, five to six times during the scan.

These plots serve to demonstrate similar conditions of motion between the Mo_vNav_all scan and the Mo_vNav_NoCo scan, due to similar PACE motion estimates. Similarly, SPM retrospective motion estimates demonstrate similar motion between the Mo_vNav_NoCo scan and the Mo_basic scan. FLIRT retrospective motion correction is very sensitive to the choice of cost function and number of degrees of freedom and consistently overestimates the motion parameters.

Shown in figure 2.6 are the FA and MD maps of a single slice for the first subject for the 5 different diffusion acquisitions, as well as the results of applying retrospective motion correction in the scan acquired using the basic sequence using SPM (Mo_basic_retro_SPM) and FLIRT (Mo_basic_retro_FLIRT), respectively. Data from the Mo_vNav_all scan have been analysed both without (Mo_vNav_noReAq) and with (Mo_vNav_ReAq) reacquisition applied.

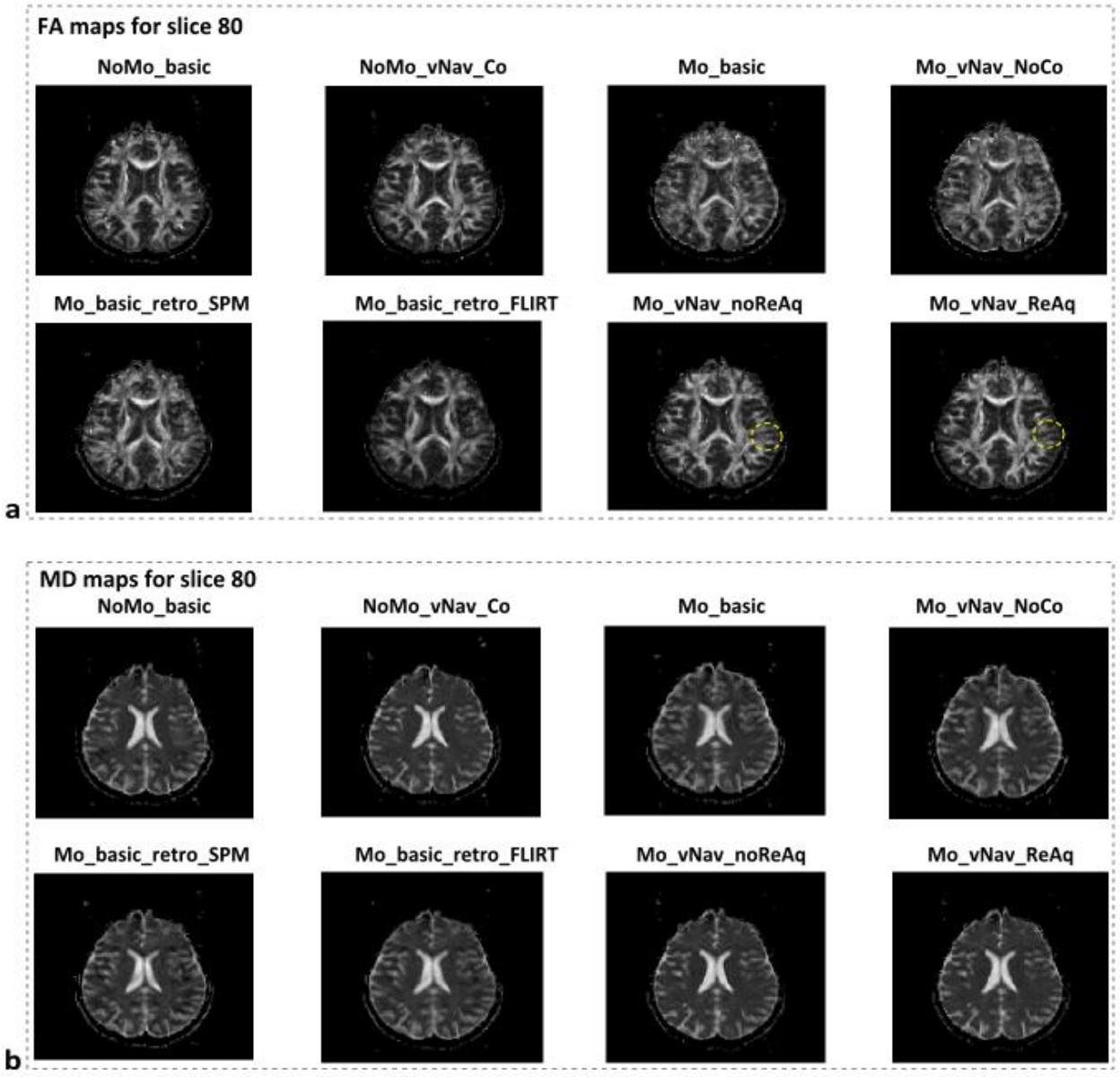

Figure 2.6: FA and MD maps of slice 80 for the first subject for five different acquisitions, as well as results of retrospective motion correction in the scan acquired using the basic sequence using SPM (Mo_basic_retro_SPM) and FLIRT (Mo_basic_retro_FLIRT), respectively. Data acquired in the Mo_vNav_all scan have been analyzed both without (Mo_vNav_noReAq) and with (Mo_vNav_ReAq) reacquisition. The two yellow circles on the FA maps demonstrate reduced blurring in the scan with reacquisition compared to the scan without reacquisition. All the maps are coregistered to the T_1 space.

Figure 2.7 presents a comparison of the WBH-FA and the WBH-MD for the different acquisitions for the same subject. This figure clearly demonstrates how motion without prospective motion correction in the Mo_basic and Mo_vNav_NoCo acquisitions, even after

applying retrospective motion correction (Mo_basic_retro, Mo_vNav_NoCo_retro), changes the distribution of the FA and the MD compared to both the at rest scans, namely the baseline scan (NoMo_basic) and the prospectively corrected navigated (NoMo_vNav_Co) scan. The distribution of the FA and the MD values are almost fully recovered when using the navigated prospective motion corrected sequence (Mo_vNav_noReAq and Mo_vNav_ReAq).

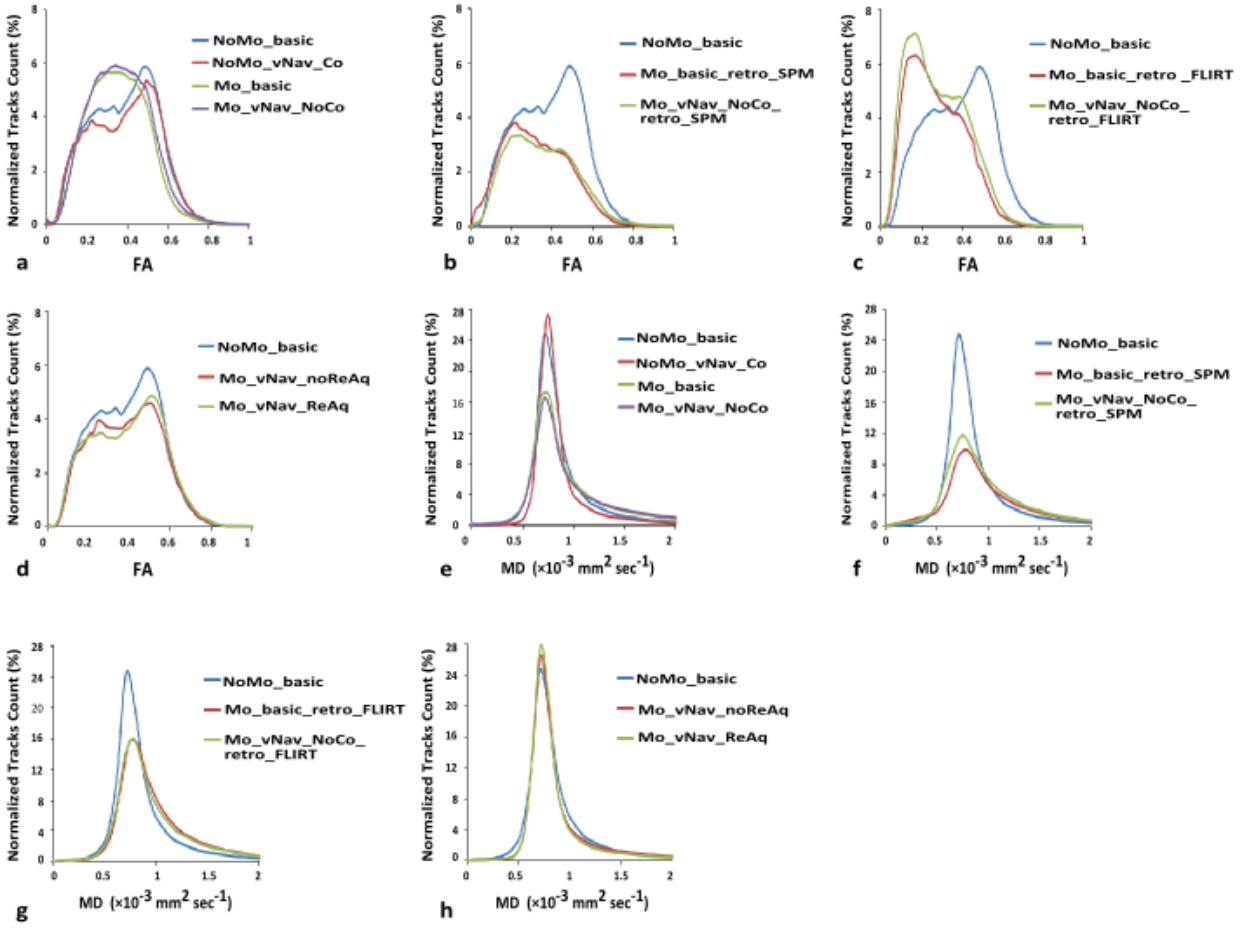

Figure 2.7: Comparison of the normalized WBH-FA (a-d) and WBH-MD (e-h) for the first subject for different scans: (a,e) Comparison of at rest scans acquired using both the basic and navigated sequence to scans with motion and no prospective motion correction acquired using both the basic and navigated sequence; (b,f) Effect of retrospective motion correction using SPM on the scans acquired without prospective motion correction; (c,g) Effect of retrospective motion correction using FLIRT on the scans acquired without prospective motion correction; and (d,h) prospective motion corrected scans acquired using the navigated sequence, both without and with reacquisition.

Tables 2.1 and 2.2 give the mean of the histogram parameters for all six subjects for FA and MD, respectively, for the different acquisitions, as well as the values obtained after applying retrospective motion correction. WBH parameters for each scan were compared with those of the at rest baseline (NoMo_basic) scan using a paired student's t-test. The mean FA and the mean MD over the whole brain volume does not differ significantly from the baseline values for scans acquired at rest using the navigated sequence without prospective correction (NoMo_vNav_NoCo), paired Student's t-test, $p = 0.73$ and $p = 0.64$, respectively. This result confirms that insertion of the navigator into the sequence does not corrupt the diffusion data.

Table 2.1

Comparison of the mean of the WBH-FA parameters for all subjects for the different scans.

WBH-FA Parameters	NoMo_ basic	NoMo_vNav _NoCo	Mo_ basic	Mo_basic _retro		Mo_vNav _noReAq	Mo_vNa v_ReAq
				SPM	FLIRT		
Mean FA (SD)	0.52 (0.02)	0.52 (0.01)	0.48* (0.02)	0.41* (0.02)	0.41* (0.02)	0.51 (0.02)	0.52 (0.01)
Peak Location (SD)	0.50 (0.01)	0.51 (0.01)	0.31* (0.03)	0.23* (0.03)	0.2* (0.1)	0.5 (0.1)	0.5 (0.1)
Skewness (SD)	0.3 (0.2)	0.2 (0.2)	0.6 (0.1)	0.6 (0.1)	0.7 (0.1)	0.3 (0.2)	0.3 (0.2)
Kurtosis (SD)	1.4 (0.1)	1.4 (0.1)	1.6 (0.2)	1.6* (0.1)	1.9* (0.1)	1.3 (0.1)	1.4 (0.1)

* $p<0.01$ paired student's t-test

Table 2. 2

Comparison of the mean of the WBH-MD parameters for all subjects for the different scans

WBH-MD Parameters	NoMo_ basic	NoMo_vNav _NoCo	Mo_ basic	Mo_basic _retro		Mo_vNav _noReAq	Mo_vNa v_ReAq
				SPM	FLIRT		
Mean MD /10^{-3} mm^2s^{-1} (SD)	0.84 (0.02)	0.83 (0.01)	0.87* (0.02)	0.78* (0.03)	0.88* (0.03)	0.85 (0.02)	0.84 (0.01)
Peak Location /10^{-3} mm^2s^{-1} (SD)	0.73 (0.02)	0.75 (0.02)	0.74 (0.03)	0.73 (0.03)	0.73 (0.01)	0.75 (0.04)	0.74 (0.02)
Skewness (SD)	3.3 (0.1)	3.4 (0.2)	2.8 (0.4)	2.7 (0.5)	2.8 (0.4)	3.4 (0.1)	3.5 (0.1)
Kurtosis (SD)	14 (1)	14 (1)	10 (2)	10 (3)	11 (3)	14 (1)	15 (1)

* $p<0.01$ paired student's t-test.

There are no significant differences in any of the WBH-FA (Table 2.1) and WBH-MD (Table 2.2) parameters between any of the navigated prospectively motion corrected sequences (Mo_vNav_noReAq and Mo_vNav_ReAq) and the at rest baseline scan (NoMo_basic). By contrast, mean FA and peak location differ significantly ($p<0.01$) for acquisitions with the basic sequence in the presence of motion, even after retrospective motion correction using SPM (Mo_basic_retro_SPM) and FLIRT (Mo_basic_retro_FLIRT). Although the FA histogram skewness and kurtosis are not altered significantly by motion in the basic sequence, the mean kurtosis is significantly higher after performing retrospective motion correction using both SPM and FLIRT. Mean MD differs significantly ($p<0.01$) from the at rest baseline value for data acquired with the basic sequence in the presence of motion (Mo_basic), even after retrospective motion correction with FLIRT and SPM. Although not significant, motion reduces the MD histogram skewness and kurtosis in the basic sequence, even after retrospective motion correction.

In order to investigate whether elimination of motion corrupted volumes in the basic acquisition improves retrospective motion correction, we eliminated for three of the subjects (2, 4, and 6) volumes that have a low signal due to motion. Figure 2.8 shows the WBH-FA for the three subjects for retrospective motion corrected data before elimination (BE) and after elimination (AE) of motion corrupted volumes. Shown also are the at rest baseline scans (NoMo_basic). Elimination of the corrupted volumes does not improve the diffusion data; there is still a significant reduction in the mean FA and in the peak location. These results demonstrate that retrospective motion correction completely fails to recover the diffusion data without prospective motion correction, even when the corrupted diffusion volumes with low signal are eliminated.

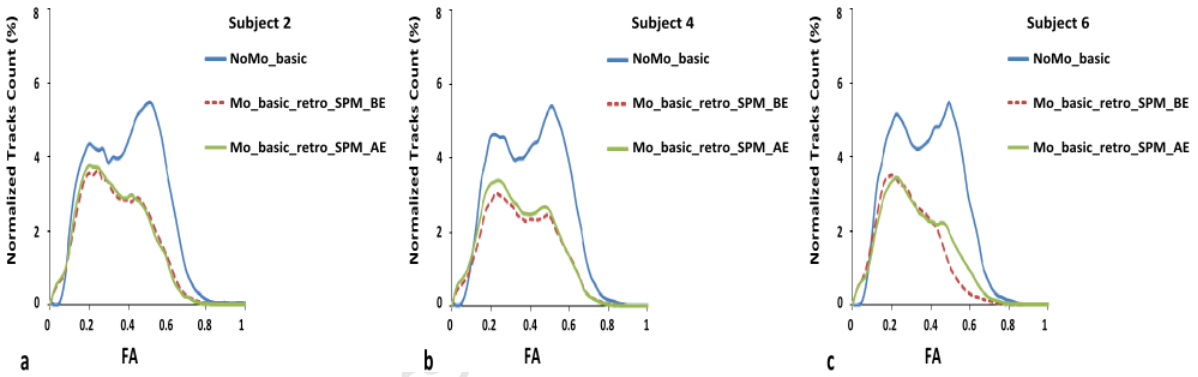

Figure 2.8: Comparison of the normalized WBH-FA in three subjects for an at rest baseline scan (NoMo_basic) compared to a scan with motion and retrospective motion correction where the suffices BE and AE, respectively, denote before and after elimination of corrupted volumes that have low signal due to motion.

Subject 6 was very restless with motion that caused PACE to terminate in the Mo_vNav_all acquisition. This acquisition was repeated but with only three reacquisitions in order to shorten the scan time. The repeated Mo_vNav_all acquisition had 11 corrupted noisy volumes, only 3 of which were reacquired. With this data we could explore the improvement offered by elimination of motion corrupted volumes in prospectively corrected data. While significantly better than scans acquired without prospective motion correction (Figure 2.9a), the prospectively corrected navigated scan in this case does not fully recover the diffusion data

(Figure 2.9b), even with reacquisition, due to the presence of uncorrected corrupted volumes. The WBH-FA was recalculated for this subject after elimination of the noisy corrupted diffusion volumes for both the Mo_vNav_noReAq (11 corrupted volumes) and the Mo_vNav_ReAq (8 corrupted volumes) data, respectively. The results presented in Figure 2.9c show that both without and with reacquisition the diffusion data improved after elimination of the corrupted volumes, but that recovery of the FA peak location was slightly better for the data with reacquisition than without. The FA peak location for both Mo_vNav_noReAq and Mo_vNav_ReAq before elimination was 0.2; after elimination it was 0.3 and 0.5 for Mo_vNav_noReAq and Mo_vNav_ReAq, respectively.

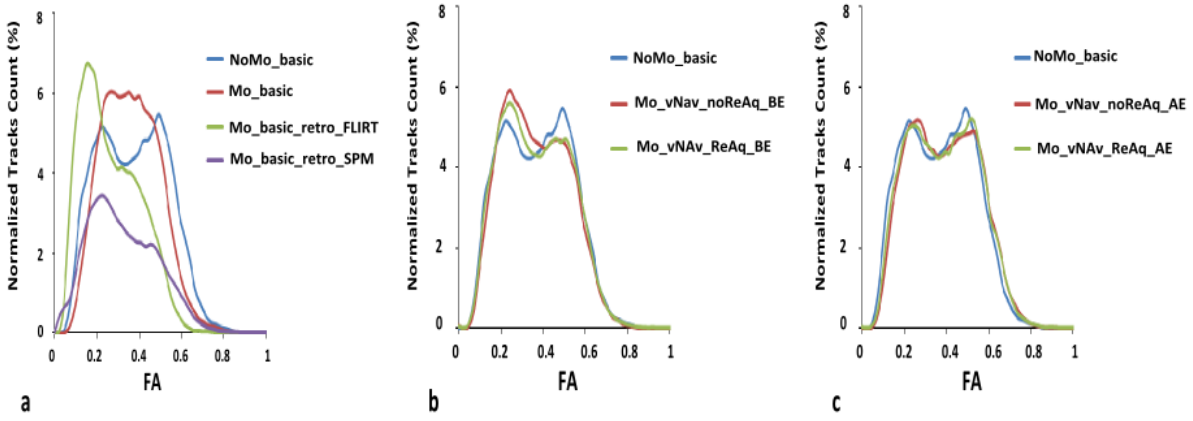

Figure 2.9: (a) The effect of motion on the normalized WBH-FA of the basic diffusion sequence (both before and after retrospective motion correction with FLIRT and SPM) for a particularly restless subject, (b) normalized WBH-FA of the navigated sequence with prospective motion correction, both without and with reacquisition, for this data with many uncorrected corrupted volumes (both before elimination (BE) of uncorrected corrupted volumes) (c) normalized WBH-FA of the navigated sequence after elimination (AE) of uncorrected corrupted volumes.

2.4 Discussion

The quantitative application of DTI in clinical or research areas relies on computation of FA and mean diffusivity (MD). The whole brain histogram (WBH) of FA and MD has been widely used to study different clinical diseases (Bozzali et al., 2001; Della Nave et al., 2007; Mori et al., 2008; Zhou et al., 2008). Subject motion influences the diffusion maps in a way that can confound the interpretation of DTI results. The accurate calculation of the diffusion tensor

and the diffusion maps requires that the diffusion weighted volumes for different diffusion directions be co-aligned. We have presented a method using a 3D-EPI navigator to track and correct in real time changes in position that result from rigid body motion.

The only increase in scan time is due to the navigator (406 ms) and waiting period for feedback (120 ms), both of which occur once per TR, increasing the TR from 9500 ms to 10026 ms. While intra-volume motion in self-navigation techniques (11,16) renders the 3D volume used for co-registration unusable, the advantage of such a short additional navigator (406 ms) is that motion at any time during the TR is unlikely to affect the navigator, and correction is applied immediately after the navigator. Only when the motion exceeds a pre-defined threshold will the motion corrupted volume be reacquired adding an additional TR. The total number of reacquisitions are, however, limited and is specified when preparing the diffusion protocol. Therefore the total acquisition time of the diffusion sequence is also limited to the value given by Equation (2.1).

The Influence of the Navigator on the Diffusion Sequence

Using both a water phantom and at rest scans in six subjects, we have confirmed that the insertion of the 3D-EPI navigator has negligible effect on the diffusion data. Figure 2.2 demonstrates that there are no artifacts or distortions in the mean diffusivity map of the water phantom that is acquired using the navigated prospective motion corrected diffusion sequence compared to the standard diffusion sequence. The results are the same for the other slices. Furthermore, the histograms of the averaged MD for the three scans over the whole volume of the water phantom for the navigated sequence and the basic sequence are similar, with no differences in peak location, skewness or kurtosis (Fig. 2.3). These results also confirm that there are no residual errors in the motion estimates derived by PACE which could corrupt the diffusion data.

For the *in vivo* data, the WBH-FA is generated from images containing gray and white matter, giving rise to 2 distinct peaks, while the WBH-MD shows a single normal distribution due to the fact that normal gray and white matter have very similar MD values. The plots in figure 2.4 show that the insertion of the navigator into the diffusion sequence does not shift or change the properties of the FA or MD histograms for *in vivo* data acquired at rest. The results

are similar for the other subjects. The average of the mean FA and the MD for all six subjects do not differ significantly between the baseline scan and the scan acquired at rest using the navigated sequence without prospective correction (Tables 2.1 and 2.2). The excellent agreement between the WBH-FA and WBH-MD shown in figure 2.7 for a single subject for the NoMo_basic and NoMo_vNav_Co acquisitions, provides further evidence for the fact that there are no residual errors in the motion estimates derived by PACE that could introduce errors in the diffusion data.

Subject Motion, Correction and Reacquisition

In the current studies there was no way to monitor the head pose inside the scanner when using the basic diffusion sequence. Even in stationary scans where subjects are instructed to remain still, they may move unexpectedly with resulting changes in the diffusion data. The navigated diffusion sequence generates the 6 parameter motion estimates that reflect the motion between every two successive diffusion volumes (Fig. 2.5). Retrospective motion correction with FLIRT yielded different motion estimates compared to PACE. In the current study, FLIRT was implemented using a least squares cost function with 6 degrees of freedom. FLIRT showed overestimation of motion parameters (Fig. 2.5e,f), while SPM motion estimates showed good agreement with PACE. Using a mutual information-based cost function and a higher number of degrees of freedom did not improve the accuracy of the FLIRT motion estimates. Using the SPM and PACE motion estimates, we could confirm that we are comparing diffusion data acquired under similar conditions of motion.

The degradation of the FA and MD maps in the presence of motion are apparent in the Mo_basic and Mo_vNav_NoCo data shown in figure 2.6. The motion adds blurring and edge artifacts, rendering the finer details of the maps inaccurate. Retrospective motion correction does reduce blurring marginally, but does not recover all the finer details. These artifacts in the FA and the MD maps are eliminated substantially with the navigated diffusion sequences Mo_vNav_noReAq and Mo_vNav_ReAq.

Motion causes a significant reduction in the mean FA of the whole brain volume for all six subjects (Table 2.1). Retrospective motion correction does not improve the mean FA, but rather causes a further significant reduction in the mean FA for both retrospective motion

correction methods (Mo_basic_retro_FLIRT and Mo_basic_retro_SPM). The mean FA is recovered substantially for the navigated prospective motion corrected acquisitions Mo_vNav_noReAq and Mo_vNav_ReAq (Table 2.1). In contrast, motion causes a significant increase in the mean MD of the whole brain volume for the six subjects. Retrospective motion correction with FLIRT yields no improvement in the mean MD. The mean MD is recovered substantially for the navigated scans Mo_vNav_noReAq and Mo_vNav_ReAq (Table 2.2).

In the presence of motion the WBH-FA for all subjects shows changes in FA toward lower anisotropy and a shift in the location of the high anisotropy peak (Fig. 2.7a). This decrease of anisotropy in the whole brain changes the unique shape of the WBH-FA with an increase in both the kurtosis (the curve becomes more peaked) as well as the skewness (the curve becomes more asymmetric) (Table 2.1). In Figure 2.7a, the double bell-shaped curve of the WBH-FA becomes distorted due to motion and the distribution moves towards a single bell-shaped curve due to a reduction in the anisotropy of the white matter and a shift towards higher diffusivity. In contrast, with subject motion the WBH-MD changes toward more diffusivity with a decrease in kurtosis (the curve becomes less peaked) as well as in skewness (the curve becomes less asymmetric) (Table 2.2, Fig. 2.7e). Retrospective motion correction does not recover the distinct peaks of the WBH-FA and moreover it causes a big increase in the height of the lower FA peak in the case of FLIRT (Fig. 2.7c) or a reduction in the lower FA peak in the case of SPM (Fig. 2.7b). Even eliminating the corrupted uncorrected volumes in the Mo_basic scan, does not improve the retrospective motion correction (Fig. 2.8). The navigated prospective motion corrected acquisition (Mo_vNav_noReAq and Mo_vNav_ReAq) recovers the properties of both the WBH-FA and the WBH-MD.

The incremental improvement of reacquisition on the diffusion data is slight, especially if there are no uncorrected diffusion volumes with low signal due to motion. The Mo_vNav_all scan for subject 6 had many corrupted noisy volumes, only 3 of which were reacquired. While significantly better than scans acquired without prospective motion correction (Figure 2.9a), the prospectively corrected navigated scan does not fully recover the diffusion data in this case (Figure 2.9b), even with reacquisition, due to the presence of uncorrected corrupted volumes. Elimination of the corrupted diffusion volumes in both the Mo_vNav_noReAq and the

Mo_vNav_ReAq acquisitions, almost fully recovers the diffusion data, but with better recovery of the FA peak location for the data with reacquisition than without.

Limitations of the 3D-EPI Navigator

Due to the long acquisition time (TR = 9500 ms) of the diffusion volume in the current protocol, real-time motion tracking by the 3D-EPI navigator once per diffusion volume might not be sufficient to detect brief fast intra-volume movements if the subject returns to their original position. Acquiring additional 3D-EPI navigators with a smaller acquisition matrix size (e.g. by partial Fourier) in between certain diffusion slices of the same volume, and not only at the end of the diffusion volume, could improve the sensitivity of the navigator. Another option would be to combine the current method with the FID navigator method proposed by Kober et al. (2011), since their volume-wise evaluation of the FID navigator is sensitive to motion throughout the volume and requires that the head position be different to the preceding repetition in at least five slices.

It is not ideal in the current implementation of the sequence that unused reacquisitions need to be acquired at the end of the scan in order to keep the scan time correct. It would be better if the sequence could terminate the scan after all the diffusion volumes have been acquired, even if there are remaining unused reacquisitions.

Finally, the allowable range of motion that can be corrected prospectively using this technique is limited by the Siemens implementation of PACE, which terminates for translations in any direction greater than 20 mm and rotations in any direction greater than 8 degrees. If the motion exceeds these limits, PACE will terminate and subsequent diffusion volumes will not be prospectively motion corrected. The navigator images will, however, still be acquired enabling offline estimation of motion parameters and retrospective motion correction.

2.5 Conclusion

In this paper we present a volumetric navigated DTI sequence that allows real-time tracking of head pose and adjustment in real time of the RF pulses and all the diffusion gradients to correct for changes in head pose. If enabled, the system also reacquires volumes during which excessive motion occurred. Apart from the reacquisition time, the only additional scan time is

526 ms per TR, which is minimal in view of the long diffusion TR of 9500 ms that is widely used in DTI protocols.

2.6 Acknowledgements

The South African Research Chairs Initiative of the Department of Science and Technology and National Research Foundation of South Africa, Medical Research Council of South Africa, NIH grants R21AA017410, R21EB008547, R21MH096559, R01HD071664, R01NS05574, P41RR014075, the Ellison Medical Foundation, and the University of Cape Town.

Addendum to Chapter 2

Revision and Correction for Chapter 2 in the Light of Thesis Examination of May 2012.

A.1 Rotation of the Diffusion Table

Leemans and Jones (2009) reported that neglecting to rotate the diffusion table introduces a bias in the estimated diffusion measures that depends on many factors such as the amount of motion, the main orientation of subject motion, the properties of the underlying microstructure as determined by First Eigenvector (FE) , FA, and MD of the diffusion tensor, and the number of gradient directions. Leemans and Jones (2009) implemented their method on a GE 3T HDx system with a single-shot spin-echo sequence along 60 gradient directions as well as using Monte Carlo simulations to demonstrate the effect of neglecting to reorient the ***B***-matrix on the estimation of diffusion measures. In contrast, our experiment was performed on a 3T Allegra Siemens scanner using the twice-refocused spin echo (TRSE: Reese et al. 2003) sequence, a single-channel head coil, the mgh_dti_30 gradient directions scheme and real human subjects were scanned with different patterns and amounts of motion. Furthermore, retrospective motion correction was implemented mainly with FLIRT in FSL.

Rotation of the diffusion table was implemented in the following way:

1) mcflirt generated the transformation matrices (4×4) for each diffusion direction or volume. Because mcflirt was used with 6 degrees of freedom instead of 12, it was easy to extract the rotation matrix from the transformation matrix.

2) The diffusion table used in this study consisted of 4 b0 and 30 diffusion directions (mgh_dti_30).

3) Each diffusion direction was multiplied by the appropriate rotation matrix .

4) The new modified diffusion table was used in Diffusion Toolkit instead of the mgh_dti_30 directions to generate new DTI maps.

Shown below are data for a healthy adult subject who was scanned with the standard diffusion sequence (basic) without motion (NoMo) and with motion (Mo). The diffusion volume images for the scan with motion (Mo_basic) were corrected retrospectively using mcflirt, 6 DOF, both with rotation (Ro) and without rotation (NoRo) of the diffusion gradient table.

Figure A.1 demonstrates that rotating the diffusion table did not change the shape of the whole brain histogram FA.

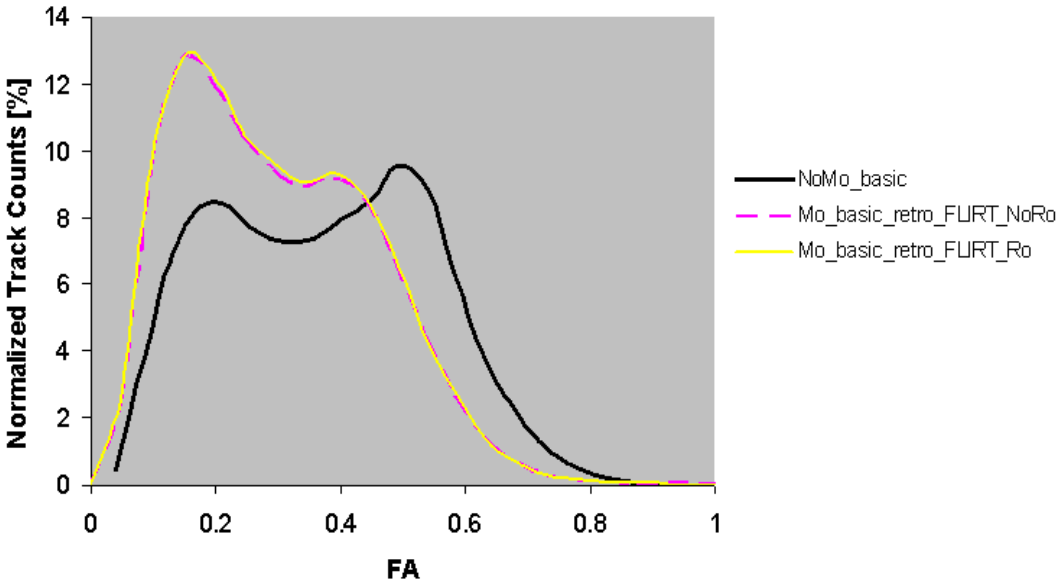

Figure A.1: Comparison of the normalized whole brain histogram (WBHs) for one subject for an at rest scan (NoMo) acquired with the standard diffusion sequence (basic) compared to a scan for the same subject with motion (Mo), with retrospective motion correction, with and without rotating (Ro) the diffusion table.

A.2 Eddy current correction

Zhuang et al. (2006) reported that eddy current can be reduced effectively in one of three ways: (i) by selecting an appropriate pulse sequence such as the twice-refocused spin echo (TRSE, Reese et al. 2003) that was employed in our study; (ii)correcting the k-space data by calibrating eddy-current artifacts in k-space (Jezzard et al., 1998; Papadakis et al., 2005); and (iii) implementing post-acquisition image processing to register the DW images to reference images. Although the last method is widely used because it does not require modification of a diffusion pulse sequence, it is limited in its ability to correct image distortion at high b-values.

In our study, we did not perform eddy current distortion correction of the real-time navigated data due to the fact that we used a sequence that has been shown to reduce eddy current effects.

There are different methods to correct for eddy currents, one of which is eddy_correct (i.e. flirt with 12 DOF) in FSL. Eddy_correct is based on a simple model for eddy current artifacts that include scaling, translation and shear of the images. All these artifacts, that include head motion, can be captured by an affine transformation, compared to 6 DOF that would correct for head motion only.

To evaluate the effects of eddy current correction on the DTI data , I applied eddy-correct with 6 and 12 DOF, respectively, in FSL to the WBH-FAs of two healthy adult subjects whose scans were deemed to be motionless (NoMo) acquired using the standard sequence (basic). The results were compared to motionless scans acquired using the navigated diffusion sequence for the same subjects (NoMo_vNav).

Figure A.2 compares the WBH-FAs for the first subject without and with eddy current correction. It is clear that eddy_correct with 6 DOF (i.e. correction for head motion) caused the mean FA and the FA histogram peak locations to decrease. Eddy current correction with 12 DOF did not recover the reduction in the mean and the FA peak location but rather caused only an increase in the peak heights. Although there is a difference in the peak heights between (NoMo_basic_No_Correction and NoMo_vNav), the mean FA and the FA peak locations are almost identical (table A.1).

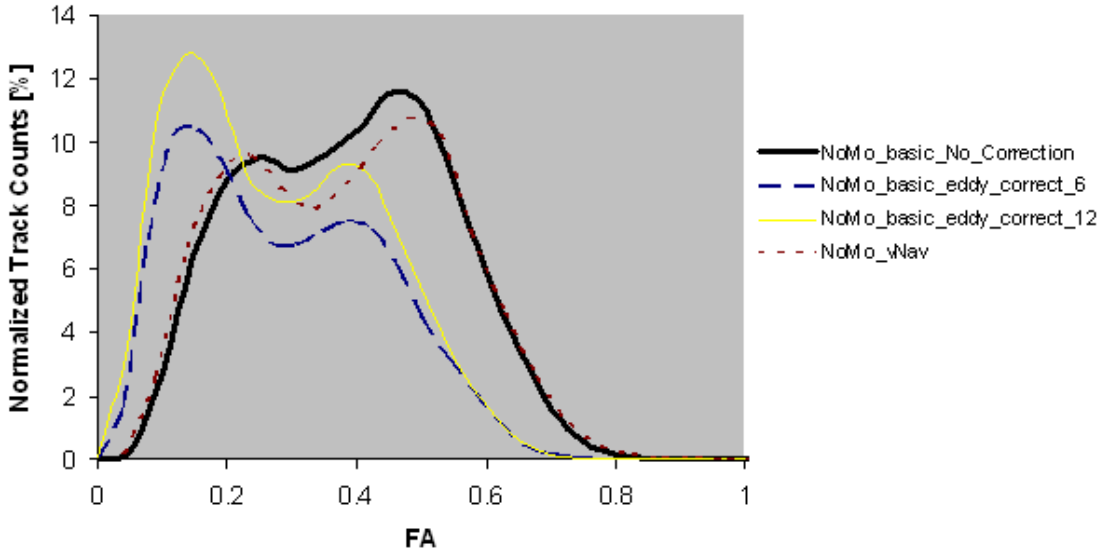

Figure A.2: Comparison of WBH-FAs for the first healthy adult volunteer for acquisitions without motion acquired using the basic and navigated sequences, without and with eddy current correction. A correlation ratio cost function was used in the eddy_correct function in FSL.

Table A.1

Comparison of mean FA's in the first healthy adult volunteer for acquisitions without motion acquired using the basic and navigated sequences, without and with eddy current correction.

	NoMo_basic_No _Correction	NoMo_basic_eddy_ Correct_6	NoMo_basic_eddy_ Correct_12	NoMo_ vNav
Mean FA	0.5	0.4	0.4	0.5

Figure A.3 and Table A.2 shows the results for the second subject. Although similar changes as in the previous subject were observed with 6DOF, eddy current correction with 12 DOF completely changed the distribution of the WBH-FA. This is due to the correlation ratio cost function that is used by default in eddy_correct rather than mutual information. After modifying the eddy_correct script to use a mutual information cost function, the WBHs-FA were recalculated with 6 and 12 DOF. The results are shown in figure A.4 and Table A.3.

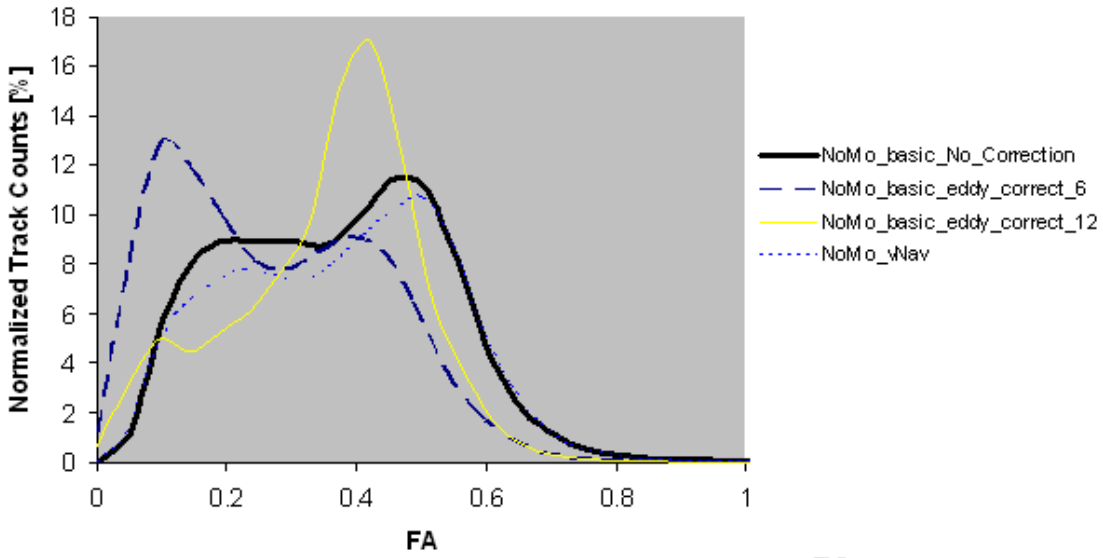

Figure A.3: Comparison of WBH-FAs for the second healthy adult volunteer for acquisitions without motion acquired using the basic and navigated sequences, without and with eddy current correction. A correlation ratio cost function was used in the eddy_correct function in FSL.

Table A.2

Comparison of mean FA's in a second adult volunteer for acquisitions without motion acquired using the basic and navigated sequences, without and with eddy current correction and a correlation ratio cost function.

	NoMo_basic_No _Correction	NoMo_basic_eddy_ Correct_6	NoMo_basic_eddy_ Correct_12	NoMo_ vNav
Mean FA	0.50	0.42	0.43	0.51

Using a mutual information cost function improves the shape of the FA, but does not recover the mean FA (Table 3) and FA peak locations. As in the previous subject, eddy current correction only enhanced the peak heights.

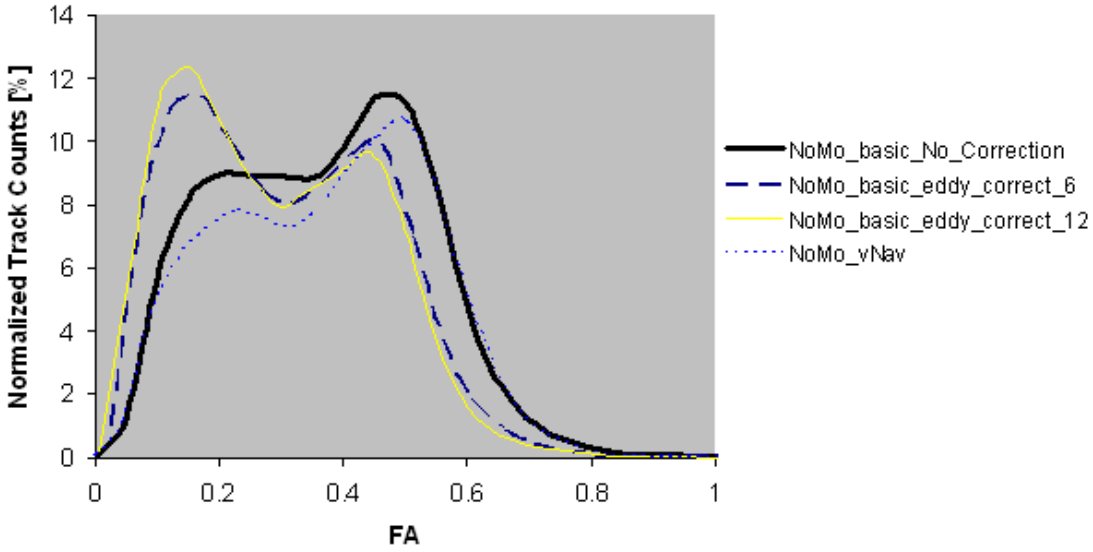

Figure A.4: Comparison of WBH-FAs for the second healthy adult volunteer for acquisitions without motion acquired using the basic and navigated sequences, without and with eddy current correction. A mutual information cost function was used in the eddy_correct function in FSL.

Table A.3

Comparison of mean FA's in a second adult volunteer for acquisitions without motion acquired using the basic and navigated sequences, without and with eddy current correction and a mutual information cost function.

	NoMo_basic_No _Correction	NoMo_basic_eddy_ Correct_6 (Mutual)	NoMo_basic_eddy_ Correct_12 (Mutual)	NoMo_ vNav
Mean FA	0.5	0.4	0.4	0.5

The above two examples clearly show how motion and eddy current correction, in the absence of motion, can corrupt the distribution of the FA data.

In order to demonstrate the effect of eddy current correction on DTI data acquired in the presence of motion, another acquisition was performed for the second subject using the standard diffusion sequence (basic) during which the subject was instructed to perform some movements (Mo). The WBHs-FA were calculated with eddy-correct implemented, respectively, with a correlation ratio cost function (Mo_basic_Eddy_Corratio_12), a mutual information cost function with 6 (Mo_basic_Eddy_Mutual_6) and 12 DOF (Mo_basic_Eddy_Mutual_12). The results were compared to the no motion (NoMo) data of the same subject acquired using the standard sequence (basic). It is evident from the plots shown in figure A.5 that retrospective motion correction with both 6 and 12 DOF failed to recover the data and that eddy_correct implemented with the default correlation ratio cost function changes the shape of the FA histogram.

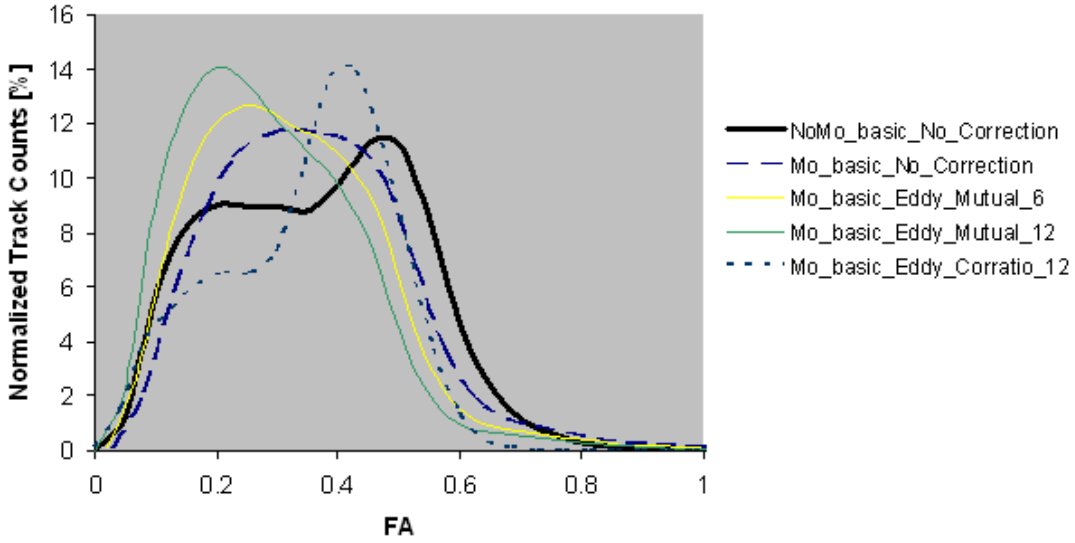

Figure A.5: WBH-FAs for the second healthy adult subject for acquisitions without (NoMo) and with motion (Mo) acquired using the basic sequence without and with different implementations of motion and eddy current correction. 'Corratio" denotes correlation ratio cost function, "mutual" denotes mutual information cost function with either 6 or 12 degrees of freedom.

In summary, the above data demonstrates that eddy_correct with both 6 and 12 DOF reduced the mean FA and the FA histogram peak locations both in the absence and presence of motion. The results also highlight the sensitivity of eddy current correction to the choice of cost function. In all cases, retrospective motion correction and eddy current correction did not recover the distribution of the WBH-FA. I have also explained that eddy current correction was not required

in the navigated data due to the choice of pulse sequence used. Further, it has been shown that rotation of the gradient table to correct for motion does not recover the DTI data.

Other studies (Freire et al., 2001; Jung K-J, 2010; Ling et al., 2012) have also reported that retrospective motion correction may induce errors in either DTI or fMRI data.

A.3 Details of Patient Motion

The navigated sequence uses PACE for motion estimates and as mentioned previously, it will terminate when motion exceeds the limits of PACE (i.e. translation in any direction >20 mm and rotation in any direction > 8 degrees). Should this happen, the navigator images will still be acquired and saved even though motion estimates will no longer be computed.

A grid (Figure A.6) was designed during scanning of the 6 adult subjects and it was placed on the head coil to help the subjects control their amount of motion in order to not exceed the limits of PACE. The subjects were asked to move freely around this grid (e.g. a – b, d – c, c – b, b – e, or a – d). The speed of motion was not a concern in this study. Each scan starts with subjects' heads at a reference point which was chosen to be 'a'. Six instructions were given to each subject throughout the scan and each time the subject received an instruction they would move their head. Table A.4 summarizes the range of motion in each direction performed by each of the 6 healthy adult volunteers.

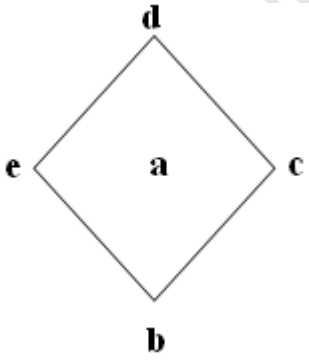

Figure A.6: Diagram of the grid that was placed on the head coil during scanning of the 6 adult subjects to help them control their amount of motion.

Table A.4

The range of motion (maximum – minimum) in each direction for each subject estimated by PACE:

Translation_X In mm	Translation_Y In mm	Translation_Z In mm	Rotation_X In degrees	Rotation_Y In degrees	Rotation_Z In degrees
2.6	0.3	3.5	0.4	10.6	0.8
2.7	9.3	3.2	4.4	11.6	14.1
2.0	15.2	3.6	5.1	6.3	9.7
2.7	7.9	3.5	1.3	6.1	11.5
1.5	12.4	3.1	6.0	5.5	12.3
2.8	4.9	4.9	1.6	6.2	5.4

Chapter 3

Potential Misinterpretation of Abnormal Diffusion Tensor Imaging Derived Metrics in the Presence of Motion[a]

A. Alhamud [1], Khader M. Hasan [4], André J.W. van der Kouwe [2,3] and Ernesta M. Meintjes [1]

[1]MRC/UCT Medical Imaging Research Unit, Department of Human Biology, University of Cape Town, South Africa

[2]Athinoula A. Martinos Center for Biomedical Imaging, MGH, Charlestown, MA, USA

[3]Department of Radiology, Harvard Medical School, Brookline, MA, USA

[4]University of Texas Health Science Center at Houston, TX, USA

[a]Chapter under review in NeuroImage.

Abstract

Several neuroimaging studies have reported significant changes with disease in metrics derived from diffusion tensor imaging (DTI), in particular fractional anisotropy (FA) and mean diffusivity (MD), within gray and white matter. Subject head motion during DTI acquisition can result in significant changes in FA and MD values. The purpose of this study is to highlight potential misinterpretation of FA and MD values that may occur as a result of subject head motion as well as to compare the effects of retrospective and prospective motion correction on these metrics. Six healthy adult subjects were scanned using (1) the standard diffusion sequence, (2) the navigated sequence without prospective motion correction, (3) the prospectively corrected navigated diffusion sequence with reacquisition, and (4) a multiecho MPRAGE sequence. FreeSurfer was used to extract volumes of interest from the structural data. In the white matter, motion caused a significant reduction in mean FA and the FA histogram peak location. In many gray matter regions, motion caused a significant increase in the mean FA and the FA histogram peak location, while MD increased slightly with motion. Retrospective motion correction resulted in a decrease in mean FA and the FA histogram peak location in white and gray matter independent of motion, and resulted in spurious fiber tracks in the corpus callosum.

These results demonstrate that subject head motion during DTI acquisition can cause significant errors in the quantitative DTI measures even with retrospective motion correction. The prospectively corrected navigated diffusion sequence with reacquisition recovers the DTI data remarkably, especially when all motion corrupted volumes have been reacquired. Abnormal DTI data should be interpreted with caution when motion may have occurred during acquisition.

Key Words: diffusion tensor imaging, prospective acquisition correction (PACE), standard diffusion sequence (basic), prospectively corrected diffusion sequence with reacquisition (vNav), whole brain histogram (WBH), fractional anisotropy (FA), mean diffusivity (MD).

3.1 Introduction

Diffusion tensor imaging (DTI) is becoming increasingly important in the assessment of many neurological diseases (Clark et al., 2000; Ellis et al., 1999; Klingberg et al., 2000; Lim et al., 1999; Mukherjee et al., 2000; Rose et al., 2008; Tievsky et al., 1999) and in advancing our understanding of human brain development and aging (Hasan et al., 2011; Neil et al., 1998; Snook et al., 2005). The basic principle of diffusion imaging is to measure signal attenuation due to the random thermal motion of water in cerebral tissue. When water movement is restricted in a specific direction, such as occurs in white matter (WM), diffusion is referred to as being anisotropic. When water diffuses freely and equally in all directions, as is the case with cerebrospinal fluid (CSF), this is referred to as isotropic diffusion. DTI provides many quantitative parameters, in particular fractional anisotropy (FA) and mean diffusivity (MD). FA is one of the most widely used parameters derived from DTI acquisitions (Pierpaoli and Basser, 1996) and provides information about the microstructural integrity of highly oriented microstructures. MD is a measure of average molecular motion independent of any tissue directionality.

Changes in FA and MD values due to brain pathology have been reported in many studies that have implemented different approaches in analysing DTI data. For example, Rose at al. (2008) studied patients with Alzheimer's disease (AD) using an automated voxel-based morphometric method and found significantly elevated MD in regions such as hippocampus, amygdala and significantly reduced FA in regions such as thalamus, parietal white matter and posterior limbs of the internal capsule. A study of schizophrenic patients (Foong et al., 2000) reported significantly increased MD and significantly reduced FA in the splenium of the corpus callosum. Whole brain histogram FA and MD of the gray and white matter in patients with multiple sclerosis were analysed by Cercignani et al. (2001). The authors found that patients with multiple sclerosis have a significantly lower histogram average FA and peak location and a significantly higher peak height. In a study of traumatic brain injury (TBI), Benson et al. (2007) found that patient whole brain white matter FA histograms were globally decreased compared with those of control subjects. The shape of the TBI histograms also differed from controls, being more peaked and skewed with a leftward shift in the FA histogram peak location.

Application of DTI in clinical or research areas relies completely on the accuracy of the diffusion tensor, which in turn depends on the quality of the diffusion volume images. Head motion during

DTI acquisition can cause misalignment of diffusion volumes and result in significant changes in the diffusion tensor. Substantial motion may also cause signal dropout in some diffusion volumes, resulting in miscalculation of the diffusion derived metrics.

While an appropriate tool may be used to correct for subject motion, dropout slices are more problematic. Dropout slices refer to slices with very low SNR due to motion during switching on of the diffusion encoding gradients. There is no way to compensate for dropout slices other than reacquisition (Benner et al., 2010; Kober et al., 2011; Alhamud et al., 2012).

Previously, volumetric navigators were introduced (Alhamud et al., 2012) to perform prospective motion correction in DTI. The FA and MD histograms of the whole brain (WBH-FA and WBH-MD) were analysed with motion, retrospective motion correction, and prospective motion correction, both with and without reacquisition of the motion corrupted diffusion volumes. Motion caused significant reduction in the mean FA of the whole brain histogram, while the mean MD of the whole brain increased significantly. At boundaries between white and grey matter, motion may increase FA in grey matter regions by introducing some orientational-dependence, while in white matter regions, FA may be decreased due to white matter being displaced by isotropic grey matter. This was clearly evident in figure 2.7(a) that showed how the distribution of FA in the whole brain changed from 2 distinct peaks to a single Gaussian in the presence of motion. Retrospective motion correction using FLIRT in FSL (FMRIB Software Library; http://www.fmrib.ox.ac.uk/fsl) and statistical parametric mapping (SPM) failed to recover the DTI parameters. The previous study also highlighted that the FA histogram's peak location is one of the most sensitive and reliable measures of motion. Motion caused a leftward shift in the FA peak location of the WBH and further shift with retrospective motion correction.

Approaches that have been used to analyze and extract information from DTI data include histograms, manual or automatic placement of regions-of-interest (ROI), voxel-based morphometry and tractography. In most of these methods, retrospective motion correction is used to correct for the misalignment in the diffusion volumes due to subject head motion. Generally, retrospective techniques have many limitations in the co-registration of conventional MR images, including blurring artifacts (Tong and Cox, 1999) and the influence of through-plane motion on the local history of magnetization (Muresan et al., 2005). Retrospective techniques face greater difficulties with diffusion weighted imaging (DWI), especially diffusion weighting with high b-values (Rohde et al., 2004).

The purpose of this study is to investigate the use of volumetric navigators using automatic tissue segmentation, provided by FreeSurfer, to explore changes in regional FA and MD measures in gray and white matter resulting from subject head motion, to compare the performance of retrospective motion correction to prospective motion correction on these measures, and to highlight potential misinterpretations that may occur in the presence of motion.

3.2 Material and Methods:

3.2.1 Navigated diffusion pulse sequence with 3D-EPI Navigator and reacquisition

A twice-refocused two-dimensional diffusion pulse sequence (Reese et al., 2003) was previously modified to acquire an additional 3D-EPI navigator (526 ms) following the acquisition of each diffusion volume (Alhamud et al., 2012). The volumetric navigator contains 3D anatomical information for direct computation of motion parameters, and is not diffusion weighted, therefore the accuracy of co-registration and motion estimates are not affected by the diffusion gradients, even at high b-values. The diffusion sequence was further modified to reacquire motion corrupted diffusion volumes during which the motion exceeded a pre-defined threshold.

3.2.2 MRI Data Acquisition

Scans were performed on a 3 T Allegra (Siemens Healthcare, Erlangen, Germany) scanner at the Cape Universities Brain Imaging Centre. Six healthy male subjects (age 24-30 years) were scanned. All subjects provided informed written consent prior to scanning according to protocols that had been approved by the Faculty of Health Sciences Human Research Ethics Committee of the University of Cape Town, South Africa.

T1-weighted Structural Acquisition

A motion navigated three dimensional multi-echo magnetization prepared rapid gradient echo (MEMPR) sequence (van der Kouwe et al., 2008) was used to acquire the structural T1-weighted image. This sequence uses volumetric navigators to ensure a consistent coordinate system from the start of the MEMPR. The MEMPR protocol was the same for all subjects: TR = 2530 ms, TE = 6.57 ms, TI = 1100 ms, flip angle = 7 degrees, slice thickness 1.3 mm, acquisition matrix size = 256 x 256 x 128, FOV 25.6 x 25.6 x 16.6 cm^3.

Diffusion Sequence Data Acquisition

The 3D-EPI navigator parameters were the same for all scans. The acquisition parameters for the navigator were: TR = 14 ms, TE = 6.6 ms, voxel size = 8 x 8 x 8 mm^3, acquisition matrix size = 32 x 32 x 28, FOV 256 x 256 x 224 mm^3, bandwidth in the readout direction = 3906 Hz/px, flip angle = 2 degrees, and total scan time = 406 ms. The acquisition parameters for the diffusion sequence were: TR = 9500 ms without the navigator (basic sequence), TR = 10026 ms with the navigator and delay for computation and feedback (vNav sequence), TE = 86 ms, 72 slices, matrix size = 112 x 112, FOV 224 x 224 mm in-plane, single channel birdcage head coil, slice thickness = 2 mm, 30 non-collinear diffusion gradient directions, b-values 0 and 1000 s mm^{-2}, and four low b-value scans. The waiting period for feedback (including all navigator-related computations in the sequence and in ICE) is 120 ms for each repetition time. Reacquisition was enabled with five reacquisitions.

The experimental protocol comprised 4 different DTI acquisitions: *at rest* (no motion) baseline scans were acquired with the basic diffusion sequence (**NoMo_basic**) and with the navigated sequence without prospective motion correction (**NoMo_vNav_NoCo**); a scan during which the subject moved, acquired with the basic sequence (**Mo_basic**); and a scan during which the subject moved, acquired using the navigated diffusion sequence with prospective motion correction and reacquisition (**Mo_vNav_all**). For the scans with motion, the subjects were instructed to change their head position upon verbal instruction five to six times during the scan. The subjects were asked to repeat the same movements for each of the scans acquired with motion. The total scan time without the navigator was 5 minutes and 33 seconds, with the navigator it was 5 minutes and 50 seconds, and with five reacquisitions it was 6 minutes and 40 seconds.

3.2.3 Data Processing

Processing of T1-weighted structural scan

The T1-weighted image for each subject was automatically segmented into cortical and sub-cortical regions using the FreeSurfer (http://surfer.nmr.mgh.harvard.edu/) software library. FreeSurfer was used in the current study as it has been tested extensively for accuracy and reliability (Fischl et al., 2002; Walimuni et al., 2010). The outcome of the segmentation process

is an atlas comprising 175 WM, GM and CSF regions with a unique label assigned to each region. Since the generated atlas was in FreeSurfer space, the "mri_convert" tool within Freesurfer was used to transfer the segmented regions from FreeSurfer space to T1 or subject space. The "fslmaths" tool within FSL, "mri_convert" within FreeSurfer, and bash scripts developed in-house were implemented to extract and create a binary mask for each volume of interest (VOI) in gray and white matter.

The VOI's that were analysed in the current study were whole brain white matter, corpus callosum (CC), left amygdala (LA), right amygdala (RA), left caudate (LC), right caudate (RC), left hippocampus (LH), right hippocampus (RH), left pallidum (LP), and right pallidum (RP).

Processing of Diffusion Data

Diffusion volumes were processed after conversion from DICOM format to NifTi using FreeSurfer tools. The diffusion data from all subjects was quantified using Diffusion Toolkit (http://trackvis.org/) which generates all the diffusion maps from the NifTi data. Retrospective motion correction using FMRIB's linear registration tool (FLIRT) was only performed on the **Mo_basic** acquisitions to align all the diffusion volumes to the b0 volume with a least squares cost function and 6 degrees of freedom.

Volume of Interest Analyses

The T1-weighted structural volume was registered to the T2-weighted (b0) volume using FSL tools; FMRIB's linear registration tool (FLIRT) was followed by a non-linear registration using FMRIB's non-linear image registration tool (FNIRT). The outcome of the non-linear registration was the field coefficients which were calculated in the diffusion space. The 'invwarp' tool within FSL was implemented to transfer the field back to the T1 space. The new inverted deformation matrix in the T1 space was applied to the FA and MD maps to transform them into the T1 space using the "applywarp" tool in FSL.

The binary masks that were created previously were applied to the FA and MD maps using the "fslmaths" tool in FSL. The FA and MD histograms for each VOI for each subject were generated and the mean histogram parameters were calculated. The average histogram parameters of each VOI for the six subjects for each acquisition were compared with those of the

at rest baseline (**NoMo_vNav_NoCo**) scan using a paired student's t-test. P-values less than 0.01 were considered statistically significant.

In order to reduce possible WM partial volume effects in the gray matter, the calculations were repeated for each VOI after applying FA < 0.2 thresholding to the gray matter masks. Similarly, a threshold of FA > 0.2 was applied to white matter masks. The corresponding FA pixels (those affected by thresholding) were mapped on the MD maps. The size of the volume before and after FA threshold was calculated in Matlab by counting the number of pixels in the volume of interest multiplied by $1 \times 1 \times 1.3$ mm^3, which is the dimension of the voxel in the T1-weighted image.

Diffusion Tensor Tractography

Diffusion tensor reconstruction and whole-brain fiber tractography was calculated using Diffusion Toolkit. The deterministic Fiber Assignment by Continuous Tracking (FACT) algorithm was applied using the entire diffusion-weighted volume as the mask image, the threshold angle (AT) of 35° was chosen and the spline filter was applied. The drawback of increasing the angle threshold is that the number of spurious tracts also increases. The recommended values of angle threshold are between 30º and 40 º to provide sufficient fiber density while minimizing the number of spurious tracts (Parizel et al., 2007).

Compact fiber tracking of the whole volume of the corpus callosum (CC) was performed using the TrackVis tool. Compact white matter refers to regions where the fibers are positioned closely such as the corpus callosum, the internal capsule and the cerebral peduncles, while non-compact white matter is present in regions such as the corona radiata and peripheral white matter. The mask of the CC for each subject and for each acquisition that was generated in the previous step was transformed to the diffusion space using the non-inverted field coefficients with the "applywarp" tool. The CC mask was further thresholded to eliminate all pixels with FA < 0.2.

The FA histogram of the whole CC and for each subject was created by the TrackVis tool. TrackVis measured the mean FA for each track in the bundle. Each track represents a single data point; the data points were binned to create the histogram. Each histogram contained 25 bins, for each of which the values were normalized by the total number of tracks estimated by TrackVis.

3.3 Results

Whole Brain White Matter Analysis

Tables 3.1 a and b give the FA histogram parameters of the whole brain WM, averaged for all six subjects for the different acquisitions before and after thresholding, respectively, as well as the values obtained after applying retrospective motion correction. The normalized FA histograms of the six subjects for the different acquisitions were averaged, before and after applying the white matter threshold and are shown in Figures 3.1a,b, respectively. It is clear that motion causes significant changes in all the FA histogram parameters when compared to the *at rest* baseline scan (**NoMo_vNav_NoCo**), and that these parameters are not recovered with retrospective motion correction. In contrast, the shape and the parameters of the FA distribution are almost fully recovered when using the navigated prospective motion corrected sequence with reacquisition (Mo_vNav_all).

Table 3.1

Comparison of the FA histogram parameters for the whole brain white matter averaged across all six subjects for the different acquisitions without FA thresholding in (a) and after thresholding in (b) (FA > 0.2).

(a) Mean FA histogram Parameters (no FA threshold)					
	NoMo_basic	NoMo_vNav _NoCo	Mo_basic	Mo_basic_ Retro_FLIRT	Mo_vNav_all
Mean FA (SD)	0.42 (0.01)	0.42 (0.01)	0.39 * (0.01)	0.343* (0.01)	0.42 (0.01)
Peak Location (SD)	0.39 (0.02)	0.40 (0.00)	0.35 * (0.00)	0.30 * (0.00)	0.39 (0.02)
(b) Mean FA histogram Parameters (after FA threshold)					
Mean FA (SD)	0.44 (0.01)	0.44 (0.01)	0.41 * (0.01)	0.38 * (0.01)	0.43 (0.01)
Peak Location (SD)	0.39 (0.02)	0.40 (0.00)	0.35 * (0.00)	0.30 * (0.00)	0.39 (0.02)

Values are means (SD).
*$p < 0.01$ (student's paired t-test compared to NoMo_vNav_NoCo).

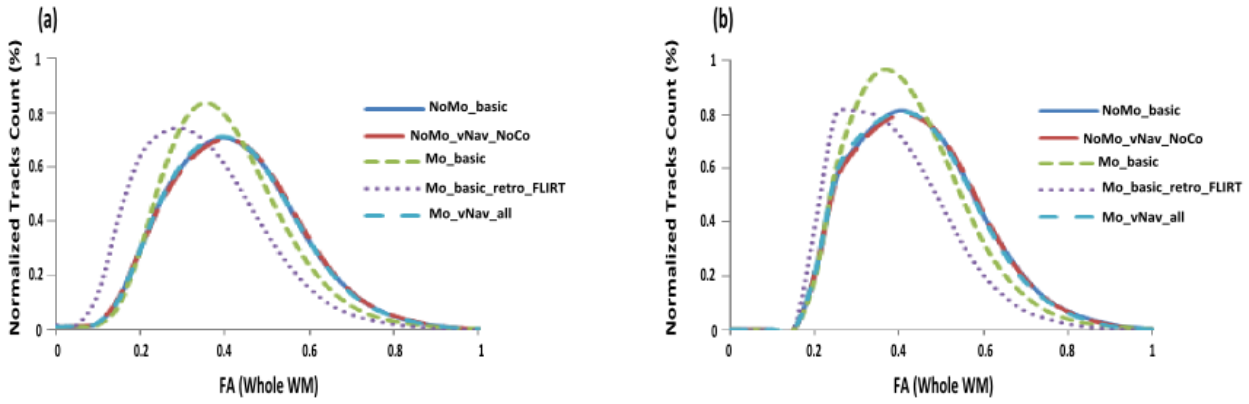

Figure 3.1: (a) Comparison of the whole brain white matter FA histograms averaged over all six subjects before applying an FA threshold and for the different acquisitions: the basic diffusion sequence (NoMo_basic), the navigated sequence without prospective motion correction (NoMo_vNav_NoCo), the basic diffusion sequence with motion (Mo_basic), the basic diffusion sequence with motion and retrospective motion correction (Mo_basic_retro_FLIRT), and the navigated sequence with prospective motion correction and reacquisition (Mo_vNav_all). (b) The same as in 'a' after applying an FA threshold (FA > 0.2).

Table 3.2 shows the mean MD histogram parameters for the whole WM volume, averaged over all six subjects, for the different acquisitions, before and after thresholding, respectively, as well as the values obtained after applying retrospective motion correction. Figure 3.2 shows the normalized MD histograms for the whole brain WM, averaged across all six subjects for the different acquisitions without white matter thresholding.

Table 3.2

Comparison of the MD ($x10^{-3}$) histogram parameters for the whole brain white matter averaged across all six subjects for the different acquisitions without FA thresholding in (a) and after thresholding in (b) (FA > 0.2).

(a) Mean MD histogram Parameters (no FA threshold)					
	NoMo_basic	NoMo_vNav _NoCo	Mo_basic	Mo_basic_ Retro_FLIRT	Mo_vNav_all
Mean FA (SD)	0.79 (0.01)	0.80 (0.01)	0.79 (0.01)	0.80 (0.01)	0.81 (0.01)
Peak Location (SD)	0.75 (0.00)	0.76 (0.02)	0.75 (0.00)	0.75 (0.00)	0.77 (0.03)
(b) Mean MD histogram Parameters (after FA threshold)					
Mean FA (SD)	0.79 (0.01)	0.80 (0.01)	0.78 (0.01)	0.78 * (0.01)	0.81 (0.02)
Peak Location (SD)	0.75 (0.00)	0.75 (0.00)	0.75 (0.00)	0.75 (0.00)	0.78 (0.03)

Values are means (SD).
*$p < 0.01$ (student's paired t-test compared to NoMo_vNav_NoCo).

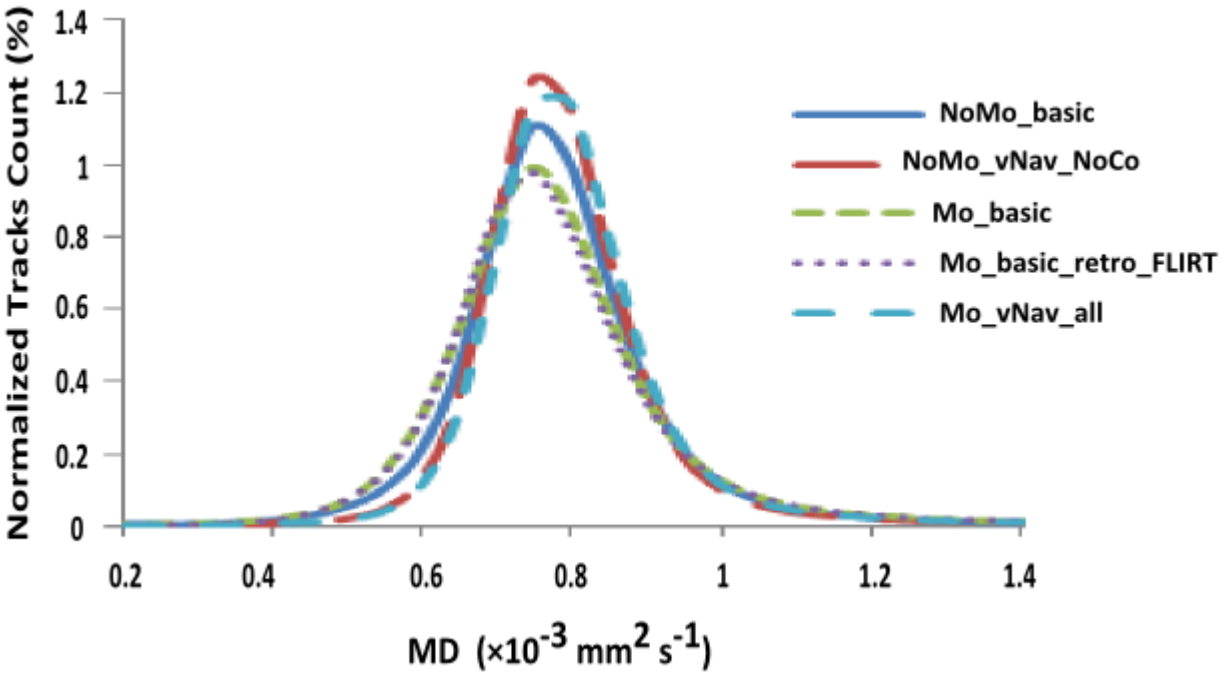

Figure 3.2: Comparison of the whole brain white matter MD histograms averaged over all six subjects for the different acquisitions without FA thresholding: the basic diffusion sequence (NoMo_basic), the navigated sequence without prospective motion correction (NoMo_vNav_NoCo), the basic diffusion sequence with motion (Mo_basic), the basic diffusion sequence with motion and retrospective motion correction (Mo_basic_retro_FLIRT), and the navigated sequence with prospective motion correction and reacquisition (Mo_vNav_all).

Table 3.3 compares the whole brain white matter volume averaged over all subjects for the different acquisitions, before and after applying the FA threshold. Applying the FA threshold reduces partially the whole brain white matter volume and significantly so with retrospective motion correction.

Table 3.3

The whole brain white matter volume (cm^3) compared for the different acquisitions before and after FA thresholding (FA > 0.2).

	NoMo_basic	NoMo_vNav _NoCo	Mo_ basic	Mo_basic _retro_FLIRT	Mo_vNav_ all
Volume before FA thresholding in cm^3 (SD)	585 (56)	585 (56)	584 (54)	579 (53)	583 (54)
Volume after thresholding in cm3 (FA > 0.2) (SD)	555 (55)	554 (54)	557 (52)	483 * (45)	553 (52)

Values are means (SD).
*$p < 0.01$ (student's paired t-test compared to NoMo_vNav_NoCo).

Corpus Callosum Fractional Anisotropy and Tractography

Figure 3.3 shows the averaged FA histograms of the whole CC of the six subjects for the different acquisitions as well as the histogram obtained after applying retrospective motion correction. The histograms were calculated using the TrackVis program and normalized for the total number of tracks. The FA histograms for scans with motion and retrospective motion correction show a leftward shift in the FA histogram peak location towards lower anisotropy.

Figure 3.4 illustrates for one subject how motion reduces the number of tracks in the CC, especially in the anterior regions, when compared to at rest baseline scans. All the other subjects show similar reduction in number of tracks with motion. The FA histogram and the tracks of the CC are recovered substantially with the Mo_vNav_all scan. Further, it is evident in figure 3.4(e) that standard retrospective motion correction introduces spurious results.

Figure 3.5 shows for one subject the effect of the FA threshold on the volume of the whole CC for the different acquisitions. The volume of the CC with motion was not influenced by the FA thresholding since FA everywhere in the CC exceeds the threshold of 0.2.

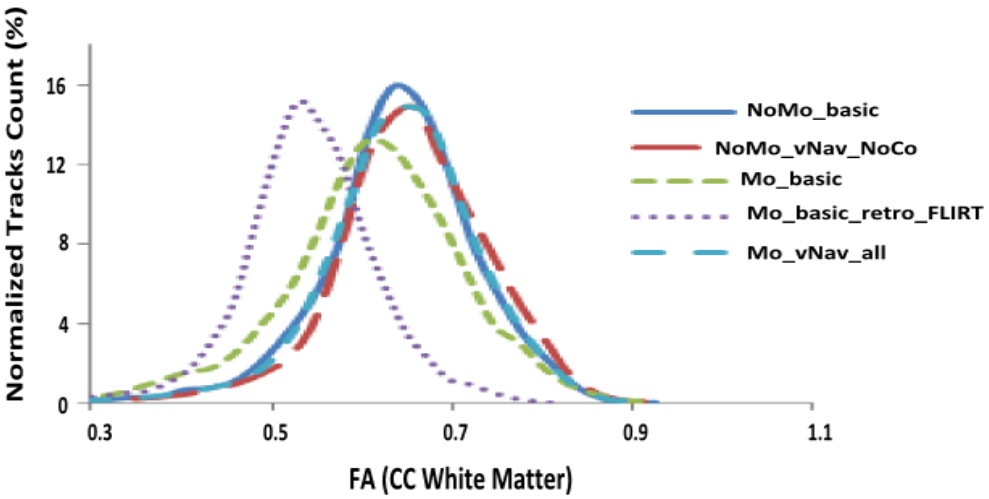

Figure 3.3: Comparison of histograms of the averaged FA for the six subjects over the whole volume of the corpus callosum CC for the different acquisitions; the basic diffusion sequence (NoMo_basic), with the navigated sequence without prospective motion correction (NoMo_vNav_NoCo), the basic diffusion sequence with motion (Mo_basic), the basic diffusion sequence with motion and retrospective motion correction (Mo_basic_retro_FLIRT), the navigated sequence with prospective motion correction and reacquisition (Mo_vNav_all). The histograms of the CC were generated by TrackVis software.

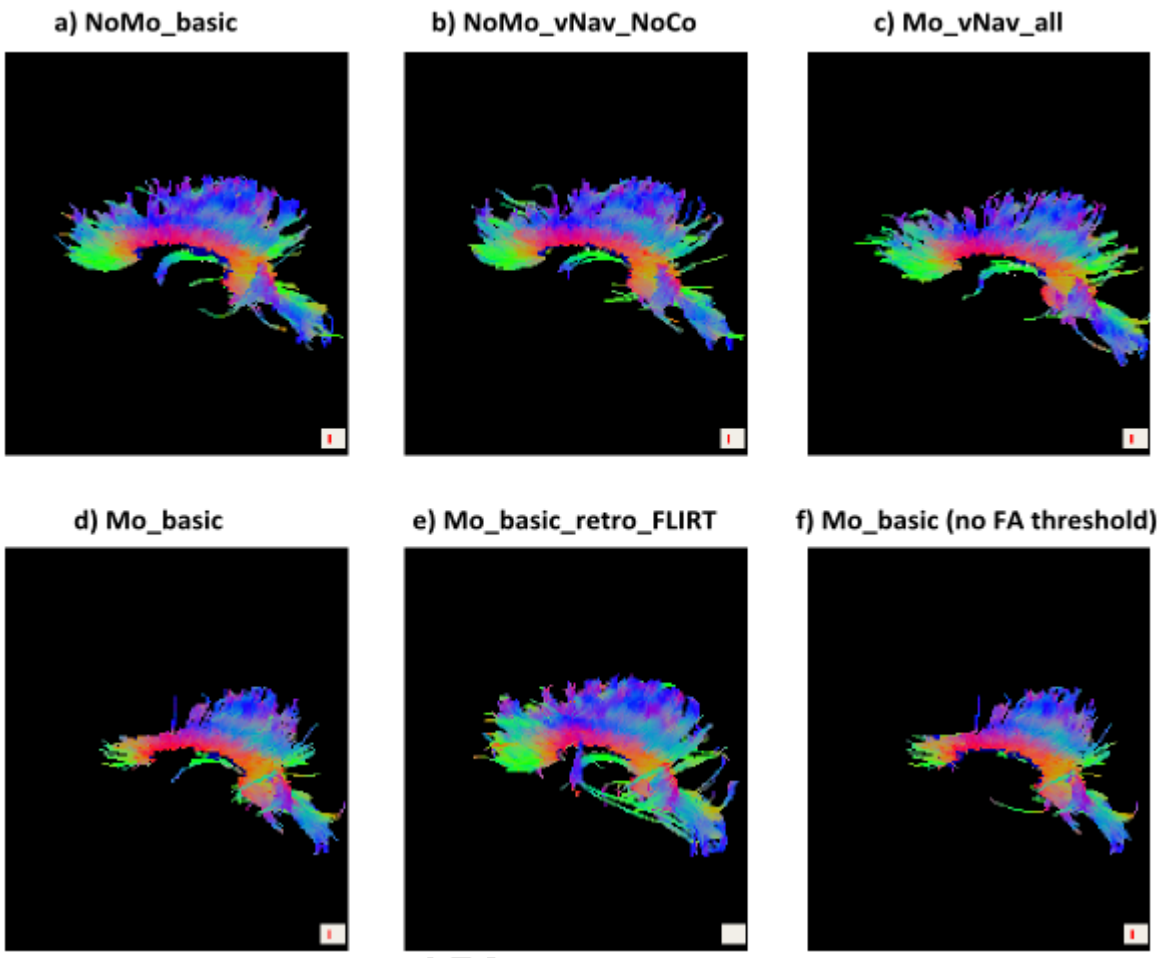

Figure 3.4: Illustration of the fiber tracks of the whole CC for one subject and for the different acquisitions after FA thresholding (i.e. FA > 0.2); (a) the at rest baseline scan with the basic diffusion sequence (NoMo_basic), (b) the navigated sequence without prospective motion correction (NoMo_vNav_NoCo), (c) the navigated sequence with prospective motion correction and reacquisition (Mo_vNav_all), (d) the basic diffusion sequence with motion (Mo_basic), (e) the basic diffusion sequence with motion and retrospective motion correction (Mo_basic_retro_FLIRT), (f) the same as in 'd' but without applying an FA threshold. The number of tracks for each acquisition was 4259, 4028, 3948, 3330, 5676, and 3647, respectively.

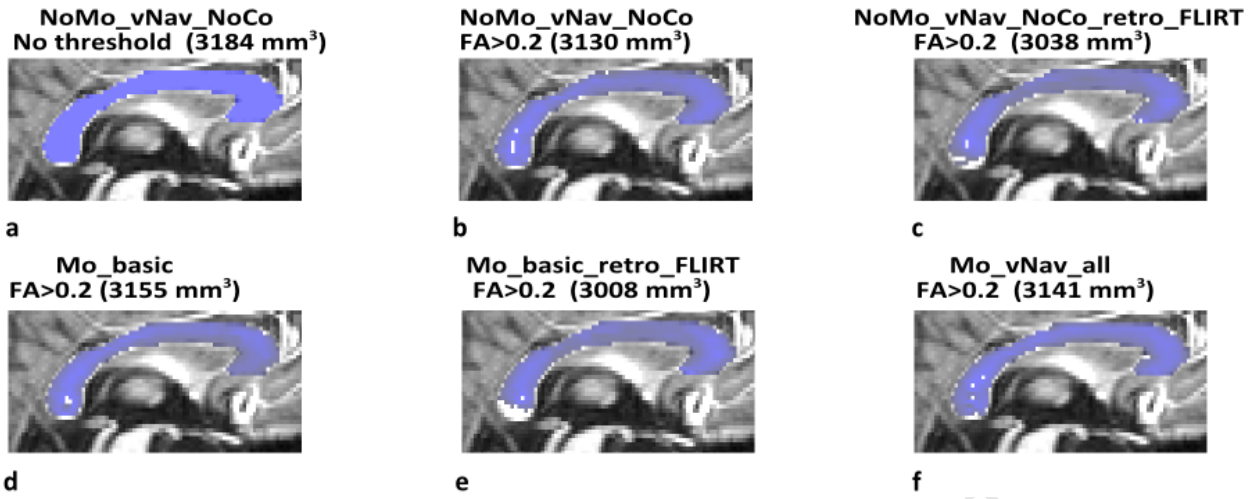

Figure 3.5: Comparison of the effect of FA thresholding on the volume of the CC, overlaid on the T1-weighted mid-sagittal slice, for one subject and for the different acquisitions: (a) the basic navigated sequence (NoMo_vNAv_NoCo) with no threshold, (b) the basic navigated sequence (NoMo_vNav_NoCo) with FA>0.2, (c) the same as in 'b' with retrospective motion correction, (d) the basic diffusion sequence with motion (Mo_basic) and with FA>0.2, (e) the basic sequence with motion and retrospective motion correction (Mo_basic_retro_FLIRT), and (f) the navigated sequence with prospective motion correction, reacquisition (Mo_vNav_all) and with FA>0.2. FLIRT was also applied to NoMo_vNav_NoCo with another cost function the mutual information, 12 degrees of freedom and the volume of the CC with FA>0.2 was 3120 mm^3.

Analysis of Gray Matter Volumes of Interest

Table 3.4 compares the effect of FA thresholding (include only voxels with FA < 0.2) on the VOI's in gray matter. FA thresholding caused a reduction in the volume size for most regions in gray matter and a further significant reduction in the presence of motion.

Table 3.4

Comparison of volumes for VOI's in gray matter (mm^3) for the different acquisitions before and after FA thresholding (FA < 0.2). Left amygdala (LA), left caudate (LC), left hippocampus (LH), left pallidum (LP), right amygdala (RA), right caudate (RC), right hippocampus (RH), and right pallidum (RP).

	No FA threshold[a]	After FA thresholding (FA <0.2)[b]				
VOI	Volume[a]	NoMo_ basic	NoMo_vNav _NoCo	Mo_ basic	Mo_basic_ Retro_FLIRT	Mo_vNav_ all
LA	1697	696	755	257 *	1133 *	724
	(89)	(143)	(185)	(99)	(68)	(187)
LC	3938	1596	1726	474 *	2136	1502
	(429)	(346)	(204)	(145)	(599)	(393)
LH	4285	1856	2036	1083 *	2884 *	1999
	(208)	(520)	(384)	(270)	(286)	(284)
LP	1846	147	174	72 *	406 *	149
	(130)	(56)	(30)	(30)	(76)	(40)
RA	1798	658	782	250 *	1302 *	796
	(235)	(260)	(145)	(151)	(169)	(189)
RC	3919	1599	1756	596 *	2177	1533
	(369)	(301)	(470)	(184)	(293)	(374)
RH	4481	2011	2267	1261 *	3169 *	2125
	(250)	(582)	(431)	(213)	(391)	(256)
RP	1636	97	114	63	300	100
	(161)	(72)	(71)	(72)	(165)	(68)

Note. [a]Without FA thresholding, the volumes are the same for the different acquisitions.
[b]With FA thresholding, the volumes differ for the different acquisitions.
Values are means (SD)
*$p < 0.01$ (student's paired t-test compared to NoMo_vNav_NoCo).

Figure 3.6 illustrates clearly the effect of the FA threshold on the volume size for left and right caudate and for the different acquisitions. Tables 3.5 and 3.6 give the mean FA and FA histogram peak locations, respectively, for different VOI's in gray matter structures, averaged across all six subjects for the different acquisitions before and after thresholding, as well as the

values obtained after applying retrospective motion correction. Motion in gray matter caused an opposite change to that in the white matter, elevating both the mean FA and the FA histogram peak location.

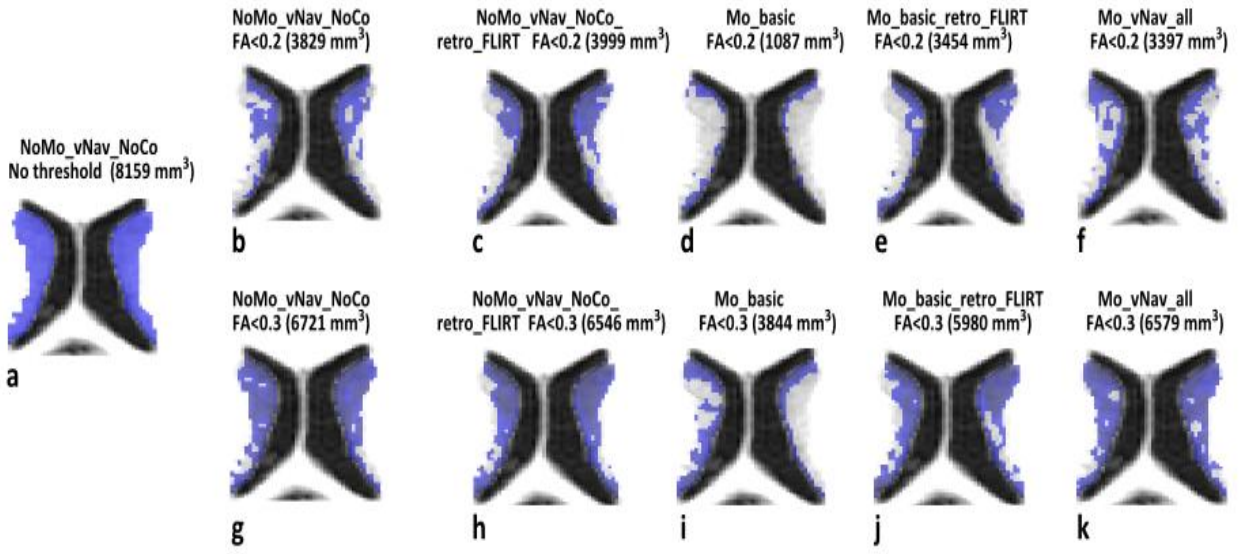

Figure 3.6: Comparison of the effect of two different FA thresholding values on the volume of the caudate, overlaid on the corresponding T1-weighted axial slice, for one subject and for the different acquisitions: (a) the basic navigated sequence (NoMo_vNAv_NoCo) with no threshold, (b) the basic navigated sequence (NoMo_vNAv_NoCo) with FA<0.2, (c) the same as in 'b' with retrospective motion correction, (d) the basic diffusion sequence with motion (Mo_basic) and with FA<0.2, (e) the basic diffusion sequence with motion and retrospective motion correction (Mo_basic_retro_FLIRT) with FA<0.2, (f) the navigated sequence with prospective motion correction and reacquisition (Mo_vNav_all) with FA<0.2. 'g, h, i, j and k' are the same as 'b, c, d, e and f' but with FA<0.3. FLIRT was also applied to NoMo_vNav_NoCo with a mutual information cost function, 12 degrees of freedom and the Caudate volume was 5100 mm^3 for FA<0.2 and 7259 mm^3 for FA<0.3.

Table 3.5

Comparison of the mean FA for different VOI's in gray matter averaged over all six subjects for the different acquisitions before applying the FA threshold in (a), and after thresholding in (b) (FA < 0.2).

VOI	NoMo_basic	NoMo_vNav _NoCo	Mo_basic	Mo_basic_ Retro_FLIRT	Mo_vNav_all
(a) Mean FA (no FA thresholding)					
LA	0.23 (0.02)	0.22 (0.02)	0.30 * (0.03)	0.18 * (0.01)	0.23 (0.01)
LC	0.24 (0.02)	0.23 (0.01)	0.32 * (0.03)	0.21 (0.03)	0.24 (0.02)
LH	0.23 (0.02)	0.22 (0.01)	0.27 * (0.01)	0.18 * (0.01)	0.23 (0.01)
LP	0.36 (0.03)	0.34 (0.02)	0.41* (0.03)	0.33 (0.04)	0.36 (0.03)
RA	0.24 (0.03)	0.23 (0.01)	0.30 * (0.03)	0.17 * (0.01)	0.23 (0.01)
RC	0.23 (0.01)	0.23 (0.02)	0.30 * (0.03)	0.21 (0.02)	0.24 (0.02)
RH	0.23 (0.02)	0.22 (0.02)	0.26 * (0.01)	0.18 * (0.02)	0.23 (0.01)
RP	0.37 (0.05)	0.35 (0.03)	0.39 (0.05)	0.34 (0.04)	0.37 (0.04)
(b) Mean FA (after FA thresholding)					
LA	0.17 (0.01)	0.16 (0.01)	0.17 (0.00)	0.15 * (0.01)	0.16 (0.01)
LC	0.16 (0.01)	0.16 (0.00)	0.17 (0.01)	0.14 * (0.01)	0.16 (0.00)
LH	0.16 (0.01)	0.16 (0.01)	0.17 (0.00)	0.14 * (0.01)	0.16 (0.01)
LP	0.16 (0.02)	0.16 (0.01)	0.16 (0.02)	0.15 (0.00)	0.17 (0.01)
RA	0.16 (0.01)	0.16 (0.01)	0.17 (0.00)	0.14 * (0.01)	0.16 (0.00)
RC	0.16 (0.00)	0.16 (0.01)	0.17 * (0.00)	0.15 * (0.00)	0.16 (0.00)
RH	0.16 (0.01)	0.16 (0.01)	0.16 (0.00)	0.14 * (0.01)	0.16 (0.00)
RP	0.17 (0.01)	0.16 (0.01)	0.16 (0.02)	0.16 (0.00)	0.17 (0.01)

Values are means (SD).
*$p < 0.01$ (student's paired t-test compared to NoMo_vNav_NoCo).

Table 3.6

Comparison of the mean FA histogram peak locations for different VOI's in gray matter structures averaged over all six subjects for the different acquisitions before applying the FA threshold in (a), and after thresholding in (b) (FA < 0.2).

(a) Mean FA histogram peak location (no FA threshold)					
VOI	NoMo_basic	NoMo_vNav _NoCo	Mo_basic	Mo_basic_ Retro_FLIRT	Mo_vNav_all
LA	0.20 (0.00)	0.20 (0.03)	0.27 (0.05)	0.16 (0.02)	0.18 (0.03)
LC	0.19 (0.02)	0.20 (0.00)	0.30 (0.07)	0.14 * (0.02)	0.22 (0.04)
LH	0.18 (0.03)	0.18 (0.03)	0.23 (0.04)	0.15 (0.00)	0.18 (0.03)
LP	0.30 (0.04)	0.33 (0.04)	0.36 (0.05)	0.21 * (0.04)	0.32 (0.05)
RA	0.22 (0.03)	0.18 (0.03)	0.28 * (0.03)	0.15 (0.00)	0.19 (0.02)
RC	0.20 (0.00)	0.19 (0.02)	0.28 (0.05)	0.16 (0.02)	0.21 (0.02)
RH	0.19 (0.02)	0.18 (0.03)	0.21 (0.02)	0.14 * (0.02)	0.19 (0.02)
RP	0.33 (0.06)	0.33 (0.04)	0.38 (0.07)	0.24 * (0.07)	0.33 (0.06)
(b) Mean FA histogram peak location (after FA threshold)					
LA	0.16 (0.02)	0.17 (0.03)	0.18 (0.03)	0.15 (0.00)	0.17 (0.03)
LC	0.15 (0.00)	0.15 (0.00)	0.18 (0.03)	0.14 (0.02)	0.15 (0.00)
LH	0.15 (0.00)	0.15 (0.00)	0.17 (0.03)	0.15 (0.00)	0.15 (0.00)
LP	0.19 (0.02)	0.18 (0.03)	0.18 (0.03)	0.15 (0.00)	0.19 (0.02)
RA	0.16 (0.02)	0.15 (0.00)	0.18 (0.03)	0.15 (0.00)	0.15 (0.00)
RC	0.15 (0.00)	0.15 (0.00)	0.18 (0.03)	0.15 (0.00)	0.15 (0.00)
RH	0.15 (0.00)	0.15 (0.00)	0.16 (0.02)	0.14 (0.02)	0.15 (0.00)
RP	0.19 (0.02)	0.19 (0.02)	0.20 (0.00)	0.16 (0.02)	0.19 (0.02)

Values are means (SD).
*$p < 0.01$ (student's paired t-test compared to NoMo_vNav_NoCo).

Table 3.7(a) and (b) show for the different acquisitions the mean MD averaged over all subjects for the different VOI's in gray matter structures, before and after thresholding, respectively. Motion generally caused a slight increase in the mean MD, which was only significant in the LC and the LH.

Table 3.7

Comparison of the mean MD ($x10^{-3}$) for different VOI's in the gray matter structures averaged for the six subjects for different acquisitions without and with thresholding.

VOI	NoMo_basic	NoMo_vNav _NoCo	Mo_basic	Mo_basic_ Retro_FLIRT	Mo_vNav_all
(a) Mean MD (no FA threshold)					
LA	1.07 (0.15)	1.00 (0.13)	1.07 (0.12)	1.00 (0.09)	1.00 (0.09)
LC	1.15 (0.10)	1.11 (0.04)	1.25 * (0.10)	1.09 (0.04)	1.14 (0.03)
LH	1.12 (0.06)	1.11 (0.05)	1.16 * (0.08)	1.10 (0.05)	1.11 (0.05)
LP	0.77 (0.05)	0.78 (0.04)	0.75 (0.02)	0.73 * (0.04)	0.79 (0.02)
RA	1.04 (0.10)	1.06 (0.15)	1.07 (0.08)	0.99 (0.06)	0.98 (0.07)
RC	1.14 (0.10)	1.11 (0.09)	1.17 (0.10)	1.08 (0.05)	1.12 (0.08)
RH	1.13 (0.08)	1.11 (0.08)	1.14 (0.08)	1.10 (0.06)	1.11 (0.07)
RP	0.77 (0.02)	0.77 (0.02)	0.72 (0.04)	0.71 * (0.04)	0.77 (0.02)
(b) Mean MD (after FA threshold)					
LA	1.16 (0.20)	1.06 (0.12)	1.03 (0.14)	1.03 (0.11)	1.07 (0.12)
LC	1.33 (0.10)	1.28 (0.06)	1.74 (0.35)	1.25 (0.04)	1.36 (0.08)
LH	1.12 (0.07)	1.12 (0.06)	1.09 (0.09)	1.12 (0.04)	1.12 (0.06)
LP	0.66 (0.24)	0.72 (0.19)	0.77 (0.25)	0.80 (0.08)	0.78 (0.11)
RA	1.09 (0.15)	1.15 (0.20)	0.97 (0.06)	1.01 (0.07)	1.03 (0.09)
RC	1.28 (0.23)	1.25 (0.13)	1.58 * (0.23)	1.20 (0.13)	1.31 (0.25)
RH	1.11 (0.09)	1.11 (0.07)	1.10 (0.07)	1.12 (0.06)	1.12 (0.07)
RP	0.73 (0.14)	0.67 (0.17)	0.63 (0.23)	0.79 (0.08)	0.73 (0.14)

Values are means (SD)

*$p < 0.01$ (student's paired t-test compared to NoMo_vNav_NoCo).

3.4 Discussion

Accurate diffusion tensor estimation requires that the diffusion-weighted volumes with different diffusion gradient strengths and orientations be aligned accurately with each other. Retrospective motion correction techniques have been used routinely for motion correction in DTI. DTI has been used to study different pathologies and the development of the human brain, and changes in FA and MD values have been widely reported. The principal direction of diffusion, which is calculated from the diffusion tensor and used in tractography, is assumed to represent the orientation of the white matter fiber tracts (Basser et al., 1994). Previously, it was shown that subject head motion and retrospective motion correction causes significant changes in the FA and the MD histogram parameters for the whole brain (Alhamud et al., 2012). These findings are very similar to those reported in studies that have been conducted on patients with neurological diseases (Della Nave et al., 2007; Mori et al., 2008; Zhou et al., 2008).

In this paper, we explored the effects of motion on DTI parameters in both white and gray matter VOI's using automatic tissue segmentation with FreeSurfer.

Data Comparison with a paired student's t-test

In the current studies it was not feasible to monitor the head pose inside the scanner when using the basic diffusion sequence. Even in stationary scans where subjects are instructed to remain still, they may move unexpectedly with resulting changes in the diffusion data. Accordingly, the data were compared to an *at rest* baseline scan that includes navigators (NoMo_vNav_NoCo), thus providing motion parameters without motion tracking even when the subject is purportedly motionless.

Whole Brain White Matter Analysis

Motion and retrospective motion correction caused a significant reduction in the mean FA and the FA histogram peak location (Table 3.1). The FA histogram peak location changed from 0.4 to 0.35 due to motion and to 0.3 after retrospective motion correction.

Motion and retrospective motion correction influenced mainly the shape of the MD histogram distribution rather than the mean and the peak location.

To reduce possible GM-CSF partial volume effects associated with the WM volume, all WM volumes were thresholded to include only pixels with FA > 0.2. Thresholding reduced partially

the white matter volumes (Table 3.3) and this explains why most of the changes in histogram parameters have the same effect with or without FA thresholding even in the presence of motion (Table 3.1a,b and Fig. 3.1a,b). By contrast, with retrospective motion correction because of the smoothing inherent in the interpolation algorithm, the FA values dropped significantly and the white matter volumes and FA histogram parameters were influenced by FA thresholding (Table 3.1b, Table 3.3). The FA histogram peak location was not affected by thresholding even in the case of retrospective motion correction, making it a good marker for detecting the presence of motion in white matter (Table 3.1a,b).

Corpus Callosum Fractional Anisotropy and Tractography

A challenging problem in DTI tractography is to estimate the correct orientation of tracks within a voxel. Tractography is based on measuring the principal direction of diffusion and FA values, both of which are calculated from the diffusion tensor. Misalignment of diffusion volumes causes changes in the DTI derived matrices. To determine whether motion and retrospective motion correction could cause changes and distortion in the tracks of the CC, the FA histogram of the whole CC was analyzed and fiber tracks for the whole CC were generated. Because the pathways traversing the CC have different mean values due to its heterogeneous structure (Hasan et al., 2009b), the FA histogram was calculated using TrackVis software. Motion and retrospective motion correction caused similar distortion and changes in the FA histogram of the CC to that observed in the whole brain white matter, namely reduction in the mean FA and a leftward shift in the FA histogram peak location (Fig. 3.3).

The fiber tracking of the CC showed a significant reduction in the number of tracks, in particular in the anterior region of the CC due to subject motion (Fig. 3.4d). Retrospective motion correction failed to recover the shape of the tracks, apparently even generating spurious tracks, compared to the at rest baseline scan (Fig. 3.4e). This can be attributed to spatial smoothing of the data due to interpolation when realigning the images. A data set with more interpolation/smoothing would produce more streamlines due to the smoothing effect (Freire et al., 2001; Jung KJ, 2010; Ling et al., 2012). The organization of the fiber tracks and the FA histogram properties of the CC were recovered substantially with the navigated diffusion sequence (Mo_vNav_all) (Fig. 3.4c). Not applying a FA threshold to the data acquired in the Mo_basic scan, does not recover the fiber tracks lost due to motion (Fig. 3.4f).

There is not a substantial reduction in the volume of the CC due to FA thresholding even in the presence of motion (Fig. 3.5). With retrospective motion correction and because of the smoothing inherent in the interpolation algorithm, the FA values dropped in some regions of the CC, especially in the anterior region even in the case of an *at rest* baseline (NoMo_vNav_NoCo) scan when applying retrospective motion correction with both cost functions. This reduction in anisotropy might result in spurious tracks.

Analysis of Gray Matter Volumes of Interest

Motion generally produces blurring and edge artifacts that increase the FA values in some voxels in the gray matter volume. In the presence of motion, thresholding the volumes to only include voxels with FA<0.2 further reduces the size of the volume (Fig. 3.6d, Table 3.4b), not due to WM partial volume errors but because motion causes a significant increase in the FA values of a large number of gray matter voxels. The volumes of the gray matter VOI's are significantly reduced after thresholding in the presence of motion compared to non-thresholded volumes (Table 3.4a) or even compared to the *at rest* baseline scan with thresholding (Table 3.4b). Changing the FA threshold to a higher value such as 0.3 shows the same effect of thresholding on volume as illustrated for the caudate in Figure 3.6. In the *at rest* baseline (NoMo_vNav_NoCo) scan, retrospective motion correction and because of the smoothing inherent in the interpolation algorithm, the volume of the caudate increased with FA>0.2 (Fig. 3.6c) and further with a mutual information cost function for both FA thresholds. In the presence of motion, retrospective motion correction and associated smoothing once again caused a reduction in FA which reduced the effect of the FA threshold (Table 3.4b), but increased the likelihood of false FA values (Fig. 3.6e,j). The volume of the caudate improved substantially with the prospectively corrected navigated (Mo_vNav_all) scan (Fig. 3.6f,k).

In gray matter structures and before FA thresholding, the effects of motion were opposite to that seen in the white matter. The mean FA and FA histogram peak location in most gray matter structures increased significantly in the presence of motion compared to the *at rest* baseline scan (Table 3.5a, 3.6a). Retrospective motion correction did not recover the DTI data but rather it caused a reduction in the mean FA and in the FA histogram peak location. The effect of the retrospective motion correction is therefore similar to that in the white matter, in which the mean

FA is significantly reduced. The prospectively corrected navigated diffusion sequence with reacquisition recovered the mean FA and the FA histogram peak location. After thresholding, motion caused a slight increase in the mean FA in RC and the mean FA histogram peak location in most of the regions (Table 3.5b, 3.6b). In contrast to white matter, FA histogram peak location for gray matter VOI's was influenced by FA thresholding (Table 3.6b).

Motion caused an increase in the mean MD for most regions, and this was significant for the left caudate and left hippocampus (Table 3.7a). Retrospective motion correction caused a reduction in the mean MD for most gray matter structures. Motion caused a significant reduction in these two parameters. The prospectively corrected navigated diffusion sequence with reacquisition recovered the MD histogram parameters substantially when compared to the *at rest* baseline scan (NoMo_vNav_NoCo). With FA thresholding, the mean MD did not show a big difference with or without motion (Table 3.7b).

In summary, the FA histogram peak location is one of the most reliable measures for detecting the presence of motion in gray and white matter. Motion causes mean FA to increase in gray matter and decrease in white matter. The smoothing inherent in retrospective motion correction causes a decrease in mean FA in gray and white matter. In the current study, retrospective motion correction failed to recover the DTI measures. In the corpus callosum, retrospective motion correction generated false fiber tracts. The pattern of DTI changes observed in the presence of motion is similar to those that have been reported in various pathologies. As such, extreme caution needs to be exercised when interpreting and reporting DTI findings.

There are a number of limitations to this current study: (1) CSF partial volume contamination within different VOI's in the gray matter may result either from the segmentation process (FreeSurfer) or the registration (FLIRT and FNIRT). (2) The noisy DTI data usually elevates FA values in both gray and white matter (Pierpaoli and Basser, 1996; Hasan et al., 2008) and this can influence the FA threshold. Because the same subject was scanned many times the effect of the noise or CSF will be added equally between different sequences on the same brain, leaving motion as the cause of the difference.

3.5 Conclusions

In this study, we have used volumetric navigators for real time motion correction in DTI with automatic tissue segmentation using FreeSurfer, to explore the changes in FA and MD in both white and gray matter. The observed changes in FA and MD properties due to subject motion are very similar to those reported in studies of neurologically diseased patients. The FA histogram peak location in both white and gray matter is the most sensitive measure for detecting motion. Thresholding FA and MD to eliminate partial volume errors is not appropriate in the presence of motion especially in gray matter. In all instances, retrospective motion correction as applied in this study fails to recover the DTI parameters.

These results demonstrate the risk of misinterpreting DTI findings in the presence of motion. It is critical that individual volumes of the DTI data be assessed for the presence of motion. The present study suggests that retrospective motion correction fails to recover the DTI data. It has been shown previously (Alhamud et al., 2012) that elimination of motion corrupted volumes in the standard diffusion sequence also does not recover the DTI data. In our experience, motion corrupted volumes should be prospectively detected and reacquired to ensure valid DTI results in the presence of motion. If prospective motion correction and reacquisition is not available, DTI scans with motion should be excluded from further analyses.

3.6 Acknowledgements

The South African Research Chairs Initiative of the Department of Science and Technology and National Research Foundation of South Africa, Medical Research Council of South Africa, NIH grants R21AA017410, R21EB008547, R21MH096559, R01HD071664, R01NS05574, P41RR014075, the Ellison Medical Foundation, and the University of Cape Town.

Chapter 4

Application of the EPI-Navigated Diffusion Tensor Imaging Sequence to Paediatric scans[a]

A. Alhamud [1], Barbara Laughton [2], André J.W. van der Kouwe [3,4] and Ernesta M. Meintjes [1]

[1]MRC/UCT Medical Imaging Research Unit, Department of Human Biology, University of Cape Town, South Africa

[2]Chidren's Infectious Diseases Clinical Research Unit, Department of Paediatrics and Child Health, Stellenbosch University and Tygerberg Hospital, Cape Town, South Africa

[3]Athinoula A. Martinos Center for Biomedical Imaging, MGH, Charlestown, MA, USA

[4]Department of Radiology, Harvard Medical School, Brookline, MA, USA

[a]Chapter written as an article to be submitted for publication.

Abstract

Diffusion tensor imaging (DTI) is a non-invasive technique with the potential to detect microstructural changes in the brain. The diffusion tensor and the anisotropy are affected by a broad range of factors. In this study we investigate in paediatric subjects the changes that head motion induces in the diffusion tensor measures, in particular to fractional anisotropy and mean diffusivity. We also compare the performance of the standard diffusion sequence to the prospectively motion corrected navigated diffusion sequence incorporating automatic tissue segmentation using Freesurfer. Sixteen paediatric subjects (aged 5-6 years) and 6 adults were scanned using: (1) the standard diffusion sequence, (2) the prospectively corrected navigated diffusion sequence with reacquisition of five uncorrected corrupted diffusion volumes, and (3) a multiecho MPRAGE sequence. FreeSurfer was used to extract volumes of interest (VOI's). In the paediatric scans acquired using the standard diffusion sequence, subject head motion caused the double bell-shaped curve of the whole brain FA histogram to move towards a single bell-shaped curve. In most of the cortical and subcortical gray matter VOI's studied, motion caused the mean FA, the FA histogram peak location and mean MD to increase significantly. While the navigated sequence yielded more reliable data than the standard sequence, the scans were still affected by motion and signal dropouts.

The results demonstrate that motion during paediatric DTI acquisition can cause changes in the quantitative DTI measures. Furthermore, reacquisition of five directions was insufficient to recover the DTI data for the patterns of movement observed in the paediatric subjects in the present study.

Key Words: diffusion tensor imaging, prospective acquisition correction (PACE), standard diffusion sequence, prospectively corrected diffusion sequence with reacquisition, whole brain histogram, fractional anisotropy, mean diffusivity.

4.1 Introduction

Diffusion tensor imaging (DTI) is a non-invasive technique that provides a sensitive measure of both microstructural changes in brain maturation (Mukherjee et al., 2001; Qiu et al., 2008; Schmithorst et al., 2002) and white matter disorders (Engelbrecht et al., 2002; Noriuchi et al., 2010; Pavuluri et al., 2009). Diffusion imaging measures signal attenuation due to the random thermal motion of water in cerebral tissue. Quantitative parameters determined from DTI include fractional anisotropy (FA) and mean diffusivity (MD). FA is one of the most widely used parameters (Pierpaoli and Basser, 1996) and provides information about the microstructural integrity of highly oriented microstructures. MD is a measure of average molecular motion independent of any tissue directionality. FA is derived from the diffusion tensor, which requires diffusion weighting to be applied along at least 6 different gradient directions. However, for a fiber tracking application, and to gain a better SNR, most DTI acquisitions apply diffusion gradients in more than 6 directions (Le Bihan et al., 2001). Echo planar imaging (EPI) has been implemented in the diffusion pulse sequence to minimize the effect of subject motion by acquiring the whole image within a single shot (Le Bihan et al., 2006). Motion artifacts may reappear in the diffusion images due to the fact that the brain is imaged repeatedly with different gradient directions in order to calculate the diffusion tensor. Head motion causes misalignment of the diffusion volumes and furthermore, individual voxels are exposed to a slightly different diffusion encoding direction/gradient than the desired one (Aksoy et al., 2008). Motion during diffusion sensitization gradients also causes signal dropouts in the images. Both uncorrected diffusion volumes and errors in diffusion encoding can cause serious artifacts in DTI, which can result in erroneous estimations of the diffusion tensor information. Generally, retrospective motion correction is used to correct for the misalignment in the diffusion volumes. Retrospective techniques have many limitations in the co-registration of conventional MR images, including blurring artifacts (Tong and Cox, 1999) and the influence of through-plane motion on the local history of magnetization (Muresan et al., 2005). Retrospective techniques face greater difficulties with diffusion weighted imaging (DWI), especially diffusion weighting with high b-values (Rohde et al., 2004).

DTI pulse sequences, such as the twice-refocused Spin Echo (Reese et al., 2003), have been implemented in paediatric scans using the same protocol parameters as with adult scans and this increases the sensitivity of the DTI measures to motion artifacts. Many neuropathological studies

have been conducted in young children and changes in FA and MD have been reported (Engelbrecht et al., 2002; Noriuchi et al., 2010; Pavuluri et al., 2009). Previously we introduced volumetric navigators to perform prospective motion correction in DTI with reacquisition (Alhamud et al., 2012). The changes observed in the DTI measures due to motion in healthy adult subjects were similar to the changes that have been reported in diseased patients among previous studies (Della Nave et al., 2007; Mori et al., 2008; Zhou et al., 2008). To the author's knowledge, no studies have been performed to highlight the potential effects of subject head motion on DTI measures in paediatric scans.

The aims of this study are: (1) to compare differences in whole brain FA between paediatric and adult scans, without and with motion, (2) to explore differences in regional FA and MD in gray and white matter resulting from subject head motion during paediatric DTI acquisition using automatic tissue segmentation by FreeSurfer, and (3) to compare the performance of the standard diffusion sequence to the prospectively motion corrected navigated diffusion sequence with reacquisition of uncorrected corrupted diffusion volumes in paediatric scans.

4.2 Materials and Methods

4.2.1 Navigated diffusion pulse sequence with 3D-EPI Navigator and reacquisition

A twice-refocused two-dimensional diffusion pulse sequence (Reese et al., 2003) was previously modified to perform prospective motion correction by acquiring an additional 3D-EPI navigator (526 ms) following the acquisition of each diffusion volume (Alhamud et al., 2012). The volumetric navigator contains 3D anatomical information for direct computation of motion parameters, and is not diffusion weighted, so that the accuracy of co-registration and motion estimates are not affected by the diffusion gradients, even at high b-values. The diffusion sequence was further modified to reacquire motion corrupted diffusion volumes during which the motion exceeds a pre-defined threshold.

4.2.2 MRI Data Acquisition

Scans were implemented on a Siemens Allegra 3 T (Siemens Healthcare, Erlangen, Germany) scanner at the Cape Universities Brain Imaging Centre and were performed according to protocols that had been approved by the Faculty of Health Sciences Human Research Ethics

Committees at the Universities of Cape Town and Stellenbosch. Sixteen young children (aged 5-6 years) were scanned. Parents/guardians provided written informed consent and children provided oral assent. We are presenting in the current study data of only one adult subject that is representative of the 6 adults who were scanned as part of a previous study (Alhamud et al., 2012).

T1-weighted structural images were acquired using the motion navigated multiecho MPRAGE (MEMPR) sequence (van der Kouwe et al., 2008). For paediatric scans the MEMPR protocol was the same for all subjects: TR 2530 ms, TE 6.57 ms, TI 1100 ms, flip angle 7 degrees, resolution 1 x 1 x 1 mm^3, acquisition matrix 224 x 224 x 144. For adult scans the MEMPR protocol was the same, except for the following changes: slice thickness 1.3 mm, acquisition matrix 256 x 256 x 128, resolution 1 x 1 x 1.3 mm^3. The MEMPR sequence uses volumetric navigators to ensure a consistent coordinate system throughout the sequence (Tisdall et al., 2011).

Diffusion images were acquired with both the standard diffusion pulse sequence (basic) and the prospectively motion corrected navigated diffusion sequence with reacquisition (vNav_all). The parameters for the diffusion sequence were TR 9500 ms without the navigator (basic sequence), TR 10026 ms with the navigator (vNav sequence), TE 86 ms, 72 slices, resolution 2 x 2 x 2 mm^3, FOV 224 mm, single channel birdcage head coil, 30 non-collinear diffusion gradient directions with b = 1000, and four non-diffusion weighted b=0 acquisitions. The waiting period for feedback in the vNav sequence (including all navigator-related computations in the sequence and in ICE) is 120 ms for each repetition time. Reacquisition was enabled in the vNav sequence with five reacquisitions. The 3D-EPI navigator parameters were TR 14 ms for each partition in the slab that includes 28 partitions without a gap, TE 6.6 ms, resolution 8 x 8 x 8 mm^3, acquisition matrix size 32 x 32 x 28, bandwidth in the readout direction 3906 Hz/px, flip angle 2 degrees, and total scan time 406 ms. The total scan time for the standard sequence is 5 minutes and 33 seconds, and for the vNav sequence with five reacquisitions it is 6 minutes and 40 seconds. The diffusion and navigator protocols were the same for both adult and pediatric scans.

For the adult scan, the subject was asked to remain motionless during the standard sequence. The subject was asked to alter their head position upon verbal instruction five to six times (roughly once every 40 s) during the navigated sequence. The paediatric scans were acquired without any verbal instruction for motion. Children were not anaesthetized or sedated during scanning and

had been trained in a mock scanner before scanning to lie as still as possible during the scan. We were interested to see how much children in this age range may move during scanning and how such random motion would affect the DTI measures. For this reason, the paediatric scans acquired with the standard sequence (basic) were visually inspected for the presence of dropout slices as an indication of motion. Accordingly, the standard diffusion sequence (basic) data was divided as follows: a group that includes all 16 paediatric subjects (all_basic), a group that includes only subjects that moved substantially during the basic acquisition (Mo_basic) as judged by the presence of dropout slices, and a group that includes only subjects with minor motion or no motion (NoMo_basic) scan. In contrast, the navigated sequence (vNav_all) data were analysed with all 16 subjects included and as such included acquisitions without and with motion.

4.2.3 Data Processing

Processing of T1-weighted structural images

The T1-weighted images of each subject were automatically segmented into cortical and subcortical regions using FreeSurfer (http://surfer.nmr.mgh.harvard.edu/) software. FreeSurfer was used in the current study as it has been tested extensively for accuracy and reliability (Fischl et al., 2002; Walimuni et al., 2010). The outcome of the segmentation process is a label volume comprising 175 white matter (WM), gray matter (GM) and cerebrospinal fluid (CSF) regions with a unique label assigned to each region. Since the generated label volume is in FreeSurfer space, the "mri_convert" tool within Freesurfer was used to transfer the segmented regions from FreeSurfer space to T1 or subject space. The "fslmaths" tool within FSL, "mri_convert" within FreeSurfer, and bash scripts developed in-house were implemented to extract and create a binary mask for each volume of interest (VOI) in gray and white matter.

The volumes of interest (VOI's) that were analysed in the current study were whole brain white matter (WM), cerebral cortex, left amygdala (LA), right amygdala (RA), left caudate (LC), right caudate (RC), left hippocampus (LH), and right hippocampus (RH).

Processing of Diffusion Data

Diffusion volumes were processed after conversion from DICOM format to NifTi using FreeSurfer tools. The diffusion data from all subjects were quantified using Diffusion Toolkit (http://trackvis.org/) which generates all the diffusion maps from the NifTi data. In the analysis of regional structures, the FA and MD histograms were calculated from the FA and MD maps and normalized to the total number of pixels. In the analysis of whole brain, the FA histograms were generated in two ways; firstly from the FA maps, and normalized for the total number of pixels and secondly by the TrackVis tools normalized for the total number of tracks.

Volume of Interest Analyses

Each subject's T1-weighted structural volume was registered to his/her T2-weighted (b0) volume using FSL tools (FMRIB Software Library; http://www.fmrib.ox.ac.uk/fsl). FMRIB's linear registration tool (FLIRT) was followed by a non-linear registration using FMRIB's non-linear image registration tool (FNIRT). The outcome of the non-linear registration is an image of the field coefficients calculated in the diffusion space. The 'invwarp' tool within FSL was implemented to transfer the field back to the T1 space. The new inverted field image in the T1 space was applied to the FA and MD maps to transform them into the T1 space using the "applywarp" tool in FSL.

The binary masks that were created previously were applied to the FA and MD maps using the "fslmaths" tool in FSL. The FA and MD histograms for each VOI were generated for each subject and the mean histogram parameters calculated. The average histogram parameters for each VOI for the Mo_basic and vNav_all groups were compared to those of the stationary group (NoMo_basic) using a paired student's t-test. P-values less than 0.05 were considered statistically significant while p-values less than 0.1 indicate a trend.

4.3 Results

The adult data presented here has been previously reported and analysed (Alhamud et al., 2012). Data for only one of the six healthy adult subjects are presented in the current work as it is representative of the sample and serves to illustrate the differences in DTI measures in young children and adults. After visual inspection of the paediatric data acquired using the standard (basic) sequence, nine subjects were considered as having remained stationary during the scan

(NoMo_basic), while seven subjects demonstrated significant movement during the acquisition (Mo_basic).

Motion Estimates

Figure 4.1a shows motion parameters estimated by the prospective acquisition correction (PACE) algorithm in the vNav sequence for a paediatric scan that included a lot of movement. These are incidental movements occurring in a random fashion. For comparison, Figure 4.1b shows motion parameters for an adult who was instructed to move at regular intervals six times during the scan.

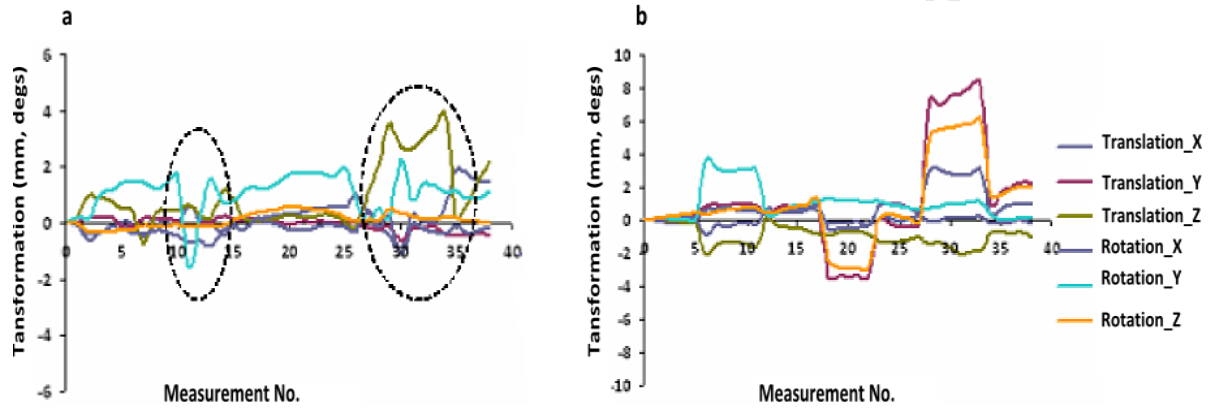

Figure 4.1: Comparison of motion parameter estimates generated by PACE in the navigated diffusion sequence (vNav_all) for (a) a paediatric scan, and (b) an adult scan. Since reacquisition was enabled, the number of measurements was 39. The circles highlight the regions where prolonged motion occurred in the paediatric scan.

Figure 4.2 shows a comparison of the range of motion in different directions averaged for all 16 children, as determined from the difference between the maximum and minimum translation and rotation estimates by PACE in the navigated sequence. Children in this age range predominantly displayed translation in the z direction (along the bore of the magnet or the superior -inferior axis) and rotation around the y direction (anterior-posterior axis).

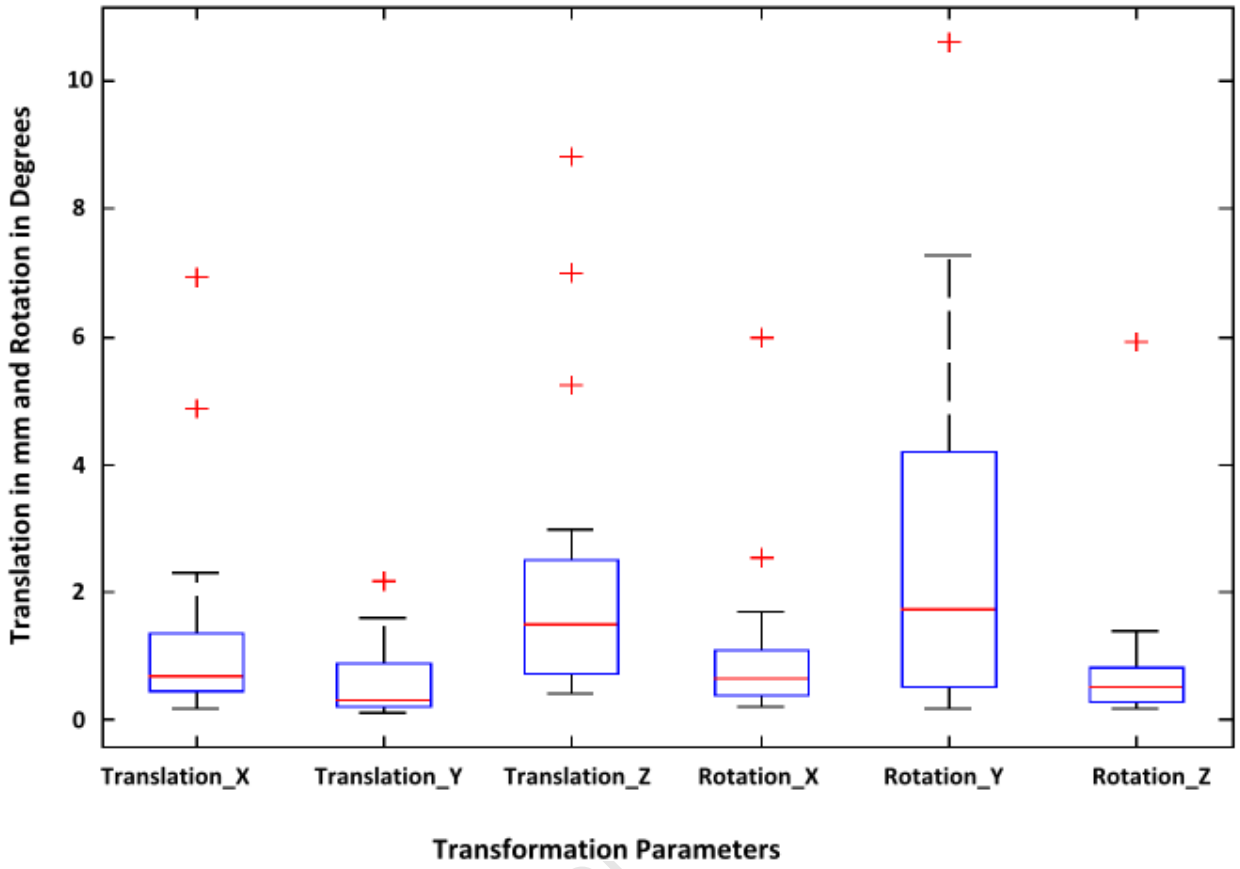

Figure 4.2: Comparison of the range of motion in different directions averaged for all 16 children, as determined from the difference between the maximum and minimum translation and rotation estimates by PACE in the navigated sequence. Children in this age range predominantly displayed translation in the z direction (along the bore of the magnet or the superior -inferior axis) and rotation around the y direction (left-right axis in the scanner coordinate system).

Age-related differences in Whole Brain FA

Figure 4.3a illustrates the difference between the whole brain histogram (WBH) of FA for one paediatric subject who did not move during either the basic or navigated acquisitions and an adult. The WBH was generated using TrackVis software. The magnitude of the low gray matter (GM) FA peak is higher in children than adults, while both the location and the magnitude of the high white matter (WM) FA peak are lower in children than in the adults. Figure 4.3b shows FA histograms for the same scans that were calculated in Matlab directly from the FA maps and normalized for the total number of pixels. These figures illustrate the microstructural changes that occur with age.

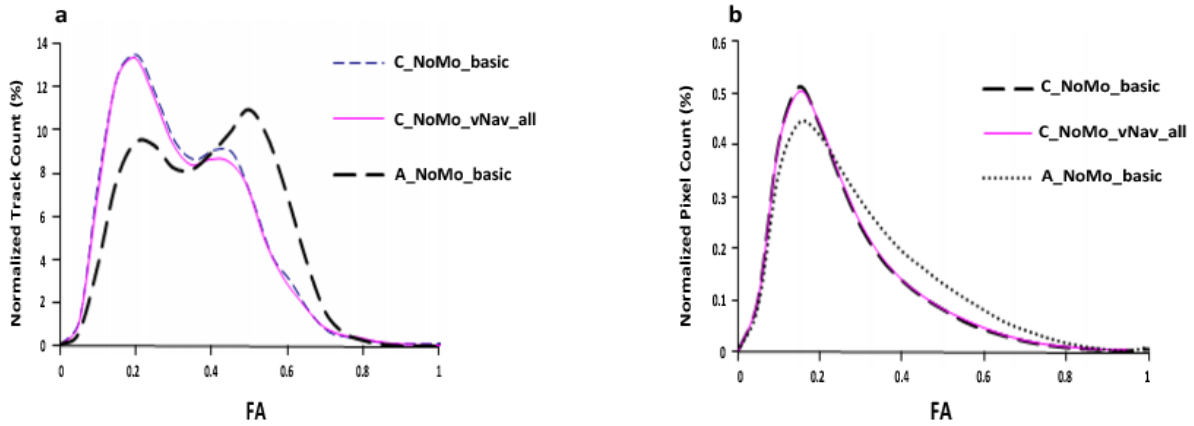

Figure 4.3: (a) Normalized whole brain histograms (WBHs) of FA for one child (C) who did not move during the standard (C_NoMo_basic) and navigated (C_NoMo_vNav_all) acquisitions. An *at rest* adult (A) scan acquired with the standard sequence (A_NoMo_basic) is superimposed on the plots. These histograms were generated in TrackVis software. (b) shows the histograms for the same scans that were generated in Matlab and normalized for the total number of pixels.

Effects of Motion on Whole Brain FA

Figure 4.4a compares the whole brain FA histograms that were generated by TrackVis software for a child (C1) who did not move during the acquisition using the basic sequence (C1_NoMo_basic), compared to those of another child (C2) who moved a lot during both the basic (C2_Mo_basic) and the navigated (C2_Mo_vNav_all) acquisitions. It is evident that motion caused significant changes to the FA histogram. The two FA peaks become less pronounced and closer together. The FA histogram shape is largely recovered using the navigated sequence. The low FA peak location was 0.20 for C1_NoMo_basic, 0.26 for C2_Mo_basic, and 0.19 for C2_Mo_vNav_all. This change towards a single bell-shaped curve is very similar to the changes that occur due to motion in adult data (figure 4.4b). The results of retrospective motion correction of the C2_Mo_basic data using FLIRT, both with and without elimination of the uncorrected corrupted diffusion volumes (8 volumes), are presented in figure 4.4c. FLIRT aligns all the diffusion volumes to the b0 volume using a least squares cost function and 6 degrees of freedom. Retrospective motion correction, even after elimination of the corrupted volumes, failed to recover the FA histogram parameters. The navigated sequence performed better than retrospective motion correction despite the fact that there were many corrupted volumes and signal dropouts in the diffusion volumes which were not eliminated prior to generating the WBH-FA .

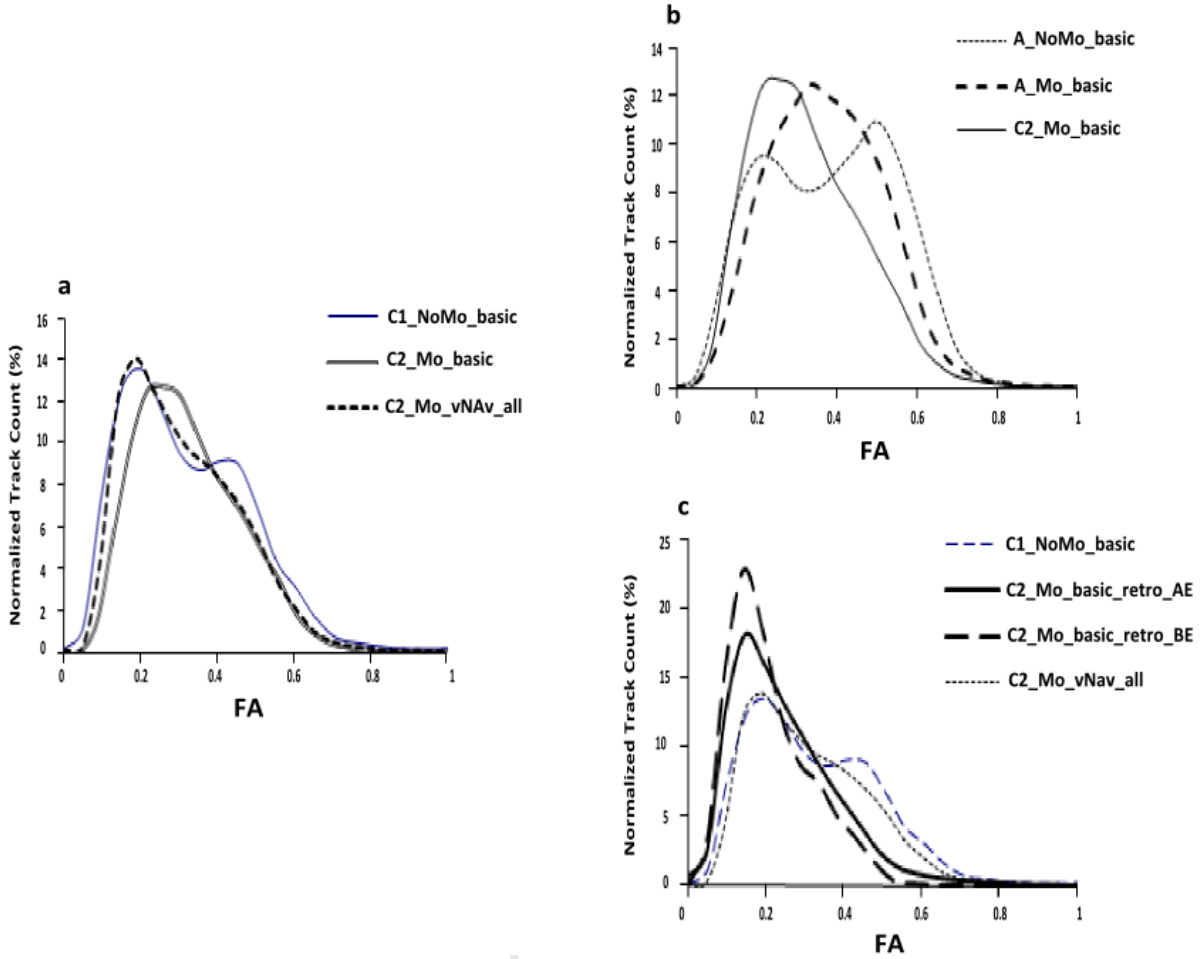

Figure 4.4: (a) Normalized whole brain histograms (WBHs) of FA of a child who did not move during the basic acquisition (C1_NoMo_basic) compared with those of a child who moved during both the basic (C2_Mo_basic) and the navigated (C2_Mo_vNav_all) acquisitions; (b) normalized WBHs of FA of an adult for an *at rest* acquisition using the basic sequence (A_NoMo_basic), and for acquisitions with motion using the basic sequence for paediatric (C2_Mo_basic) and adult (A_Mo_basic) subjects respectively; and (c) effect of retrospective motion correction using FLIRT on normalized WBHs of FA of a child who moved, both without (C2_Mo_basic_retro_BE) and with (C2_Mo_basic_retro_AE) elimination of corrupted volumes, compared to the navigated acquisition (C2_Mo_vNav_all) and the FA histogram of a child who did not move during the basic scan (C1_NoMo_basic).

Effects of motion in Whole Brain white matter

Table 4.1 presents the mean FA histogram parameters of the whole brain white matter, averaged for each group, ie. data for all 16 paediatric subjects from the basic acquisition (all_basic), only subjects with no motion (NoMo) during the basic scan, only subjects who moved (Mo) during the basic scan, and data for all 16 subjects from the vNav_all acquisition.

The FA histogram parameters of the whole brain white matter were not affected by subject motion.

Table 4.1

Comparison of the mean FA histogram parameters of paediatric subjects for the whole brain white matter averaged for each group.

Sequence	Basic Sequence			Navigated DTI
Histogram Parameters	all_basic[a]	NoMo_basic[b]	Mo_basic[b]	vNav_all
N	16	9	7	16
Mean FA	0.38 (0.01)	0.38 (0.01)	0.38 (0.01)	0.38 (0.01)
Peak Location	0.34 (0.02)	0.33 (0.03)	0.34 (0.02)	0.33 (0.02)

Note. [a]Group includes all 16 paediatric subjects imaged with the standard sequence (basic)
[b]Subjects were subdivided according to those who did not (N=9) and those who did (N=7) move during the basic acquisition, as determined by the presence of dropout slices.
Values are means (SD)

Table 4.2 presents the mean MD histogram parameters of the whole brain white matter for each group. The MD histogram peak location was significantly lower for children who moved during the basic scan than those who did not. The navigated sequence recovered all the parameters of the MD histogram for the whole brain WM.

Table 4.2

Comparison of the mean MD histogram parameters for the whole brain white matter for each group.

Sequence	Basic			Navigated DTI
Histogram Parameters	all_basic[a]	NoMo_basic[b]	Mo_basic[b]	vNav_all
N	16	9	7	16
Mean MD /10^{-3} mm^2s^{-1}	0.88 (0.02)	0.88 (0.01)	0.88 (0.03)	0.89 (0.02)
Peak Location /10^{-3} mm^2s^{-1}	0.84 (0.02)	0.85 (0.00)	0.83 (0.03)*	0.85 (0.03)

Note. [a]Group includes all 16 paediatric subjects imaged with the standard sequence (basic)
[b]Subjects were subdivided according to those who did not (N=9) and those who did (N=7) move during the basic acquisition, as determined by the presence of dropout slices.
Values are means (SD)
*$p < 0.05$ (paired student's t-test compared to NoMo_basic).

Effects of Motion in Cerebral Cortex

Table 4.3 presents the mean FA histogram parameters of the cerebral cortex, averaged for each group. There is a significant increase in the peak location and mean FA in children who moved during the basic scan compared to those who did not. The navigated sequence recovered all the FA histogram parameters despite significant motion and the presence of volumes with dropout slices. Figure 4.5 shows the distribution of the mean FA histogram peak location for the basic and navigated scans. For the navigated scans, the mean FA histogram peak location is 0.15 for 81% of the children. By comparison, the peak location for the basic scan data is 0.15 for 56% of the children and 0.20 for 44% of the children. Those with the higher FA include all the children who moved during the basic acquisition.

Table 4.3

Comparison of the mean FA histogram parameters for the cerebral cortex for each group.

Sequence	Basic			Navigated DTI
Histogram Parameters	all_basic[a]	NoMo_basic[b]	Mo_basic[b]	vNav_all
N	16	9	7	16
Mean FA	0.21 (0.02)	0.20 (0.01)	0.23 (0.02)*	0.21 (0.02)
Peak Location	0.17 (0.03)*	0.16 (0.02)	0.20 (0.00)*	0.16 (0.03)

Note. [a]Group includes all 16 paediatric subjects imaged with the standard sequence (basic)
[b]Subjects were subdivided according to those who did not (N=9) and those who did (N=7) move during the basic acquisition, as determined by the presence of dropout slices.
Values are means (SD)
*$p < 0.05$ (paired student's t-test compared to NoMo_basic).

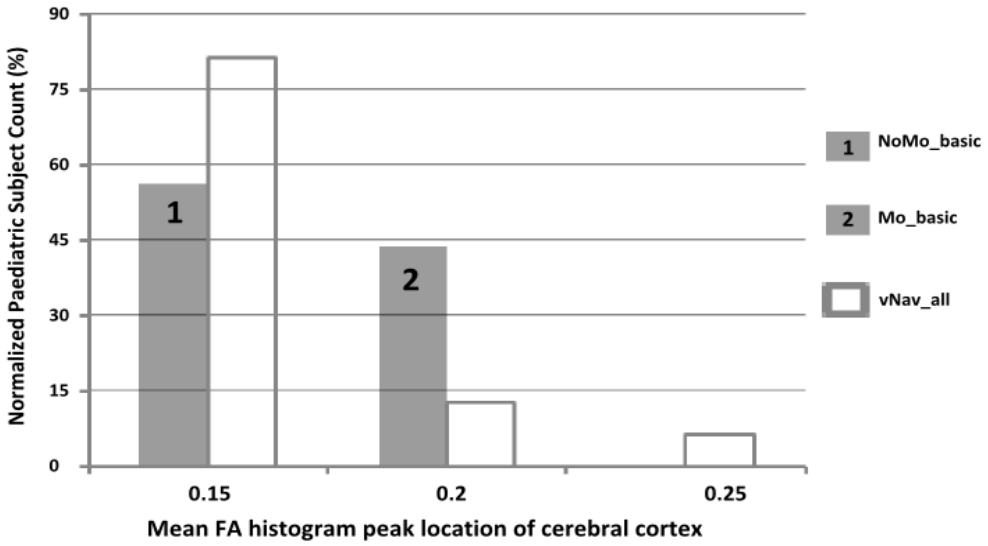

Figure 4.5: Distribution of the mean FA histogram peak location for the basic and navigated acquisitions. For the basic acquisition, the numbers indicate that all the children with peak location 0.15 did not move during the scan (1), while all the children with peak location 0.2 did move (2).

Table 4.4 shows the mean MD histogram parameters of the cerebral cortex, averaged for each group. The mean MD was increased significantly in children who moved during the basic acquisition compared to those who did not. The navigated sequence recovered all the parameters of the MD histogram for the cerebral cortex, even though there were scans with motion and signal dropout.

Table 4.4

Comparison of the mean MD histogram parameters for the cerebral cortex averaged for each group.

Sequence	Basic			Navigated DTI
Histogram Parameters	all_basic[a]	NoMo_basic[b]	Mo_basic[b]	vNav_all
N	16	9	7	16
Mean MD /10^{-3} mm^2s^{-1}	0.99 (0.04)	0.97 (0.03)	1.01 (0.04)*	0.98 (0.04)
Peak Location /10^{-3} mm^2s^{-1}	0.87 (0.03)	0.86 (0.02)	0.89 (0.04)	0.88 (0.04)

Note. [a]Group includes all 16 paediatric subjects imaged with the standard sequence (basic)
[b]Subjects were subdivided according to those who did not (N=9) and those who did (N=7) move during the basic acquisition, as determined by the presence of dropout slices
Values are means (SD)
*$p < 0.05$ (paired student's t-test compared to NoMo_basic).

Effects of Motion in Subcortical Gray Matter VOI's

Tables 4.5 and 4.6 present the mean FA and the mean FA histogram peak location, respectively, for the different subcortical gray matter VOI's, averaged for each group. In most of the subcortical VOI's considered, motion caused both the mean FA and the mean FA histogram peak location to increase (p<0.1). In the left hippocampus and right (caudate, amygdale, and hippocampus) the increase in FA was significant, while the increase in the FA histogram peak location was significant in the left hippocampus.

Table 4.5

Comparison of the mean FA in different subcortical gray matter VOI's averaged for each group.

	Mean FA(SD)			
VOI[1]	all_basic (N=16)	NoMo_basic (N=9)	Mo_basic (N=7)	vNav_all (N=16)
LA	0.21 (0.02)	0.21 (0.02)	0.22 (0.03)	0.21 (0.03)
LC	0.21 (0.03)	0.20 (0.02)	0.23 (0.03)†	0.20 (0.03)
LH	0.21 (0.02)	0.20 (0.01)	0.22 (0.02)*	0.21 (0.01)
RA	0.22 (0.02)	0.21 (0.01)	0.23 (0.02)*	0.22 (0.03)
RC	0.20 (0.02)	0.19 (0.02)	0.21 (0.02)*	0.20 (0.02)
RH	0.21 (0.01)	0.21 (0.01)	0.22 (0.01)*	0.21 (0.02)

Note.[1]The subcortical gray matter VOI's were: left amygdala (LA), left caudate (LC), left hippocampus (LH), right amygdala (RA), right caudate (RC), right hippocampus (RH).
Values are means (SD)
*$p < 0.05$, $^{\dagger}p < 0.1$ (paired student's t-test compared to NoMo_basic).

Table 4.6

Comparison of the mean FA histogram peak location in the different subcortical gray matter VOI's averaged for each group.

	mean FA Histogram Peak Location (SD)			
VOI[1]	all_basic (N=16)	NoMo_basic (N=9)	Mo_basic (N=7)	vNav_all (N=16)
LA	0.18 (0.03)	0.17 (0.03)	0.2 (0.0)	0.17 (0.03)
LC	0.17 (0.03)	0.16 (0.02)	0.19 (0.04)†	0.17 (0.04)
LH	0.17 (0.03)	0.16 (0.02)	0.19 (0.03)*	0.17 (0.02)
RA	0.18 (0.03)	0.17 (0.03)	0.20 (0.03)†	0.17 (0.03)
RC	0.16 (0.02)	0.16 (0.02)	0.17 (0.03)	0.16 (0.02)
RH	0.17 (0.02)	0.16 (0.02)	0.18 (0.03)†	0.17 (0.03)

Note.[1]The subcortical gray matter VOI's were: left amygdala (LA), left caudate (LC), left hippocampus (LH), right amygdala (RA), right caudate (RC), right hippocampus (RH).
Values are means (SD)
*$p < 0.05$, $^{\dagger}p < 0.1$ (paired student's t-test compared to NoMo_basic).

Table 4.7 shows the mean MD, for the different subcortical gray matter VOI's, averaged for each group. In the left caudate, left hippocampus, and right hippocampus there is a significant increase in the mean MD in children who moved during the basic scan compared to those who did not. The navigated sequence fully recovers the mean MD in the different subcortical gray matter VOI's, despite the presence of scans with motion and signal dropout.

Table 4.7

Comparison of the mean MD ($\times 10^{-3}$) in different subcortical gray matter VOI's averaged for each group.

	mean FA Histogram Peak Location (SD)			
VOI[1]	all_basic (N=16)	NoMo_basic (N=9)	Mo_basic (N=7)	vNav_all (N=16)
LA	1.12 (0.16)	1.12 (0.18)	1.11 (0.13)	1.06 (0.10)
LC	1.15 (0.13)	1.09 (0.09)	1.24 (0.13)*	1.15 (0.11)
LH	1.15 (0.07)	1.12 (0.05)	1.19 (0.07)*	1.15 (0.07)
RA	1.08 (0.13)	1.06 (0.12)	1.12 (0.15)	1.07 (0.12)
RC	1.13 (0.12)	1.13 (0.13)	1.15 (0.11)	1.14 (0.10)
RH	1.14 (0.06)	1.11 (0.05)	1.17 (0.05)*	1.14 (0.06)

Note.[1]The subcortical gray matter VOI's were: left amygdala (LA), left caudate (LC), left hippocampus (LH), right amygdala (RA), right caudate (RC), right hippocampus (RH).
Values are means (SD)
*$p < 0.05$ (paired student's t-test compared to NoMo_basic).

4.4 Discussion

DTI has been performed extensively on children in studies of brain development (Hasan et al., 2011; Miller et al., 2003; Snook et al., 2005) and been used to detect many neuropathological diseases (Engelbrecht et al., 2002; Noriuchi et al., 2010; Pavuluri et al., 2009). Most of these studies have found changes in DTI measures, especially in the FA and MD. Previous studies on healthy adult subjects using volumetric navigators for real time motion correction (Alhamud et al., 2012) demonstrated that motion during DTI acquisition can cause significant changes to the DTI measures. The current study aims to explore the effects of motion on DTI measures in paediatric subjects.

Paediatric Scans

In the current study, DTI acquisitions were performed at the end of the scanning session, approximately 35 minutes from the start of the scan. By this time, most of the children were very tired and restless resulting in a significant amount of motion and the presence of signal dropouts. The amount of motion was even worse with the navigated sequence, which was the last acquisition in the session. Therefore, for approximately 5 of the navigated diffusion acquisitions, the reacquisition of 5 uncorrected corrupted diffusion volumes was insufficient to recover the DTI data.

Motion Estimates

The prospectively corrected navigated sequence generates motion parameters during the DTI acquisition (Fig. 4.1a,b). For the standard diffusion sequence (basic), the dicom volume images were inspected visually for motion by looking for the presence of dropout slices. We experienced two scenarios during the paediatric acquisitions with both sequences (basic, vNav_all): children either displayed little motion or were almost asleep, while other children exhibited significant motion and signal dropouts or both.

Figure 4.1a shows an example of a child who moved a lot during the acquisition. Movements of this nature can corrupt many diffusion volumes. Fortunately, the design of the current navigated diffusion sequence, in addition to prospective motion correction, enables reacquisition immediately following the detection of motion and signal dropouts, thus avoiding corruption of other diffusion volumes with different directions or strengths.

For the 5 to 6 year old children scanned as part of this study, the largest motions observed were translation in the z direction and rotation around the left-right axis (Fig. 4.2) which corresponds to nodding movement. Using a special foam pillow to restrain motion in these directions may improve the DTI data.

Age-related Differences in Whole Brain FA

Good agreement is shown in (Fig. 4.3a) between the normalized WBH's of FA of the standard sequence (C_NoMo_basic) and the navigated sequence (C_NoMo_vNav_all) thereby confirming that the navigators and PACE do not introduce errors in the diffusion data.

In a previous study of healthy adult subjects (Alhamud et al., 2012) it was found that the FA histogram of the whole brain is characterized by two distinct peaks: a lower gray matter FA peak and a higher white matter FA peak. The number of tracks in the higher peak was greater than the lower peak in the adult brain due to white matter maturation (Fig. 4.3b). In contrast to the adult brain, the FA histogram of the whole brain in children was characterized by a greater low FA peak (Fig. 4.3b). Although most of the myelination in brain white matter is complete by the age of 5 years, maturation of brain white matter continues into at least the 3rd decade of life (Schmithorst et al., 2002). Schmithorst et al. (2002) also reported an increase in both white matter density and organization during childhood and adolescence. Figure 4.3b shows an FA histogram based on brain volume rather than track numbers. This figure reflects a greater number of pixels with higher anisotropy (FA) in adults compared to childhood, which may be due to the fact that the white matter is fully mature in adult brains. All the paediatric and adult scans without motion displayed similar characteristics.

Effects of Motion on Whole Brain FA

Motion caused similar changes to the FA histogram of children (Fig. 4.4a) as seen in adults (Fig. 4.4b). The double bell-shaped curve of the WBH-FA becomes distorted due to motion and the distribution changes to a single bell-shaped curve (Fig. 4.4b). Retrospective motion correction in the basic acquisition failed to recover the FA histogram properties, even after elimination of the motion corrupted diffusion volumes. Although the navigated sequence was affected by a lot of motion and signal dropouts in the example shown, it was more successful in recovering the DTI data than the standard sequence, both without and with retrospective motion correction (Fig. 4.4c).

Effects of Motion in Whole Brain White Matter

The FA properties of the whole white matter were not affected by paediatric motion (Table 4.1). This may be due to the fact that white matter is still immature at this age (5-6 years). By contrast, the MD histogram peak location was reduced significantly (Table 4.2) in children who moved during the basic scan compared to children who did not. It should be noted that when the data were combined for children who moved and did not move during the basic scan (all_basic), we observe no changes in the MD histogram parameters.

Effects of Motion in Cerebral Cortex

All the FA histogram parameters were significantly different for children who moved during the basic scan compared to children who did not move (Table 4.3). The mean FA histogram peak location and mean FA were significantly higher. The mean FA histogram peak location was also significantly higher when combining all the children who moved and did not move during the basic scan into a single group (all_basic). Figure 4.5 illustrates the good agreement between the FA histogram peak location for subjects who remain stationary during the basic scan and scans acquired with the navigated sequence. The value of the peak location for 81% of the vNav_all acquisitions, was identical to that of the children who did not move during the basic scan. For the 44% who moved during the basic scan, the peak location was higher. The FA histogram peak location in the cerebral cortex is a good indicator for the presence of motion. The mean MD was increased significantly for children who moved during the basic scan compared to those who did not (Table 4.4).

Effects of Motion in Subcortical Gray Matter VOI's

In most of the subcortical VOI's, motion tended ($p < 0.1$) to increase the mean FA and FA histogram peak location. The increase in mean FA was significant in the LH, RC, RA and RH, while the FA histogram peak location was significantly higher in the LH (Tables 4.5 and 4.6). None of the histogram parameters were affected when combining children who moved and who did not move into a single group (all_basic). Although the paediatric scans with the navigated sequence (vNav_all) were acquired in the presence of substantial motion and signal dropouts, the mean FA and the mean FA histogram peak locations for subcortical VOI's were more accurate than for the standard sequence in the presence of motion (Mo_basic). In the left caudate, left hippocampus and right hippocampus motion caused the mean MD to increase significantly for children who moved during the basic scan compared to those who did not (Table 4.7).

There are a number of limitations to the current study: (1) CSF partial volume contamination, particularly within different VOI's in gray matter, may result either from the segmentation process (FreeSurfer) or the registration (FLIRT and FNIRT). (2) Noisy DTI data usually elevates FA values in both gray and white matter (Pierpaoli and Basser, 1996; Hasan et al., 2008). The noise could be larger in the present study due to the use of a Siemens head coil that is designed

specifically for scanning adult subjects or because of the use of only one average in the diffusion protocol. Using a specific head coil for children or increasing the number of averages in the diffusion protocol could enhance the diffusion volume's images and would help in the registration and segmentation process.

Contrary to our expectations, motion generally did not affect the histogram parameters when all the subjects who moved and did not move were combined into a single group. Since fewer than half of the children in our study moved during the basic scan, this may be very different if more of the children in the sample move. When the data of the children who did move during the basic scan were analysed separately, significant changes in DTI measures were evident. As such, it is imperative that data be inspected for the presence of motion before drawing conclusions regarding abnormal DTI. Despite significant subject motion, the vNav_all acquisition successfully recovered the DTI measures.

4.5 Conclusion

In this study, we have highlighted the potential effects of head motion on DTI measures in paediatric scans. This study, similar to a previous study on adult subjects (Alhamud et al., 2012), also demonstrates that navigators do not influence paediatric diffusion data and that there are no potential or residual errors from PACE, which would have introduced diffusion errors. In the presence of motion, the observed changes in the FA properties of the whole brain of children are very similar to the changes observed in adults. In the regional analyses of paediatric brains using automatic tissue segmentation by FreeSurfer, most of the changes due to motion in the DTI measures were shown to be in gray matter. FA histogram peak location in gray matter, is the most sensitive measure for detecting motion in paediatric scans.

The results of this work demonstrate the risk of misinterpreting DTI findings in paediatric scans, in the presence of motion. It is critical that individual volumes of the DTI data be assessed for the presence of motion prior to analysis. The results of this study are in agreement with a previous study (Alhamud et al., 2012), in which retrospective motion correction, with or without elimination of motion corrupted volumes, fails to recover the diffusion data. This study also highlights that motion corrupted volumes should be prospectively detected and reacquired to ensure valid DTI results in the presence of motion. If prospective motion correction and reacquisition is not available, DTI scans with motion should be excluded from further analyses.

4.6 Acknowledgements

The South African Research Chairs Initiative of the Department of Science and Technology and National Research Foundation of South Africa, Medical Research Council of South Africa, NRF grant CPRR78737, NIH grants R21AA017410, R21EB008547, R21MH096559, R01HD071664, R01NS05574, P41RR014075, the Ellison Medical Foundation, and the University of Cape Town.

Chapter 5

Discussion

To accurately solve the six parameters of the diffusion tensor ***D*** from the measured data, each voxel must correspond to the same anatomical location in all the measurements. Subject motion and distortions violate this assumption and typically the images are realigned before model fitting. Several methods have been proposed to improve the properties of the DTI data, either by registering each diffusion weighted image to a reference image (i.e. retrospective motion correction), introducing non-linear reconstruction algorithms to reconstruct the diffusion tensor, or collecting more data during DTI acquisition using navigators. Despite these efforts and the sophisticated algorithms that have been introduced for motion correction in DTI, the correction is still influenced by the diffusion weighting, even when using navigators. Another controversial issue relates to updating the diffusion matrix in retrospective motion correction.

In this work we have presented a motion tracking technique that is completely independent of the diffusion contrast to perform prospective motion correction in diffusion tensor imaging (DTI). This technique involved modifying the standard twice-refocused spin echo diffusion pulse sequence to acquire a 3D-EPI navigator following the acquisition of each diffusion volume. The standard diffusion sequence was further modified to include an optional function in the diffusion protocol for reacquisition of diffusion volumes during which large motion occurred.

5.1 Comparison of the vNav to Current Techniques

DTI information cannot be extracted from one image or volume, but requires repeated scanning of the brain with several diffusion gradients and directions in order to calculate the diffusion tensor. Several diffusion volume images are acquired and each diffusion volume has to be aligned with the others for accurate calculation of the diffusion tensor. The long acquisition of the DTI sequence renders the diffusion volume images sensitive to subject head motion.

Retrospective Motion Correction

Retrospective motion correction is typically used for motion correction in DTI. Retrospective motion correction basically aligns each diffusion volume to a target volume image, usually the first volume with no diffusion sensitization (the b0 volume image). The b0 volume is selected as the target because it is less distorted and has a higher signal-to-noise ratio (SNR) than the DW images. Following retrospective motion correction, each voxel is assumed to correspond to the same anatomical location in all diffusion volumes. One problem with retrospective methods is that volumes acquired with different gradient directions have different contrasts. Even with a mutual information (MI) cost function that is commonly used in DWI registration, the differences in contrast between the DW images and the target image result in poor registration, especially in images with high b values (Rohde et al., 2004).

In the current work retrospective motion correction was implemented with two different algorithms, namely FLIRT and SPM. FLIRT was implemented with different cost functions such as mutual information (MI) and least squares. The results of the current study demonstrate that FLIRT not only fails to recover the diffusion data, but also overestimates the motion parameters (Fig. 2.5). Moreover, in the corpus callosum (CC) FLIRT generates spurious tracts and exaggerates the number of tracts (Fig. 3.4e). Although SPM uses a mutual information cost function for image registration, SPM also fails to recover the diffusion data (Fig 2.7b,f and Fig. 2.8).

A recent and noteworthy abstract by Kwan-Jin Jung (2010) details a study of DW images acquired from the head of an *anesthetized, immobilized monkey* as well as images acquired from the head of a volunteer using an eddy-current compensated sequence. The authors reported: "The anisotropic attenuation of the WM by the DW gradient can induce a false motion estimation when the motion is estimated by the available method. This has to be considered in correcting the motion of the DW images in particular at a higher b value. ***Therefore, it is necessary to develop a new motion estimation method that can detect the motion reliably from the DW images without the need of the acquisition of b=0 images. Besides, a new motion estimation method is important for the new DTI analysis method which does not require the b=0 images***."

In the case of multishot data the situation is even more complex (Aksoy et al., 2008) and the 2-step method for tensor estimation, that is 1) the reconstruction of individual diffusion-weighted images followed by 2) multivariate regression, cannot be used.

Robust Tensor Fitting Model

Robust tensor fitting applied at a voxel-wise level has been proposed for mitigating the effects of artifactual data points that manifest themselves as outlier data (Chang 2005). Techniques such as RESTORE (Robust Estimation of Tensor by Outlier Rejection) by Chang et al. (2005) identify the outliers in the measurement data and exclude them. Retrospective motion correction is, however, performed prior to implementing RESTORE. As a result, if retrospective motion correction introduces spurious data or fails to realign the diffusion images, RESTORE may under or over estimate the measurement data and as such fail to remove the corrupted data. Another disadvantage of robust tensor fitting approaches is increased computational time, so that diffusion tensor images cannot be displayed "on the fly" during or immediately after the acquisition. The tensor fitting model may also not be suitable for other diffusion imaging modalities such as HARDI (*High Angular Resolution Diffusion Imaging)* at very high b-values.

Basic Model-based Registration

More recently a Model-Based Registration technique by Bai and Alexander (2008) has been introduced to improve the registration and remove the errors that traditional motion correction approaches introduce. The basic principle of this method is to use different reference images to register diffusion-weighted images with diffusion weightings in different directions, so that the contrast differences of measurements are taken into account. Because this technique uses diffusion weighted images for motion correction, it is still sensitive to the diffusion weightings and will be less accurate at high b-values.

Navigation in Diffusion MRI

Motion correction in diffusion MRI using navigators has been performed either by collecting information from extra pulses in the standard diffusion sequence (Ordidge et al., 1994; Anderson and Gore, 1994; Crespingy et al., 1995; Butts et al., 1997; Atkinson et al., 2000, Norris

et al., 2001) or by using inherent information from the sequence itself (Pipe et al., 2002; Benner et al., 2010; Kober et al., 2011). Despite the advanced strategies in the design of the navigators used for diffusion MRI, the navigators used to date were all influenced by the diffusion weighting. This is due to the fact that most of the navigator pulses are inserted before the readout gradients. Benner et al. (2010) and Kober et. al. (2011) perform motion correction by registering each diffusion weighted image to a reference image, in this way avoiding the need for extra pulses in the standard diffusion sequence. Although these techniques do not require extra pulses, they are still influenced by the diffusion weightings and moreover the time for registering a whole diffusion weighted image to a reference image online is time consuming, causing the scan time to increase (Kober et al., 2011).

To address several of the concerns raised above and also to develop a technique that is independent of the diffusion contrast, a separate motion tracking technique has been introduced in this work using a volumetric 3D-EPI navigator. This technique performs 3 functions simultaneously: correcting in real time the image misalignment, updating in real time the diffusion gradient, and reacquiring in real time a pre-determined number of corrupted diffusion volumes. The technique presented here can be applied without any limitations to multishot diffusion sequences. Motion detection and motion correction are performed completely independently of the diffusion contrast. This has two major advantages for diffusion imaging. Firstly, the navigator contrast does not change for every diffusion measurement, even for diffusion weightings with high b values (Alhamud et al., 2011). This makes the technique suitable for applications such as q-space imaging (Assaf and Cohen, 1999), Q-ball imaging (Tuch et al., 2003), and diffusion spectrum imaging (Wedeen et al., 2005). Secondly, the navigator data are used directly to estimate the motion parameters so that no additional b0 volume image needs to be acquired every time motion is detected (Kober et al., 2011). The scan time of the navigators, motion estimation by (PACE), and the period required for updating all the diffusion gradients and the RF pulses, is 526 ms. This is a relatively short time when compared to the duration of the diffusion volume measurement (TR = 9500 ms in the current diffusion protocol) (Fig. 1.12).

5.2 Effect of Motion on the B-Matrix

As mentioned above, motion causes diffusion images to be realigned before diffusion model fitting. Motion also causes the subject to be exposed to different diffusion-encoding gradients than the desired one (Rohde et al., 2004). A study that is based on Monte Carlo simulation and *in vivo* subject data by Leemans and Jones (2009) demonstrate that neglecting to reorient the B-matrix introduces significant bias in diffusion measures (e.g. FA and MD) and fiber orientation estimates. The situation becomes more complex with multishot diffusion pulse sequences where motion introduces a different diffusion-weighting matrix for each interleaf (Aksoy et al., 2008).

A recent study by Ling et al. (2012) reported *that the relationship between head motion and diffusion values such as fractional anisotropy (FA) and mean diffusivity (MD) is currently not well understood. While simulation studies suggest that head motion may introduce either a positive or negative bias, this has not been quantified in clinical studies*.

The results of our study reported in the addendum to chapter 2 (A-1) concur with the findings of Ling et al. (2012), namely that retrospective motion correction (i.e. correction of both images and gradient table) with or without elimination of motion corrupted volumes, is likely to be insufficient for removing motion bias.

While it is absolutely true that the accurate estimation of a diffusion tensor depends on the exact diffusion gradient direction, the question arises whether the B-matrix can be reoriented retrospectively or whether this needs to be done prospectively? In contrast to the results reported by Leemans and Jones (2009), rotation of the B-matrix following retrospective motion correction did not recover the shape of the whole brain histogram in the present study. The table below highlights the differences between these studies, which may help explain the different findings.

Table 5. 1

Differences between the Leemans and Jones (2009) study and the present work.

Leemans and Jones (2009)	Alhamud et al., (2012)
Retrospective motion correction and eddy current correction were performed using the method that was developed by Rohde et al. (2004)	Retrospective motion correction was performed using FLIRT in FSL and SPM in a few cases. No eddy current correction was required due to the fact that an optimised twice-refocused spin echo (TRSE) pulse sequence (Reese et al., 2003) was used.
Cardiac gating was employed	Cardiac gating was not employed
Whole body scanner, GE 3T HDx	Head-only scanner, Siemens 3T Allegra
No gold standard data were available for the *in vivo* scans to which retrospective motion corrected data with or without b-matrix rotation could be compared.	Gold standard data with confirmed absence of motion were available from the navigated diffusion acquisitions (Alhamud et al., 2012).
A voxelwise analysis was used to evaluate the effect of reorienting the B-matrix on the DTI measures.	Whole brain histograms were used to evaluate the effect of reorienting the B-matrix on the DTI parameters.
The subjects were healthy volunteers familiar with MRI who did not know that this study was investigating the effects of subject motion. Subjects who are familiar with MRI will, in general, move less than diseased subjects or children. Each subject was scanned only once.	The subjects were healthy volunteers familiar with MRI who knew that the study was investigating the effects of motion. Each subject was scanned twice with the standard sequence, once the subject was asked to remain still and the other time the subject was instructed to move. As such, significant motion will be expected during the acquisitions with motion.

One important point, which is evident from the above comparison, is the difference in the way that the DTI data was analyzed and visualized. Reorienting the B-matrix introduces both positive and negative bias in different regions in the voxelwise data presented by Leemans and Jones (2009). Using the whole brain histogram, the local effects of reorienting the B-matrix may not be apparent as regions of increase and decrease will be averaged out, resulting in very little change to the whole brain histogram. Further, subjects moved significantly more in the acquisitions with motion in the current study than the incidental motion that occurred during the Leemans and Jones (2009) study of adults who were trying to remain motionless.

In the absence of prospective motion correction, further studies are required in different populations with different patterns of motion, different scanners, different methods of retrospective motion, different diffusion encoding schemes, and different methods for analyzing the DTI data in order to address these unresolved issues.

5.3 DTI Data Analysis with the Standard and the Navigated Diffusion Sequences

5.3.1 Validation of the Navigator

As mentioned in chapter 1, inserting additional elements in a diffusion pulse sequence can improve the diffusion data substantially, but at the same time these might generate other complexities as was the case with spin echo or EPI pulses (1.2.2**)**. Acquiring a 3D-EPI navigator following each diffusion measurement might corrupt the diffusion data. For this reason, we performed several scans on a water phantom and on six *at rest* adult subjects. The results demonstrate that the diffusion data is not affected or biased by the navigator and further to this, that there are no residual errors in the motion estimates derived by PACE since these would have corrupted the diffusion data (Table 2.1, 2.2, Fig. 2.2, 2.3, 2.4).

5.3.2 Age-related Differences in Whole Brain Histogram FA

The FA histogram of the whole brain of healthy adult subjects is characterized by two distinct peaks (Fig. 2.4): a lower gray matter FA peak and a higher white matter FA peak. The location and number of tracts in the high FA peak was greater than the low FA peak in the adult brain due to white matter maturation. In contrast to the adult brain, the FA histogram of the

whole brain in children was characterized by a greater number of tracts in the low FA peak (Fig. 4.2). Snook et al. (2004) found that during the transition from childhood to young adulthood, a great number of brain regions demonstrate increases in FA and decreases in MD, suggesting a progressive pattern of myelination/axon growth during this critical period of neurodevelopment.

5.3.3 Effects of Motion and motion correction on Whole Brain Histogram FA in Adults and Children

Several methods have been employed to extract information from DTI data. The majority of studies have adopted the region-of-interest (ROI) method, by manually defining ROIs on the unregistered images. The major limitations of the region of interest method are operator dependence and *a priori* knowledge bias (Della Nave et al., 2007). Since the same subject was scanned several times with different sequences in our study, manual segmentation was avoided. Instead we implemented the whole brain histogram approach and automatic tissue segmentation using FreeSurfer to analyse the DTI data.

Although there were substantial differences in the characteristics of whole brain histograms between adults and children, the effects of motion on the properties of the WBH-FA were identical. In both adults and children, motion caused the unique shape of the WBH-FA to become distorted and to change from a double bell-shaped curve to a single bell-shaped curve. Retrospective motion correction using FLIRT and SPM for scans acquired using the standard diffusion sequence during which motion occurred, failed to recover the shape and the parameters of the WBH-FA, instead resulting in a further reduction in the mean FA and the FA histogram peak location (Table 2.1, 2.2, Fig. 2.7 and 2.8 for adult; Fig. 4.3 for paediatric subject). Even eliminating the corrupted diffusion volumes did not improve retrospective motion correction (Fig. 2.8 for adults; Fig. 4.3 for children).

5.3.4 Effects of Motion and motion correction on Regional FA and MD in Adults and Children

In chapter 2 we analysed the whole brain histograms of FA and MD to avoid any bias in DTI data that could be introduced by manual segmentation of ROI's. In chapters 3 and 4, we performed a regional analysis of the FA and MD in different VOI's in gray and white matter that were automatically segmented using FreeSurfer. Freesurfer was used in the current study as it

has been tested extensively for accuracy and reliability (Fischl et al., 2002; Walimuni et al., 2010).

Whole brain white matter (WM)

In adults we observed a significant reduction in the mean FA and FA histogram peak location (Table 3.1, Fig. 3.1) in the presence of motion. In contrast to the changes observed in the histogram parameters of the WBWM-FA of adults, the histogram parameters of the WBWM-FA of children were not affected by motion, not even the FA histogram peak location (Table 4.1). This might be due to impending white matter maturation at ages 5-6. In both adults and children, retrospective motion correction using FLIRT caused a reduction in the mean FA and FA histogram peak location. This reduction would affect gray-white matter segmentation using an FA threshold, as is frequently done (Table 3.3).

Motion and retrospective motion correction influenced mainly the shape of the MD histogram distribution rather than the mean MD (Fig. 3.2). The mean MD and MD histogram peak location for adults did not show changes due to motion (Table 3.2), while a significant reduction in the mean MD histogram peak location of children was observed (4.2). In view of this, the median MD should be reported together with the mean FA to take into account changes in the shape of the MD histogram.

Subcortical gray matter

The effects of motion on subcortical gray matter were identical for both adults and children. In most of the gray matter VOI's, motion resulted in increased mean FA and FA histogram peak locations (Tables 3.5 and 3.6 for adults; Tables 4.5 and 4.6 for children). These results highlight the fact that FA thresholding may not be appropriate in the presence of motion since parts of the anatomical VOI may be excluded due to increases in the GM FA as a result of motion (Table 3.4 and Fig. 3.6).

The prospectively navigated diffusion sequence substantially recovers the properties of both the regional and the whole brain FA and MD. Even for paediatric subjects in whom a lot of motion and signal dropouts occurred during the navigated sequence, the accuracy and reliability of the DTI data are much improved compared to the standard sequence.

5.4 Limitations to this Study

There are a number of limitations to the current study summarised as follows:

1) Real time motion tracking by the 3D EPI navigator once per diffusion volume may not be sufficient to detect rapid motion, especially in paediatric scans. The use of double 3D EPI navigators, each with half the scan time of the current navigator (406/2 ms), inserted between diffusion volumes could improve the performance of this technique. A second option would be to combine the current method with the FID navigator method proposed by (Kober et al., 2011). Another option is to add a new function to the image reconstruction that creates a profile image of the signal intensities of each slice in the diffusion volume, which can then be compared to a reference profile. Substantial changes in the intensity profile would indicate that significant motion occurred during the diffusion volume. A signal would then be sent to the scanner to reacquire this volume, together with the motion parameters required to update the scanner coordinate system to the subject coordinate system.

2) When reacquisition is enabled on the modified diffusion protocol and the number of reacquisitions are specified, that number of reacquisitions must be performed in the current implementation of the sequence, even if no significant motion (or fewer instances than specified) occurred during the scan. In such a case, the final diffusion volume will be reacquired however many times is necessary to use up any remaining reacquisitions. The main reason why the sequence was designed this way was to keep the scan time on the scanner accurate. We can terminate reacquisition at the end of the diffusion measurements by adjusting some flags in the diffusion pulse sequence.

3) Motion estimation in the current implementation of the navigated diffusion sequence relies completely on the Siemens implementation of PACE, which terminates for translations in any direction greater than 20 mm and rotations in any direction greater than 8 degrees. Although PACE terminates and no further motion estimates are generated, the sequence will continue to run and navigator images will still be acquired enabling offline estimation of motion parameters and retrospective motion correction. PACE could be replaced with a different algorithm for image registration. This could,

however, affect the waiting period for the feedback which is 120 ms in the current version of the sequence.

4) CSF partial volume contamination in the different VOI's in the gray matter may result either from segmentation or registration errors. Because the same subject was scanned repeatedly using different sequences, CSF partial voluming should affect the different acquisitions equally so that the observed differences can be attributed to motion.

5) Noisy DTI data usually elevates FA values in both gray and white matter and may influence the segmentation and registration process. In the current study we acquired only one average in the diffusion protocol. By increasing the number of averages in the diffusion protocol the SNR of the DTI data could be improved. Because we used the same Siemens head coil for the paediatric and adult scans, SNR of the paediatric DTI data may also be lower due to poorer coil filling. Using a smaller head coil that is suitable for small children could improve the SNR of the paediatric data. SNR should, however, be similar for the different acquisitions that are being compared in this study, so that differences may be attributed to motion.

6) In the paediatric study, the navigated diffusion acquisition was performed at the end of a long imaging protocol, by which time children were very restless and moved more than normal. As such, there were more instances of significant motion than the specified number of reacquisitions. Ideally all these instances should have been reacquired. This reduced the effectiveness of the prospective motion correction. In future studies the DTI acquisition should be performed near the beginning of the imaging protocol to avoid this problem.

Chapter 6

Conclusion

A novel technique has been presented that performs real-time tracking of head pose and adjusts in real time the RF pulses and all the diffusion gradients to correct for any head motion. The additional scan time required is 526 ms for each diffusion TR (9500 ms). The technique uses an echo planar imaging readout to rapidly acquire a low-resolution volumetric navigator (vNav) following the acquisition of each diffusion volume. Registration of successive vNavs to the reference vNav provides robust head position and orientation estimates that are used to update the scanner's current coordinate system once each TR. If enabled, the system also reacquires volumes during which excessive motion occurred. The reacquisition was programmed to take place immediately following the detection of corrupted volumes and not at the end of the scan (Benner et al., 2011). Architecture such as this is highly suitable to paediatric scans because of the prolonged incidental movements that could corrupt other diffusion volumes with different diffusion directions and strengths. The sequence was validated using phantom data, as well as *in vivo* adult and paediatric scans. It was shown that introducing the navigator does not corrupt the diffusion data and that the navigated sequence can successfully recover the DTI data in the presence of motion.

The changes observed in the FA and MD due to subject motion are very similar to those that have been reported in studies of neurologically diseased patients. Although changes in the FA histogram peak location have been reported in neurologically diseased patients, it was a sensitive marker for detecting the presence of motion in all the adult and paediatric data presented here, except for paediatric white matter. Motion affects white and gray matter FA differently; in white matter motion reduces the high FA values while in gray matter motion increases the low FA values. Thresholding FA and MD to eliminate partial volume errors is not appropriate in the presence of motion, especially in gray matter.

In all instances where retrospective motion correction was applied in this study, both with and without elimination of motion corrupted volumes, it failed to recover the DTI parameters. Because of the smoothing inherent to the interpolation algorithm in retrospective methods,

retrospective motion correction reduces the diffusion anisotropy in both gray and white matter and, moreover, false values can be generated.

Because of the flexibility in the design of the current navigated diffusion sequence, which allows easily adding or removing blocks in the sequence and in the image reconstruction pipeline, future studies should examine the benefits of real-time shim correction in DTI. It has been shown previously (Hess et al., 2011) in Magnetic Resonance Spectroscopy (MRS) that both real-time shim and motion correction are necessary to correct for motion in MRS. The shim changes caused by motion during DTI and the effects of these changes on the DTI data need to be assessed. This will entail inserting a second volumetric navigator with a different echo time into each volume of the DTI acquisition in order to measure shim changes throughout the DTI scan. From these two navigators, frequency and main magnetic field (B0) changes that occur due to motion can be computed and corrected in real time.

In the current implementation of the navigated sequence, corrupted diffusion volumes were reacquired when motion exceeded some pre-set thresholds. This pattern of reacquisition may be sufficient if there is no continuous motion following the reacquisition, such as we observed in the 5-year old children. Future work should develop an automated method to detect volumes with dropout slices in order to optimise reacquisition of only severely corrupted slices. One possible approach is to only reacquire volumes that have a significantly low signal. Also, it may be better to allow reacquisition of all severely corrupted volumes rather than specifying before the scan the number of allowed reacquisitions.

Multishot EPI and spiral sequences are more sensitive to subject motion compared to single shot EPI and spiral sequences, because each interleaf accrues a different (typically nonlinear) phase in the image domain (Aksoy et al., 2008). The insertion of the 3D-EPI navigator in the multishot sequences may be an efficient way to detect and correct the motion in real time for each interleaf.

In this work, PACE was implemented in the diffusion sequence to evaluate motion parameters. As mentioned previously, PACE terminates when motion exceeds certain limits. In this scenario, the navigator images could be used retrospectively for estimating motion. Alternatively,

developing or implementing another algorithm to replace PACE in the image reconstruction pipeline (ICE) is another option. The design of the current pulse sequence is very flexible in terms of implementing and replacing any function in the image reconstruction pipeline.

High resolution 3D sequences offer many advantages over conventional 2D sequences in terms of signal to noise ratio and improved spatial resolution, but may suffer from even longer scan times. It will be of interest to investigate the feasibility of using a 3D echo-planar imaging sequence for DTI acquisition.

The results of this work demonstrate the risk of misinterpreting DTI findings in adult and paediatric scans in the presence of motion. It is critical that individual volumes of DTI data be assessed for the presence of motion. This study also highlights that motion corrupted volumes should be prospectively detected and reacquired to ensure valid DTI results in the presence of motion. If prospective motion correction and reacquisition is not available, DTI scans with motion should be excluded from further analyses.

References

Aksoy, M., Liu, C., Moseley, M. E., Bammer, R., 2008. Single-step nonlinear diffusion tensor estimation in the presence of microscopic and macroscopic motion. Magn. Reson. Med. 59,1138-1150.

Aksoy, M., Forman, C., Straka, M., Skare, S., Holdsworth, S., Hornegger, J., Bammer, R., 2011. Real-time optical motion correction for diffusion tensor imaging. Magn. Reson. Med. 66,366-378.

Alhamud, A., Hess, A. T., Tisdall, M. D., Meintjes, E. M., van der Kouwe, A. J. W., 2011. Implementation of real time motion correction in diffusion tensor imaging. In: Proceedings of the 19th Annual Meeting of ISMRM; Montréal, Canada, (# 3942).

Alhamud, A., Tisdall, M. D., Hess, A. T., Hasan, K. M., Meintjes, E. M., van der Kouwe, A. J. W., 2012. Volumetric navigators for real-time motion correction in diffusion tensor imaging. Magn. Reson. Med. doi: 10.1002/mrm.23314.

Anderson, A. W., Gore, J. C.,1994. Analysis and correction of motion artifacts in diffusion weighted imaging. Magn. Reson. Med. 32:379-87.

Ashburner, J., Andersson, J.L., Friston, K.J., 1999. High-dimensional image registration using symmetric priors. Neuroimage 9:619-28.

Assaf, Y., Cohen, Y., 1999. Structural information in neuronal tissue as revealed by q-space diffusion NMR spectroscopy of metabolites in bovine optic nerve. NMR Biomed. 12,335-344.

Atkinson, D., Porter, D. A., Hill, D. L., Calamante, F., Connelly, A., 2000. Sampling and reconstruction effects due to motion in diffusion-weighted interleaved echo planar imaging. Magn. Reson. Med. 44:101-9.

Bai, Y., Alexander, D. C., 2008. Model-based registration to correct for motion between acquisitions in diffusion MR imaging, The fifth IEEE international symposium on biomedical imaging (ISBI 2008).

Basser, P. J., Mattiello, J., LeBihan, D., 1994. MR diffusion tensor spectroscopy and imaging. Biophys. J. 66,259-267.

Basser, P. J., Pierpaoli, C., 1996. Microstructural and physiological features of tissues elucidated by quantitative-diffusion-tensor MRI. J. Magn. Reson. B. 111,209-219.

Basser, P.J., Pajevic, S., Pierpaoli, C., Duda, J., Aldroubi, A, 2000. In vivo fiber tractography using DT-MRI data. Magn. Reson. Med 44:625-32.

Benner, T., van der Kouwe, A. J. W., Sorensen, A. G., 2010. Diffusion imaging with prospective motion correction and reacquisition. Magn. Reson. Med. doi: 10.1002/mrm.22837. .

Benson, R. R., Meda, S. A., Vasudevan, S., Kou, Z., Govindarajan, K. A., Hanks, R. A., Millis, S. R., Makki, M., Latif, Z., Coplin, W., 2007. Global white matter analysis of diffusion tensor images is predictive of injury severity in traumatic brain injury. J. Neurotrauma. 24,446-459.

Bozzali, M., Franceschi, M., Falini, A., Pontesilli, S., Cercignani, M., Magnani, G., Scotti, G., Comi, G., Filippi, M., 2001. Quantification of tissue damage in AD using diffusion tensor and magnetization transfer MRI. Neurology 57,1135-1137.

Brown R., 1828. On the general existence of active molecules in organic and inorganic bodies. Philos. Mag., Ann. Philos. New Series, 4.
http://sciweb.nybg.org/science2/pdfs/dws/Brownian.pdf

Butts K, Pauly J, de Crespigny A, Moseley M., 1997. Isotropic diffusion-weighted and spiral-navigated interleaved EPI for routine imaging of acute stroke.Magn. Reson. Med. 38:741-9.

Cercignani, M., Inglese, M., Pagani, E., Comi, G., Filippi, M., 2001. Mean diffusivity and fractional anisotropy histograms of patients with multiple sclerosis. AJNR Am. J. Neuroradiol. 22,952-958.

Chang, L. C., Jones, D. K., Pierpaoli, C., 2005. RESTORE: robust estimation of tensors by outlier rejection.Magn. Reson. Med.53:1088-95.

Chung, S. W., Pelletier, D., Sdika, M., Lu, Y., Berman, J. I., Henry, R. G., 2008. Whole brain voxel-wise analysis of single-subject serial DTI by permutation testing. Neuroimage 39,1693-1705.

Clark, C. A., Werring, D. J., Miller, D. H., 2000. Diffusion imaging of the spinal cord in vivo: estimation of the principal diffusivities and application to multiple sclerosis. Magn. Reson. Med. 43,133-138.

de Crespigny, A. J., Marks, M. P., Enzmann, D. R., Moseley, M. E., 1995. Navigated diffusion

imaging of normal and ischemic human brain. Magn. Reson. Med. 33:720-8.

de Figueiredo, E. H., Borgonovi, A. F. N. G., Doring, T. M., 2011. Basic concepts of MR imaging, diffusion MR imaging, and diffusion tensor imaging. Magn. Reson. Imaging Clin. N. Am. 19,1-22.

Della Nave, R., Foresti, S., Pratesi, A., Ginestroni, A., Inzitari, M., Salvadori, E., Giannelli, M., Diciotti, S., Inzitari, D., Mascalchi, M., 2007. Whole-brain histogram and voxel-based analyses of diffusion tensor imaging in patients with leukoaraiosis: correlation with motor and cognitive impairment. AJNR Am. J. Neuroradiol. 28,1313-1319.

Derbyshire, J. A., Wright, G. A., Henkelman, R. M., Hinks, R. S., 1998. Dynamic scan-plane tracking using MR position monitoring. J. Magn. Reson. Imaging 8,924-932.

Ehman, R. L., Felmlee, J., 1989. Adaptive technique for high-definition MR imaging of moving structures. Radiology 173,255-263.

Ellis, C., Simmons, A., Jones, D., Bland, J., Dawson, J., Horsfield, M., Williams, S., Leigh, P., 1999. Diffusion tensor MRI assesses corticospinal tract damage in ALS. Neurology 53,1051-1051.

Engelbrecht, V., Scherer, A., Rassek, M., Witsack, H. J., Mödder, U., 2002. Diffusion-weighted MR Imaging in the Brain in Children: Findings in the Normal Brain and in the Brain with White Matter Diseases1. Radiology 222,410-418.

Eviatar, H., Schattka, B., Sharp, J. C., Rendell, J., Alexander, M. E., 1999. Real time head motion correction for functional MRI. In: Proceedings of the 7th Annual Meeting of ISMRM; Philadelphia, PA, USA, (# 262).

Fischl, B., Salat, D. H., Busa, E., Albert, M., Dieterich, M., Haselgrove, C., van der Kouwe, A., Killiany, R., Kennedy, D., Klaveness, S., 2002. Whole Brain Segmentation:: Automated Labeling of Neuroanatomical Structures in the Human Brain. Neuron 33,341-355.

Foong, J., Maier, M., Clark, C., Barker, G., Miller, D., Ron, M., 2000. Neuropathological abnormalities of the corpus callosum in schizophrenia: a diffusion tensor imaging study. J. Neurol. Neurosurg. Psychiatry. 68,242-244.

Freire, L., Mangin, J. F., 2001. Motion correction algorithms may create spurious brain activations in the absence of subject motion. Neuroimage14: 709-722.

Friston, K. J., Ashburner, J., Frith, C. D., Poline, J. B., Heather, J. D., Frackowiak, R. S. J., 1995. Spatial registration and normalization of images. Hum. Brain Mapp. 3,165-189.

Fu, Z. W., Wang, Y., Grimm, R. C., Rossman, P. J., Felmlee, J. P., Riederer, S. J., Ehman, R. L., 1995. Orbital navigator echoes for motion measurements in magnetic resonance imaging. Magn. Reson. Med. 34,746-753.

Hasan, K. M., Halphen, C., Boska, M. D., Narayana, P. A., 2008. Diffusion tensor metrics, T2 relaxation, and volumetry of the naturally aging human caudate nuclei in healthy young and middle-aged adults: Possible implications for the neurobiology of human brain aging and disease. Magn. Reson. Med. 59,7-13.

Hasan, K. M., Iftikhar, A., Kamali, A., Kramer, L. A., Ashtari, M., Cirino, P. T., Papanicolaou, A. C., Fletcher, J. M., Ewing-Cobbs, L., 2009a. Development and aging of the healthy human brain uncinate fasciculus across the lifespan using diffusion tensor tractography. Brain Res. 1276,67-76.

Hasan, K. M., Kamali, A., Iftikhar, A., Kramer, L. A., Papanicolaou, A. C., Fletcher, J. M., Ewing-Cobbs, L., 2009b. Diffusion tensor tractography quantification of the human corpus callosum fiber pathways across the lifespan. Brain Res. 1249,91-100.

Hasan, K. M., Walimuni, I. S., Abid, H., Frye, R. E., Ewing-Cobbs, L., Wolinsky, J. S., Narayana, P. A., 2011. Multimodal Quantitative Magnetic Resonance Imaging of Thalamic Development and Aging across the Human Lifespan: Implications to Neurodegeneration in Multiple Sclerosis. J. Neurosci. 31,16826-16832.

Helton, K. J., Phillips, N. S., Khan, R. B., Boop, F. A., Sanford, R. A., Zou, P, Li, C. S., Langston, J. W., Ogg, R. J., 2006. Diffusion tensor imaging of tract involvement in children with pontine tumors. AJNR Am. J. Neuroradiol. 27(4):786-793.

Hess, A. T., Tisdall, M. D., Andronesi, O. C., Meintjes, E. M., van der Kouwe, A. J.,2011. Real-time motion and B0 corrected single voxel spectroscopy using volumetric navigators. Magn. Reson. Med. 66(2):314-23.

Hsu, E. W., Mori, S., 1995. Analytical expressions for the NMR apparent diffusion coefficients in an anisotropic system and a simplified method for determining fiber orientation. Magn. Reson. Med. 34:194-200.

Jones, D. K., Horsfield, M. A., Simmons, A., 1999. Optimal strategies for measuring diffusion in anisotropic systems by magnetic resonance imaging. Magn Reson Med. 42:515-25.

Klingberg, T., Hedehus, M., Temple, E., Salz, T., Gabrieli, J. D. E., Moseley, M. E., Poldrack, R. A., 2000. Microstructure of Temporo-Parietal White Matter as a Basis for Reading

Ability:: Evidence from Diffusion Tensor Magnetic Resonance Imaging. Neuron 25,493-500.

Kober, T., Gruetter, R., Krueger, G., 2011. Prospective and retrospective motion correction in diffusion magnetic resonance imaging of the human brain. Neuroimage 59,389-398.

Kwan-Jin Jung, 2010. Sensitivity of Motion Estimation to the anistropic diffusion of white matter in diffusion MRI. In: Proceedings of the 18th Annual Meeting of ISMRM; Stockholm, Sweden, (# 4036).

Le Bihan, D., Turner, R., Moonen, C. T. W., Pekar, J., 1991. Imaging of diffusion and microcirculation with gradient sensitization: design, strategy, and significance. J. Magn. Reson. Imaging 1,7-28.

Le Bihan, D., Mangin, J. F., Poupon, C., Clark, C. A., Pappata, S., Molko, N., Chabriat, H., 2001. Diffusion tensor imaging: concepts and applications. J. Magn. Reson. Imaging 13,534-546.

Le Bihan, D., Poupon, C., Amadon, A., Lethimonnier, F., 2006. Artifacts and pitfalls in diffusion MRI. J. Magn. Reson. Imaging 24,478-488.

Leemans, A., Jones, D. K., 2009. The B-matrix must be rotated when correcting for subject motion in DTI data.Magn. Reson. Med. 61:1336-49.

Lim, K. O., Hedehus, M., Moseley, M., de Crespigny, A., Sullivan, E. V., Pfefferbaum, A., 1999. Compromised white matter tract integrity in schizophrenia inferred from diffusion tensor imaging. Arch. Gen. Psychiatry. 56,367.

Ling, J., Merideth, F., Caprihan, A., Pena A, Teshiba, T., Mayer, A. R., 2012. Head injury or head motion? Assessment and quantification of motion artifacts in diffusion tensor imaging studies. Hum. Brain Mapp. 33:50-62.

Maes F, Collignon A, Vandermeulen D, Marcha G, Suetens P. Multimodality image registration by maximization of mutual information, 1997. IEEE Trans Med Imaging;16:187–198.

McRobbie, D. W., Moore, E. A., Graves, M. J., Prince, M. R., 2007. The textbook of : MRI from picture to ptoton. Cambridge University Press. 3rd edition, 2007.

Miller, J. H., McKinstry, R. C., Philip, J. V., Mukherjee, P., Neil, J. J., 2003. Diffusion-tensor MR imaging of normal brain maturation: a guide to structural development and myelination. AJR Am. J Roentgenol. 180,851-859.

Mori, S., van Zijl, P. C., 1995. Diffusion weighting by the trace of the diffusion tensor within a single scan.Magn. Reson. Med. 33:41-52.

Mori, N., Miki, Y., Fushimi, Y., Kikuta, K., Urayama, S., Okada, T., Fukuyama, H., Hashimoto, N., Togashi, K., 2008. Cerebral infarction associated with moyamoya disease: histogram-based quantitative analysis of diffusion tensor imaging--a preliminary study. Magn. Reson. Imaging 26,835-840.

Mugler, J. P., Brookeman, J. R., 1990. Three-dimensional magnetization-prepared rapid gradient-echo imaging (3D MP RAGE). Magn. Reson. Med. 15,152-157.

Mukherjee, P., Bahn, M. M., McKinstry, R. C., Shimony, J. S., Cull, T. S., Akbudak, E., Snyder, A. Z., Conturo, T. E., 2000. Differences between Gray Matter and White Matter Water Diffusion in Stroke: Diffusion-Tensor MR Imaging in 12 Patients1. Radiology 215,211-220.

Mukherjee, P., Miller, J. H., Shimony, J. S., Conturo, T. E., Lee, B. C. P., Almli, C. R., McKinstry, R. C., 2001. Normal Brain Maturation during Childhood: Developmental Trends Characterized with Diffusion-Tensor MR Imaging1. Radiology 221,349.

Muresan, L., Renken, R., Roerdink, J. B. T. M., Duifhuis, H., 2005. Automated correction of spin-history related motion artefacts in fMRI: simulated and phantom data. IEEE Trans. Biomed. Eng. 52,1450-1460.

Nagy, Z., Weiskopf, N., 2008. Efficient fat suppression by slice-selection gradient reversal in twice-refocused diffusion encoding. Magn. Reson. Med. 60,1256-1260.

Neil, J. J., Shiran, S. I., McKinstry, R. C., Schefft, G. L., Snyder, A. Z., Almli, C. R., Akbudak, E., Aronovitz, J. A., Miller, J. P., Lee, B., 1998. Normal brain in human newborns: apparent diffusion coefficient and diffusion anisotropy measured by using diffusion tensor MR imaging. Radiology 209,57-66.

Noriuchi, M., Kikuchi, Y., Yoshiura, T., Kira, R., Shigeto, H., Hara, T., Tobimatsu, S., Kamio, Y., 2010. Altered white matter fractional anisotropy and social impairment in children with autism spectrum disorder. Brain Res. 1362,141-149.

Norris, D. G., Driesel, W., 2001. Online motion correction for diffusion-weighted imaging using navigator echoes: Application to RARE imaging without sensitivity loss. Magn. Reson. Med. 45:729-33.

Ooi, M. B., Krueger, S., Thomas, W. J., Swaminathan, S. V., Brown, T. R., 2009. Prospective real-time correction for arbitrary head motion using active markers. Magn. Reson. Med. 62,943-954.

Ordidge, R. J., Helpern, J. A., Qing, Z. X., Knight, R. A., Nagesh, V., 1994. Correction of motional artifacts in diffusion-weighted MR images using navigator echoes. Magn. Reson. Med. 12:455-60.

Parizel, P. M., Van Rompaey, V., Loock, V. R., Van Hecke, W., Van Goethem, J., Leemans, A., Sijbers, J., 2007. Influence of User-Defined Parameters on Diffusion Tensor Tractography of the Corticospinal Tract. The Neuroradiology Journal 20:139-147.

Pavuluri, M. N., Yang, S., Kamineni, K., Passarotti, A. M., Srinivasan, G., Harral, E. M., Sweeney, J. A., Zhou, X. J., 2009. Diffusion tensor imaging study of white matter fiber tracts in pediatric bipolar disorder and attention-deficit/hyperactivity disorder. Biol. Psychiatry 65,586-593.

Pierpaoli, C., Basser, P. J., 1996. Toward a quantitative assessment of diffusion anisotropy. Magn. Reson. Med. 36:893-906.

Pipe, J. G., Farthing, V. G., Forbes, K. P., 2002.Multishot diffusion-weighted FSE using PROPELLER MRI.Magn. Reson. Med. 47:42-52.

Pipe, J. G., 1999. Motion correction with PROPELLER MRI: application to head motion and free-breathing cardiac imaging. Magn. Reson. Med. 42,963-969.

Qin, L., van Gelderen, P., Derbyshire, J. A., Jin, F., Lee, J., de Zwart, J. A., Tao, Y., Duyn, J. H., 2009. Prospective head-movement correction for high-resolution MRI using an in-bore optical tracking system. Magn. Reson. Med. 62,924-934.

Qiu, D., Tan, L. H., Zhou, K., Khong, P. L., 2008. Diffusion tensor imaging of normal white matter maturation from late childhood to young adulthood: voxel-wise evaluation of mean diffusivity, fractional anisotropy, radial and axial diffusivities, and correlation with reading development. Neuroimage 41,223-232.

Reese, T., Heid, O., Weisskoff, R., Wedeen, V., 2003. Reduction of eddy-current-induced distortion in diffusion MRI using a twice-refocused spin echo. Magn. Reson. Med. 49,177-182.

Rohde, G., Barnett, A., Basser, P., Marenco, S., Pierpaoli, C., 2004. Comprehensive approach for correction of motion and distortion in diffusion-weighted MRI. Magn. Reson. Med. 51:103-114.

Rosas, H. D., Lee, S.Y., Bender, A.C., Zaleta, A.K., Vangel, M., Yu, P., Fischl, B., Pappu, V., Onorato, C., Cha, J. H., Salat, D. H., Hersch, S. M., 2010. Altered white matter microstructure in the corpus callosum in Huntington's disease: implications for cortical "disconnection". Neuroimage 49:2995-3004.

Rose, S. E., Janke PhD, A. L., Chalk, J. B., 2008. Gray and white matter changes in Alzheimer's disease: a diffusion tensor imaging study. J. Magn. Reson. Imaging 27,20-26.

Schmithorst, V. J., Wilke, M., Dardzinski, B. J., Holland, S. K., 2002. Correlation of White Matter Diffusivity and Anisotropy with Age during Childhood and Adolescence: A Cross-sectional Diffusion-Tensor MR Imaging Study. Radiology 222,212-218.

Snook, L., Paulson, L. A., Roy, D., Phillips, L., Beaulieu, C., 2005. Diffusion tensor imaging of neurodevelopment in children and young adults. Neuroimage 26,1164-1173.

Stejskal, E., Tanner, J., 1965. Spin diffusion measurements: spin echoes in the presence of a time-dependent field gradient. J. Chem. Phys. 42,288.

Studholme, C., Hill, D.L., Hawkes, D. J., 1997. Automated three-dimensional registration of magnetic resonance and positron emission tomography brain images by multiresolution optimization of voxel similarity measures. Med. Phys. 24:25–35.

Thesen, S., Heid, O., Mueller, E., Schad, L. R., 2000. Prospective acquisition correction for head motion with image-based tracking for real-time fMRI. Magn. Reson. Med. 44,457-465.

Tievsky, A. L., Ptak, T., Farkas, J., 1999. Investigation of apparent diffusion coefficient and diffusion tensor anisotropy in acute and chronic multiple sclerosis lesions. AJNR Am. J Neuroradiol. 20,1491-1499.

Tisdall, M. D., Hess, A. T., Reuter, M., Meintjes, E. M., Fischl, B., van der Kouwe, A. J. W., 2011. Volumetric navigators for prospective motion correction and selective reacquisition in neuroanatomical MRI. Magn. Reson. Med. doi: 10.1002/mrm.23228. .

Tong, R., Cox, R. W., 1999. Rotation of NMR images using the 2D chirp-z transform. Magn. Reson. Med. 41,253-256.

Tuch, D. S., Reese, T. G., Wiegell, M. R., Wedeen, V. J., 2003. Diffusion MRI of complex neural architecture. Neuron 40,885-895.

van der Kouwe, A. J. W., Benner, T., Dale, A. M., 2006. Real-time rigid body motion correction and shimming using cloverleaf navigators. Magn. Reson. Med. 56,1019-1032.

van der Kouwe, A. J. W., Benner, T., Salat, D. H., Fischl, B., 2008. Brain morphometry with multiecho MPRAGE. Neuroimage 40,559-569.

Walimuni, I. S., Abid, H., Hasan, K. M., 2010. A computational framework to quantify tissue microstructural integrity using conventional MRI macrostructural volumetry. Comput. Biol. Med. 41,1073-1081.

Ward, H. A., Riederer, S. J., Grimm, R. C., Ehman, R. L., Felmlee, J. P., Jack Jr, C. R., 2000. Prospective multiaxial motion correction for fMRI. Magn. Reson. Med. 43,459-469.

Wedeen, V. J., Hagmann, P., Tseng, W. Y. I., Reese, T. G., Weisskoff, R. M., 2005. Mapping complex tissue architecture with diffusion spectrum magnetic resonance imaging. Magn. Reson. Med. 54,1377-1386.

Welch, E. B., Manduca, A., Grimm, R. C., Ward, H. A., Jack Jr, C. R., 2002. Spherical navigator echoes for full 3D rigid body motion measurement in MRI. Magn. Reson. Med. 47,32-41.

White, N., Roddey, C., Shankaranarayanan, A., Han, E., Rettmann, D., Santos, J., Kuperman, J., Dale, A., 2010. PROMO: Real-time prospective motion correction in MRI using image-based tracking. Magn. Reson. Med. 63,91-105.

Wong, E. C., Cox, R. W.,Song, A. W.,1995. Optimized isotropic diffusion weighting. Magn. Reson. Med. 34: 139–143.

Zaitsev, M., Dold, C., Sakas, G., Hennig, J., Speck, O., 2006. Magnetic resonance imaging of freely moving objects: prospective real-time motion correction using an external optical motion tracking system. Neuroimage 31,1038-1050.

Zaitsev, M., Armstrong, B. S. R., Andrews-Shigaki, B., Kusik, T. P., Barrows, R. T., Gumus, K., Kadashevich, I. Y., Prieto, T., Speck, O., Ernst, T. M., 2010a. Prospective Motion Correction for MRI with a Single Retro-Grate Reflector Target and a Single Camera. In: Proceedings of the 18th annual meeting of International Society of Magnetic Resonance in Medicine. Vol. M. p. 5027.

Zhou, Y., Lin, F., Zhu, J., Zhuang, Z., Li, Y., Tao, J., Qian, L., Xu, J., Lei, H., 2008. Whole brain diffusion tensor imaging histogram analysis in vascular cognitive impairment. J. Neurol. Sci. 268,60-64.